University of Alberta

Finite Deformation of Elastic Curves and Surfaces

by

Ali Asghar Atai

A thesis submitted to the Faculty of Graduate Studies and Research in partial fulfillment of the requirements for the degree of Doctor of Philosophy

Department of Mechanical Engineering

Edmonton, Alberta
Fall 1998

National Library of Canada
Acquisitions and Bibliographic Services
395 Wellington Street
Ottawa ON K1A 0N4
Canada

Bibliothèque nationale du Canada
Acquisitions et services bibliographiques
395, rue Wellington
Ottawa ON K1A 0N4
Canada

Your file Votre référence

Our file Notre référence

The author has granted a non-exclusive licence allowing the National Library of Canada to reproduce, loan, distribute or sell copies of this thesis in microform, paper or electronic formats.

L'auteur a accordé une licence non exclusive permettant à la Bibliothèque nationale du Canada de reproduire, prêter, distribuer ou vendre des copies de cette thèse sous la forme de microfiche/film, de reproduction sur papier ou sur format électronique.

The author retains ownership of the copyright in this thesis. Neither the thesis nor substantial extracts from it may be printed or otherwise reproduced without the author's permission.

L'auteur conserve la propriété du droit d'auteur qui protège cette thèse. Ni la thèse ni des extraits substantiels de celle-ci ne doivent être imprimés ou autrement reproduits sans son autorisation.

0-612-34730-3

Canada

University of Alberta

Library Release Form

Name of Author: Ali Asghar Atai

Title of Thesis: Finite Deformation of Elastic Curves and Surfaces

Degree: Doctor of Philosophy

Year this Degree Granted: 1998

Permission is hereby granted to the University of Alberta Library to reproduce single copies of this thesis and to lend or sell such copies for private, scholarly, or scientific research purposes only.

The author reserves all other publication and other rights in association with the copyright in the thesis, and except as hereinbefore provided, neither the thesis nor any substantial portion thereof may be printed or otherwise reproduced in any material form whatever without the author's prior written permission.

A. A. Atai

Ali Asghar Atai
#206, R.H. Michener Park,
Edmonton, Alberta, Canada
T6H 4M5

Date: Sept. 21, 98

University of Alberta

Faculty of Graduate Studies and Research

The undersigned certify that they have read, and recommend to the Faculty of Graduate Studies and Research for acceptance, a thesis entitled **Finite Deformation of Elastic Curves and Surfaces** submitted by **Ali Asghar Atai** in partial fulfillment of the requirements for the degree of Doctor of Philosophy

David Steigmann

Dr. D. J. Steigmann (Supervisor)

Dr. A. Mioduchowski (Co-Supervisor)

Dr. S. A. Lukasiewicz

Dr. J. K. Szymanski

Gary Faulkner

Dr. M. G. Faulkner

Peter Schiavone

Dr. P. Schiavone

A W Lipsett

Dr. A. W. Lipsett

Ru Chang Ding

Dr. C. Q. Ru

Date: Aug. 11, 98

Abstract

Cable and membrane structures have always been under consideration by engineers as structural elements because of advantages like high strength to weight ratio and low cost over other structures. But due to the highly non-linear geometrical and material behavior of such structures, their design and analysis is a difficult task. Also, treatments that consider both elements in a structure and their interaction is rare to find. In this work, the equilibrium equations for the coupled finite deformations of perfectly flexible elastic membranes and cables is established. In order to incorporate the necessary conditions for stability of the equilibrium configuration, *relaxed* strain energy functions for cable and membrane are used which eliminate the possibility of the existence of compressive stresses (which cannot be carried by cables and membranes) in the structures and introduce wrinkles. The difference form of the equations of equilibrium is derived using Green's theorem and a numerical method called *dynamic relaxation* (which considers the problem as a damped dynamic one) is used to obtain the equilibrium configuration as the steady state response to the dynamical problem. Several examples are solved

using this method. Two interesting cases among them are neutral holes (elliptic and circular) and inclusion. It is seen that the cable reinforcement reduces the sharp strain gradients specially at singular points. Qualitative behavior of cable reinforcement is shown in an experiment.

Dedication

This work is dedicated to my parents, to my wife, and to my son Amir Hossein.

Acknowledgment

I want to thank Drs. D.J. Steigmann and A. Mioduchowski for their supervision of this work whose support and guidance, helped me finish this work. I also want to thank the partial financial support of Ministry of Culture and Higher Education of Iran and Natural Sciences and Engineering Research Council of Canada. I would also like to thank Warner Shelters company in Calgary, Alberta for providing the pattern data for the six–pole tent example. The help of Dr. D. Budney and technicians Berni Faulkner and Ian Buttar with the experimental part of my work is highly appreciated. Last and not the least, I wanted to thank my wife who was a great support for me and stood by me all the way.

Contents

1 Introduction 1

2 Elastic curves and surfaces 5
- 2.1 Elastic curves (cables) 5
- 2.2 Elastic surfaces 10

3 Variational Theory 15
- 3.1 Equilibrium 20
- 3.2 Additional necessary conditions 27
- 3.3 Relaxed theory 29
  - 3.3.1 Relaxed membrane energy 31
  - 3.3.2 Relaxed cable energy 37

4 Discretization and numerical solution 39
- 4.1 Discretization 39
- 4.2 Numerical method 47

5 Numerical Examples 52
- 5.1 Examples involving plane deformation of membranes 52
  - 5.1.1 Varga material 55
  - 5.1.2 Harmonic materials 57
  - 5.1.3 Neo-Hookian material 65
- 5.2 Neutral holes 70
  - 5.2.1 Circular hole 72
  - 5.2.2 Elliptic neutral hole 75
- 5.3 Planar deformation of membrane with orthotropic material . . 81
- 5.4 Plane deformation of a square sheet 84
- 5.5 Inclusion 89

5.6 Suturing 96
5.7 Three dimensional tents 98

6 Experimental results **110**

7 Conclusion and Summary **124**

A Boundary-Fitted Orthonormal Grids **131**

B Source Code **136**

List of Tables

5.1 Comparison of numerical and analytical stretches for elliptic inclusion 94
5.2 Numerical stretches for extended circle inclusion 96

List of Figures

2.1 A single cable undergoing general deformation in 3D space . . 6
2.2 A single cable under distributed and end forces 9
2.3 A membrane in x_1–x_2 plane undergoing general 3D deformation 11

3.1 Examples of attached cable reinforcement 17
3.2 Examples of shearless cable reinforcement 18
3.3 Two pieces of membrane sutured together 24

4.1 Discretized regions for finite–difference approximations of equations of equilibrium 40
4.2 Green integration path for two pieces that are to be sutured . 43

5.1 Meshed reference configuration of an annular membrane with $r_i/r_o = 0.5$ 58
5.2 Deformed configuration with $\rho_o = 1.2r_o$. Varga material. No cable reinforcement 59
5.3 Distribution of stretches vs. radius for Varga material with no cable reinforcement 60
5.4 Distribution of stretches vs. radius for Varga material with cable reinforcement of $E/2\mu r_i = 2.0$ 61
5.5 Distribution of stretches vs. radius for standard harmonic material ($\bar{\lambda}/\mu = 2.0$) with no cable reinforcement 63
5.6 Distribution of stretches vs. radius for standard harmonic material ($\bar{\lambda}/\mu = 2.0$) and cable reinforcement of $E/2\mu r_i = 2.0$ 64
5.7 Distribution of stretches vs. radius for neo–Hookian material with no cable reinforcement 67
5.8 Distribution of stretches vs. radius for neo–Hookian material with cable reinforcement of $E/\mu r_i = 2.0$ 68

5.9 Deformed configuration of an annular with $r_i/r_o = 0.5$, $\rho_o = r_o$, and applied radial traction of $\mathbf{t} = -\mathbf{e}_r$ on the inside 69
5.10 Distribution of stretches vs. radius for neo–Hookian material with no cable reinforcement and applied radial traction 71
5.11 Distribution of stretches vs. radius for standard harmonic material ($\bar{\lambda}/\mu = 2.0$) and cable reinforcement of $E/2\mu r_i = 3.0$ 74
5.12 Geometry of the elliptic hole before and after deformation . . 76
5.13 Elliptic hole with dimensions $a = 2.5b = r_o/2$ inside a circular domain of radius r_o 79
5.14 Distribution of stretches vs. horizontal axis for the elliptic hole. Varga material. Applied stretches of $\lambda_1 = 1.46$ and $\lambda_2 = 2.5$ on the outside 80
5.15 Deformed configuration of an annular membrane with $r_i/r_o = 0.5$. Linear orthotropic material. Twist of 20 degrees ccw in the inside 82
5.16 Deformed configuration of the annular membrane with applied twist and a slit along the horizontal radial line 83
5.17 A 10 by 10 square mesh with side L 85
5.18 Spurious deformed configuration of the square with diagonal pull–out of the corners 86
5.19 Initial configuration of a square with side L 87
5.20 Deformed configuration of the square with diagonal pull–out of the corners 88
5.21 Deformed configuration of the square with corners pulled out and attached cable reinforcement on the edges 90
5.22 Deformed configuration of the square with corners pulled out and shearless cable reinforcement on the edges 91
5.23 Initial configuration of a square of side L with an elliptic inclusion at the center 93
5.24 Initial configuration of a square of side L with an extended circle inclusion at the center 95
5.25 Undeformed configuration of two chevron shaped pieces fixed at the vertical edges and sutured along the facing edges 97
5.26 Deformed configuration of two chevron shaped pieces sutures together 99
5.27 Undeformed configuration of a chevron shaped piece and a square one that are to be sutured 100

5.28 Deformed configuration of a chevron shaped piece and a square one sutured together 101
5.29 Undeformed configuration of a 6–pole tent. 16 pieces are to be sutured together 102
5.30 Angle–view of the deformed configuration of the 6–pole tent . 104
5.31 Overlapping meshes of two extended triangles that are to be sutured 105
5.32 Side–view of the deformed configuration of the single pole tent with no cable reinforcement 107
5.33 Side–view of the deformed configuration of the single pole tent with attached cable reinforcement along the edges 108
5.34 Side–view of the deformed configuration of the single pole tent with shearless cable reinforcement along the edges 109

6.1 Schematic of setup for the tensile test of the rubber 111
6.2 Results of the uniaxial tensile test on the rubber 113
6.3 Grid used for stretch calculations 114
6.4 Distribution of stretches vs. radius for the rubber. No hole and no reinforcement 116
6.5 Deformed configuration for the rubber sheet with a hole and no reinforcement 117
6.6 Distribution of stretches vs. radius for the rubber with a hole and no reinforcement 118
6.7 Undeformed configuration of the rubber sheet with a hole and one reinforcement ring 119
6.8 Distribution of stretches vs. radius for the rubber with a hole and one reinforcement ring 120
6.9 Deformed configuration of the rubber with a hole and two reinforcement rings 122
6.10 Distribution of stretches vs. radius for rubber with a hole and two reinforcement rings 123

A.1 A few grids generated by orthogonal mapping 135

Chapter 1

Introduction

Membrane and cable structures have long been under consideration as structural elements because of advantages like high strength to weight ratio and low cost. But what makes their design difficult is the inherent non–linearity of the deformation and the material. These elements have been used to model a wide variety of phenomena ranging from bioelasticity and fluid capillarity to rubber elasticity and mechanics of structural networks. But a treatment of both these elements and their interaction in a system under three–dimensional large deformations is rarely found. In this work, we try to establish such a framework. We use ideal models of perfectly flexible one and two dimensional continua and solve boundary value problems that normally involve cases in which compressive stresses appear in parts of the structure. This stress state represents a localized buckling phenomenon and it typically involves wrinkling under small compressive stress with most of the tensile stress carried along the wrinkle trajectories. The shape of the wrinkles is mainly determined by the bending stiffness of the material. Since the ideal model considered here neglects flexural stiffness, such a pattern of deformation cannot be described by this model. Moreover, the presence of the compressive stresses in equilibrium solution generates instability (Steigmann, 1986). The use of theories for structures (such as rods and shells) that are capable of describing these patterns has its own complications and entails

substantial additional analytical and computational work. In this work, since the flexural rigidity for both of these elements is neglected, cables are represented by straight lines and membranes are shown by flat surfaces in the wrinkled regions and the details of deformation in the wrinkled region are not given. However, in most cases, we are after the global behavior of the structure and this is not affected by these local patterns. Therefore, we make use of the *relaxed* theories of perfectly flexible continua, in which we modify the constitutive equations in such a way that the compressive stresses are automatically excluded for all strains. Atai and Steigmann (1997) and Haseganu and Steigmann (1994a) have discussed this issue for cables and membranes, respectively. A deformation that involves a state of strain that would cause destabilizing compression according to the original theory can now be viewed as resulting from a continuous distribution of wrinkles under negligible compressive stress. Pipkin (1986) showed that states of strain associated with unstable compressive stresses in conventional membrane theory may instead be constructed as limits of energy–minimizing sequences of deformations involving closely spaced wrinkles. He derived a *relaxed strain energy* that automatically accounts for such states.

We begin in Chapter 2 with a brief discussion of deformation of elastic curves (cables) and surfaces (membranes) and their equilibrium. Chapter 3 deals with applications of variational theory to the potential energy for a system of combined cables and membranes. Two different cable arrangements (attached and shearless) are considered. And the equations of equilibrium plus the coupling boundary conditions for both types of cables are discussed. The possibility of having several disjoint pieces of membrane as the undeformed configuration and connecting them together (suturing) and analysing the resultant structure is taken into account. This feature along with the two cable-attachment models is a new aspect in this work and it allows for a better modeling of practical structural design. The necessary conditions for the equilibrium configuration to be the minimizer of the potential energy are

also discussed. Several material models for the membrane are discussed and their relaxed form is presented. This multiple definition of the strain energy function automatically satisfies the conditions required for stability. The materials are mostly isotropic but a very simple orthotropic material is also considered. A linear elastic cable model is discussed and the stability conditions for both types of cable attachments are presented. In Chapter 4, the discretization of the domain of the membrane and the finite difference form of the equations of equilibrium are presented. A numerical method that does not need the calculation of stiffness matrix (and hence avoids ill–conditioning due to lack of stiffness) and has the advantage of low memory requirements is discussed and the procedure for implementing it in solving the discretized equations of equilibrium is discussed. Chapter 5 shows some numerical examples of combinations of cable and membrane structures. Wherever possible, the analytical results are also obtained and a comparison is made with the numerical ones. Two very interesting examples of this case are circular and elliptic neutral holes. Here we consider finite deformations as opposed to small deformations considered by Mansfield (1953) but the condition on the outer boundary and the shape of the original hole are as he suggested. The significant effect of cable reinforcement on membrane structures is shown in the stretch of a square sheet and it is seen there that the reinforcement tends to bring down the sharp stretch gradients specially at singular points. A few 2 and 3 dimensional suturing examples are presented and the results seem to be plausible. The 6–pole and single pole tent cases are interesting examples of suturing. In the single–pole tent case, it is seen how a very rough attempt to diminish the high strains at the pole tip is successful simply by having an undeformed configuration that is stretched near the position of the pole. An example that uses the orthotropic material is also discussed. In Chapter 6, an experimental case is discussed and the results are compared with the analytical and numerical ones. In Chapter 7 we discuss the conclusions of this work and possible future extensions. Appendix A covers the pro-

cedure for generating boundary–fitted orthogonal coordinate system which helps generate meshes for numerical calculations that minimize the error in approximations of equations of equilibrium.

Chapter 2

Elastic curves and surfaces

In this chapter, the equilibrium equations for *perfectly* flexible elastic curves (cables) and surfaces (membranes) are briefly discussed. The reader is referred to Atai and Steigmann (1997) and Haseganu and Steigmann (1994a) for more detail.

2.1 Elastic curves (cables)

Let's consider a single cable with unstretched length L undergoing a general deformation in 3D space (Figure 2.1). The cable is assumed to be unstretched in the reference configuration so that the arclength measure s varies in the range [0,L]. $\mathbf{x}(s)$ is the position vector of a point on the cable in the reference configuration with respect to the fixed frame with orthonormal vectors $\mathbf{e}_i, i \in \{1,2,3\}$ and $\mathbf{r}(s)$ is its corresponding vector in the deformed configuration.

The deformation gradient is given by

$$\mathbf{r}'(s) = \frac{d\mathbf{r}}{ds} = \frac{d\mathbf{r}}{dS}\frac{dS}{ds} = \lambda \mathbf{t} \tag{2.1}$$

where S is the measure of arclength in the deformed configuration, λ is the stretch in the cable, and $\mathbf{t}$ is the unit tangent to the cable in the deformed

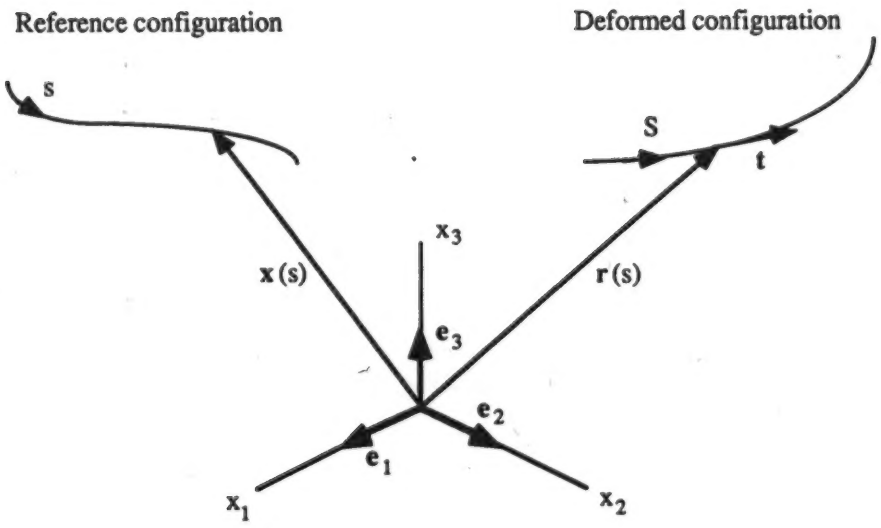

Figure 2-1: A single cable undergoing general deformation in 3D space

configuration. From now on, prime denotes differentiation with respect to the indicated argument. We can assume the existence of a strain energy density, B, per unit arclength s, that depends in some way on the deformation gradient $\mathbf{r}'(s)$. Although non-uniform materials can be considered allowing B to depend explicitly on s, this dependency is suppressed in this work.

It is logical to assume that superposed rigid motions do not affect the strain energy for a given deformation. This invariance results in the necessary and sufficient condition of

$$B(\mathbf{r}'(s)) = \hat{B}(\lambda); \qquad \lambda(s) = |\mathbf{r}'(s)|. \tag{2.2}$$

The strain energy stored in an elastic cable with reference length L can be written as

$$\int_0^L B(\mathbf{r}'(s))ds = \int_0^L \hat{B}(\lambda(s))ds. \tag{2.3}$$

The force exerted by the part $(s, L]$ of the cable on the part $[0, s]$ is (Atai and Steigmann, 1997)

$$\mathbf{f}(s) = \hat{\mathbf{f}}(\mathbf{r}'(s)) = (\partial B/\partial r_i')\mathbf{e}_i, \tag{2.4}$$

where $r_i(s)$ are the components of $\mathbf{r}(s)$ corresponding to $\mathbf{e}_i$ and from now on, summation rule applies on the repeated indices. Then from (2.2) we can write

$$\frac{\partial B}{\partial r_i'} = \frac{\partial \hat{B}}{\partial r_i'} = \frac{\partial \hat{B}}{\partial \lambda}\frac{\partial \lambda}{\partial r_i'} = \frac{\partial \hat{B}}{\partial \lambda}(\frac{r_i'}{\lambda}) = \frac{\partial \hat{B}}{\partial \lambda}t_i = f(\lambda)t_i, \tag{2.5}$$

where

$$f(\lambda) = \hat{B}'(\lambda) \tag{2.6}$$

is the magnitude of the force derived from the constitutive relation and the relation

$$\lambda^2 = r_i' r_i' \tag{2.7}$$

derived from $(2.2)_2$ is used to get (2.5). Thus

$$\mathbf{f}(s) = f(\lambda(s))\mathbf{t}(s). \tag{2.8}$$

Eqn (2.8) shows that the force is everywhere tangential to the curve defined by $\mathbf{r}(\cdot)$.

Now consider a cable under distributed force with density $\mathbf{b}(s)$ per unit reference arclength (Figure 2.2). Then the equilibrium equation for the cable will be (Atai and Steigmann, 1997)

$$\mathbf{f}'(s) + \mathbf{b}(s) = \mathbf{0}, \quad s \in [0, L], \tag{2.9}$$

and if in addition, end forces $\mathbf{f}_L$ and $-\mathbf{f}_0$ are applied at $s = L$ and $s = 0$, respectively, then the boundary conditions result in

$$\mathbf{f}(0) = \mathbf{f}_0 \text{ and } \mathbf{f}(L) = \mathbf{f}_L. \tag{2.10}$$

In this case, $\mathbf{f}_0$, $\mathbf{f}_L$ and $\mathbf{b}(s)$ must be chosen such that

$$\mathbf{f}_L = \mathbf{f}_0 - \int_0^L \mathbf{b}(s)ds. \tag{2.11}$$

Alternatively, if either of the ends of the curve is constrained against movement then eqn (2.10) defines the reaction force at the end in question, and eqn (2.11) is automatically satisfied in any equilibrium configuration.

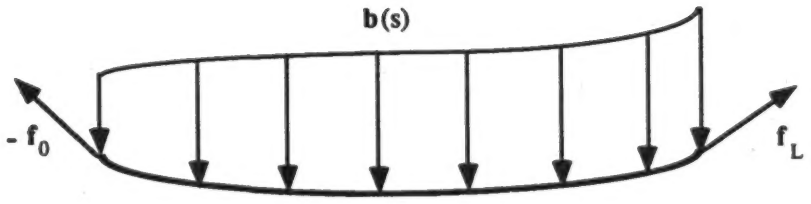

Figure 2-2: A single cable under distributed and end forces

2.2 Elastic surfaces

In this section, we discuss the analysis of perfectly flexible elastic surfaces. This can be considered as the 2D generalization of the perfectly flexible cables theory. In this work, we consider the reference configuration to be flat and stress–free. We assume that the reference configuration occupies a bounded region Ω in the (x_1, x_2) plane with piecewise smooth boundary $\partial\Omega$ (Figure 2.3). Each point of the membrane in this configuration is identified by its position vector $\mathbf{x} = x_\alpha \mathbf{e}_\alpha$ where Greek indices range over $\{1, 2\}$ and $\{\mathbf{e}_1, \mathbf{e}_2\}$ is a fixed orthonormal basis that spans Ω.

A general 3D deformation maps the position vector $\mathbf{x}$ to the deformed position vector $\mathbf{y}(\mathbf{x}) = y_i(\mathbf{x})\mathbf{e}_i$, where Latin indices range over $\{1, 2, 3\}$ and $\mathbf{e}_3 = \mathbf{e}_1 \times \mathbf{e}_2$. The deformation gradient $\mathbf{F}$, that maps the element $d\mathbf{x}$ in the reference plane onto $d\mathbf{y}(\mathbf{x}) = \mathbf{F}d\mathbf{x}$ tangent to the deformed surface can be expressed by

$$\mathbf{F}(\mathbf{x}) = \text{grad}\mathbf{y}(\mathbf{x}) = F_{i\alpha}(\mathbf{x})\mathbf{e}_i \otimes \mathbf{e}_\alpha; \qquad F_{i\alpha} = y_{i,\alpha}, \tag{2.12}$$

where $(\cdot)_{,\alpha} = \partial(\cdot)/\partial x_\alpha$ and summation takes place over the repeated indices. Then as in conventional continuum mechanics, the associated Cauchy–Green strain tensor is

$$\mathbf{C} = \mathbf{F}^T\mathbf{F} = C_{\alpha\beta}\mathbf{e}_\alpha \otimes \mathbf{e}_\beta; \qquad C_{\alpha\beta} = F_{i\alpha}F_{i\beta}. \tag{2.13}$$

It can be easily seen that for every vector $\mathbf{v} \in \mathrm{R}^3$, $\mathbf{v} \cdot \mathbf{C}\mathbf{v} = |\mathbf{F}\mathbf{v}|^2 \geq 0$. So $\mathbf{C}$ is a positive semi–definite tensor and therefore, it can be represented in the following spectral form

$$\mathbf{C} = \lambda_1^2 \mathbf{u}_1 \otimes \mathbf{u}_1 + \lambda_2^2 \mathbf{u}_2 \otimes \mathbf{u}_2, \tag{2.14}$$

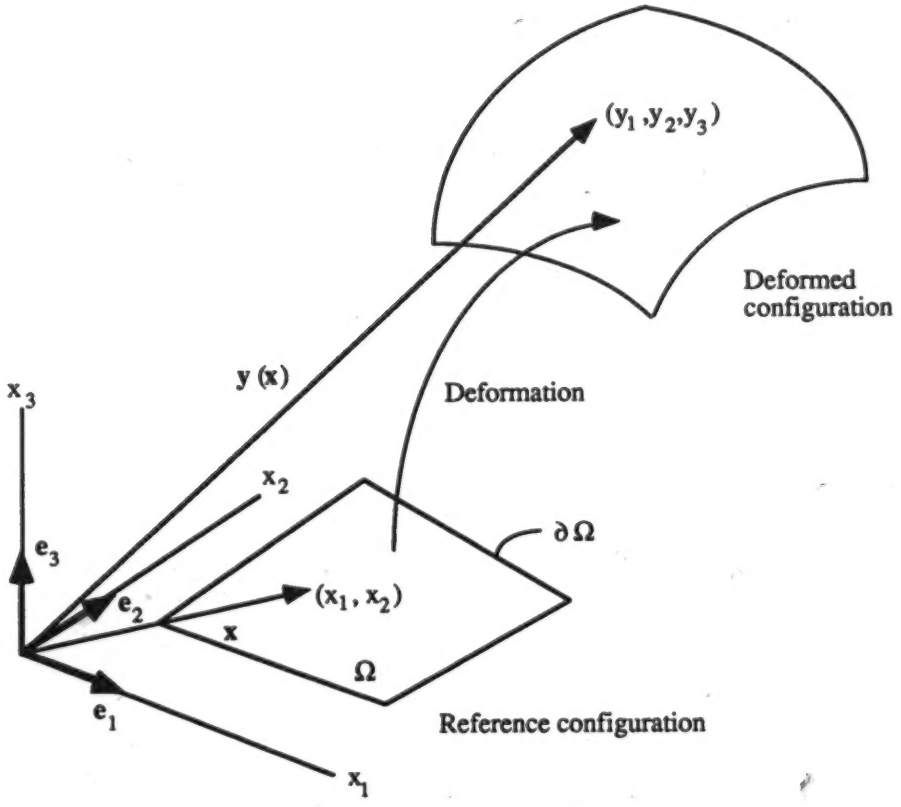

Figure 2-3: A membrane in x_1-x_2 plane undergoing general 3D deformation

where $\mathbf{u}_1$, $\mathbf{u}_2$ are the orthonormal principal vectors of strain and $\lambda_\alpha = |\mathbf{F}\mathbf{u}_\alpha| = (\mathbf{u}_\alpha \cdot \mathbf{C}\mathbf{u}_\alpha)^{1/2}$ (≥ 0). These can be used to define the unit vectors

$$\mathbf{U}_\alpha = \lambda_\alpha^{-1}\mathbf{F}\mathbf{u}_\alpha. \tag{2.15}$$

Since $\mathbf{u}_1$ and $\mathbf{u}_2$ are orthonormal vectors, the unit tensor $\boldsymbol{\Delta}$ in 2D space can be written as $\boldsymbol{\Delta} = \mathbf{u}_\alpha \otimes \mathbf{u}_\alpha$. Then

$$\mathbf{F} = \mathbf{F}\boldsymbol{\Delta} = \mathbf{F}\mathbf{u}_1 \otimes \mathbf{u}_1 + \mathbf{F}\mathbf{u}_2 \otimes \mathbf{u}_2 = \lambda_1\mathbf{U}_1 \otimes \mathbf{u}_1 + \lambda_2\mathbf{U}_2 \otimes \mathbf{u}_2 \tag{2.16}$$

and the Cauchy–Green strain tensor is

$$\begin{aligned} \mathbf{C} &= \mathbf{F}^T\mathbf{F} = \lambda_1^2\mathbf{u}_1 \otimes \mathbf{u}_1 + \lambda_2^2\mathbf{u}_2 \otimes \mathbf{u}_2 \\ &\quad +\lambda_1\lambda_2\mathbf{U}_1 \cdot \mathbf{U}_2(\mathbf{u}_1 \otimes \mathbf{u}_2 + \mathbf{u}_2 \otimes \mathbf{u}_1). \end{aligned} \tag{2.17}$$

Comparing (2.17) with (2.14) and noticing that $\mathbf{u}_1 \cdot \mathbf{u}_2 = 0$, we see that $\mathbf{U}_1 \cdot \mathbf{U}_2 = 0$. In other words, $\mathbf{U}_1$ and $\mathbf{U}_2$ are orthonormal vectors that span the plane tangent to the deformed surface and λ_1 and λ_2 are the stretches along those directions.

Again as in the case of elastic curve, we assume the existence of a strain energy W, per unit area of Ω, that responds only to changes in the local intrinsic or metric geometry of the surface. This formalizes the intuitive notion of a perfectly flexible surface (membrane). Thus, we assume that

$$W(\mathbf{F}) = \hat{W}(\mathbf{F}^T\mathbf{F}) = \hat{W}(\mathbf{C}). \tag{2.18}$$

It can be seen that W is invariant under superimposed rigid motion. Non-uniform elastic properties may be taken into account letting $\hat{W}$ depend explicitly on $\mathbf{x}$.

The surface analog of the 2nd Piola–Kirchhoff stress is (Haseganu and Steigmann, 1994a):

$$\mathbf{S} = S_{\alpha\beta}\mathbf{e}_\alpha \otimes \mathbf{e}_\beta; \qquad S_{\alpha\beta} = S_{\beta\alpha} = \partial\hat{W}/\partial C_{\alpha\beta} + \partial\hat{W}/\partial C_{\beta\alpha}, \tag{2.19}$$

and the Piola stress is

$$\mathbf{T} = \mathbf{FS} = T_{i\alpha}\mathbf{e}_i \otimes \mathbf{e}_\alpha; \qquad T_{i\alpha} = F_{i\beta}S_{\beta\alpha} = \partial W/\partial F_{i\alpha}. \tag{2.20}$$

This furnishes the force per unit reference length, $\boldsymbol{\tau}$, exerted by the material to the right of an embedded curve on the material to the left, according to the formula

$$\boldsymbol{\tau} = \mathbf{T}\boldsymbol{\nu} \tag{2.21}$$

where $\boldsymbol{\nu} = \mathbf{x}'(s) \times \mathbf{e}_3$ is the *rightward* unit normal to the curve and $\mathbf{x}(s)$ is the arclength parametrization of the curve on Ω. If the surface is in equilibrium under applied or reactive edge forces, and the distributed forces (e.g. weight, pressure) are negligible, then the Piola stress must satisfy

$$\mathrm{div}\mathbf{T} = \mathbf{0}; \qquad T_{i\alpha,\alpha} = 0 \qquad \text{in } \Omega. \tag{2.22}$$

For isotropic materials, the strain energy is expressible as a symmetric function of the principal stretches (Naghdi and Tang, 1977; Haseganu and Steigmann, 1994a):

$$W(\mathbf{F}) = \hat{W}(\mathbf{C}) = w(\lambda_1, \lambda_2) = w(\lambda_2, \lambda_1) \tag{2.23}$$

The 2nd Piola–Kirchhoff stress is then given by

$$\mathbf{S} = \lambda_1^{-1} w_1 \mathbf{u}_1 \otimes \mathbf{u}_1 + \lambda_2^{-1} w_2 \mathbf{u}_2 \otimes \mathbf{u}_2 \tag{2.24}$$

where

$$w_\alpha = \partial w / \partial \lambda_\alpha. \tag{2.25}$$

Then the Piola stress can be calculated from (2.20) to be

$$\mathbf{T} = w_1 \mathbf{U}_1 \otimes \mathbf{u}_1 + w_2 \mathbf{U}_2 \otimes \mathbf{u}_2. \tag{2.26}$$

It should be noted that for orthotropic materials, $\mathbf{u}_\alpha$ and $\mathbf{U}_\alpha$ are the unit vectors along the orthogonal fibers before and after the deformation respectively and λ_α are the stretches along them.

Chapter 3

Variational Theory

In this work we formulate conservative boundary value problems as minimization problems for appropriately defined potential energies. The so–called *relaxation* of the associated variational theory furnishes a rationale for the description and analysis of wrinkling in elastic surfaces and curves (Pipkin, 1986; Atai and Steigmann, 1997). Moreover, minimum energy states are relevant to the study of stable equilibria [e.g. Knops and Wilkes (1973); Como and Grimaldi (1995)].

The question of the existence of minimizers is not addressed here and such matters have been studied extensively elsewhere (Ball, 1977; Dacarogna, 1989). Rather, we suppose that a given configuration minimizes a potential energy functional to be defined, and investigate restrictions on the configuration imposed by certain well known necessary conditions in the calculus of variations. Chief among these are the Euler equations and certain inequalities generated by the *quasiconvexity* condition (Dacarogna, 1989). We then introduce a *relaxed* version of the theory which is quasiconvex in all configurations. The physical interpretation of the relaxed theory in terms of slackening is indicated briefly. Such interpretations have been thoroughly discussed in (Pipkin, 1986; Haseganu and Steigmann, 1994a; Atai and Steigmann, 1997). In some cases the relaxed theory admits a dual variational formulation leading to a minimum complementary energy principle and a uniqueness theorem

for the equilibrium stress distribution.

These issues are addressed here in the context of the potential energy functional

$$E[\mathbf{y}] = \int_{\Omega} W(\mathbf{F})da + U[\mathbf{y}] \tag{3.1}$$

in which the integral represents the strain energy of the deformed elastic surface and the functional U represents the energetic contribution of one or more elastic curves (cables) interacting with the surface, and $\mathbf{y}$ is an arbitrary but kinematically admissible configuration. This framework encompasses a wide variety of applications involving coupled one– and two–dimensional elastic elements [e.g. Steigmann and Li, 1995; Steigmann and Ogden, 1997]. The often striking features of such interactions have recently been illustrated by Libai and Simmonds (1998).

In the applications considered here, the elastic cable is attached to a subset $P \subset \partial\Omega$ of the boundary of the membrane consisting of one or more arcs. We consider two types of attachment: (1) the cable is fixed to the membrane at each of its points and deforms with it as an embedded (material) curve (Figure 3.1); and (2) the endpoints of P are fixed and the configurations of the cable and the boundary of the membrane are congruent, but the interior points of the cable do not maintain fixed correspondences with points of the membrane (Figure 3.2). Thus, the cable and membrane may slide relative to each other without separating. In the context of tension structure design, the first alternative may be used to describe the stiffening effect of a seam–line along which the membrane is folded to provide a finished edge or to prevent fraying. The second alternative furnishes an idealized model of cables that slide freely through hoops stationed at intervals along the membrane boundary. In this application the stress in the membrane is controlled, at least to some degree, by the tensile force in the cable.

The functionals $U[\mathbf{y}]$ associated with the two types of attachments are

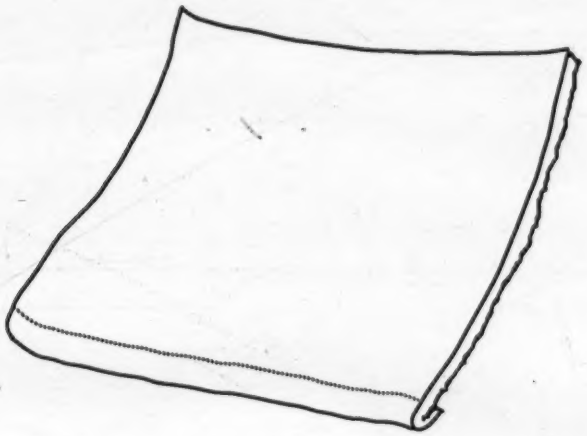

(a)

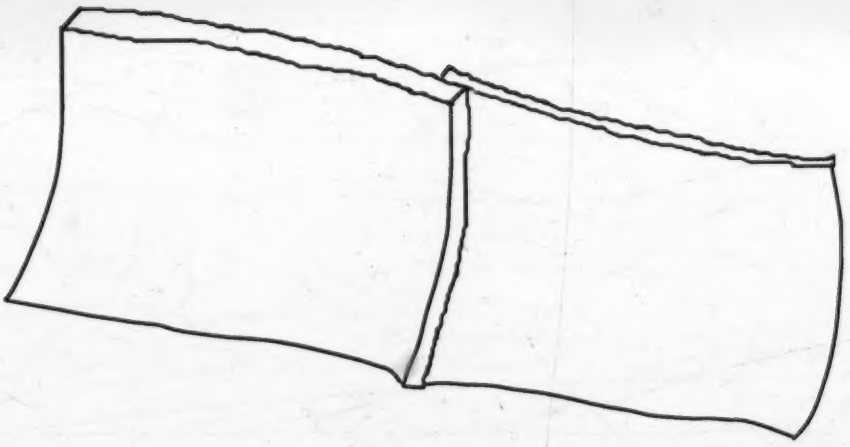

(b)

Figure 3.1: Examples of attached cable reinforcement; (a) folded edge of the membrane, (b) overlap of two pieces at the place of suture

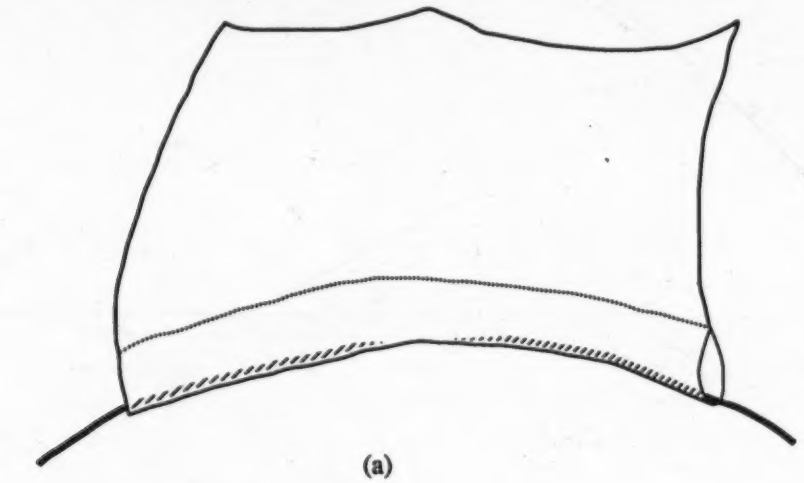

(a)

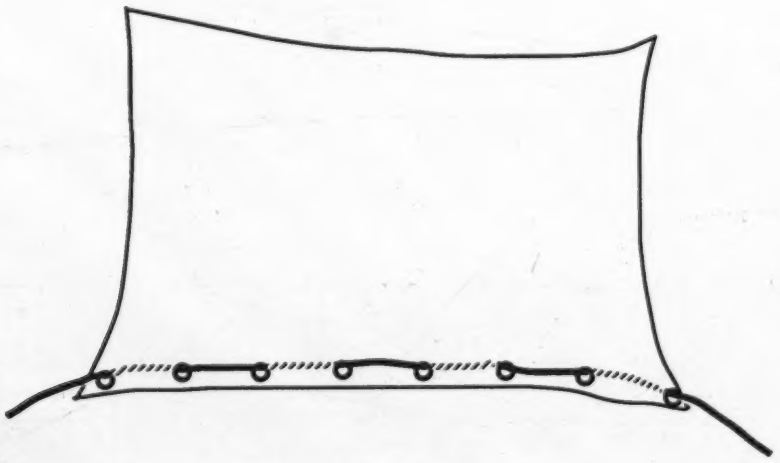

(b)

Figure 3.2: Examples of shearless cable reinforcement; (a) Cable passing through the hem, (b) cable passing through the hoops

$$U_1[\mathbf{y}] = \int_P B(\mathbf{y}'(s))ds \tag{3.2}$$

in the first instance, where $B(\cdot)$ is the cable strain energy function defined in Chapter 2, and

$$U_2[\mathbf{y}] = G(l[\mathbf{y}]) \equiv \int_L^{l[\mathbf{y}]} f(x/L)dx \tag{3.3}$$

in the second instance, where

$$l[\mathbf{y}] = \int_P g(\mathbf{y}'(s))ds; \qquad g(\mathbf{y}) \equiv |\mathbf{y}'| \tag{3.4}$$

is the total arclength of the image of P in a configuration $\mathbf{y}(P)$, $f(\cdot)$ is the force–extension relation of the elastic cable, and L is the arclength of P in the reference configuration. This can be thought of as the energy stored in (or work done by) a uniform spring when its total length x varies from free length L to a deformed length $l[\mathbf{y}]$ and the force in the spring (which is a function of the change in length) is given by $f(x/L)$. Another way of defining U_2 is to integrate the strain energy function for the cable $\hat{B}(\lambda(s))$ [Cf. (2.3)] but since the cable is uniformly strained, $\lambda = l[\mathbf{y}]/L$ is constant along the length of the cable and so is $\hat{B}(\lambda)$. So it can be taken out of the integral and we can write

$$\begin{aligned} U_2[\mathbf{y}] &= \hat{B}(\lambda)L = \hat{B}(l[\mathbf{y}]/L)L = L\int_1^{l[\mathbf{y}]/L} \hat{B}'(\lambda)d\lambda = L\int_1^{l[\mathbf{y}]/L} f(\lambda)d\lambda \\ &= L\int_1^{l[\mathbf{y}]/L} f(x/L)d(x/L) \\ &= L\int_L^{l[\mathbf{y}]} f(x/L)dx/L = \int_L^{l[\mathbf{y}]} f(x/L)dx \end{aligned} \tag{3.5}$$

which is the original definition of U_2. It should be noted that for the strain energies considered, $P \subset \partial\Omega$ is taken to consist of a single connected arc but more arcs can be considered by simply adding the strain energy for each arc together.

The functional U_2 represents the strain energy stored in a *homogeneously* strained cable. This form is used because the freely sliding cable is not subject to any tangential force distribution along its length. It then follows from eqns (2.8) and (2.9) that an elastically uniform cable is homogeneously strained in equilibrium configurations. The functional (3.3) is well defined for configurations that are not in equilibrium, but it is then to be interpreted as a potential rather than the total cable strain energy. In this respect U_2 is similar to the potentials associated with pressure acting at the boundary of a three–dimensional body (Fisher, 1988; Podio-Guidugli, 1988), or over the domain of a two–dimensional body (Steigmann, 1991; Bufler and Schneider, 1994). The *distribution* of pressure used in the definition of the potential is typically chosen to an *equilibrium* distribution for the fluid medium that transmits the pressure to the body in question. The same potential is then used to define a total potential energy functional for *all* kinematically admissible configurations, not just for those that are statically admissible as well. Apparently this subtle point has not been emphasized in the literature on configuration–dependent conservative loading. Functionals of this kind nevertheless furnish potentials for the problems considered.

3.1 Equilibrium

The equilibrium equations for the coupled response of the elastic membrane and cable are obtained as a condition of minimization of the energy $E[\mathbf{y}]$. Let $\mathbf{y}(\mathbf{x};\epsilon)$ be a one–parameter family of deformations with $\epsilon \in (-\epsilon_0, \epsilon_0)$ for some $\epsilon_0 > 0$. Then (3.1) can be written as

$$E[\epsilon] = \int_\Omega W(\text{grady}(\epsilon))da + U[\mathbf{y}(\epsilon)]. \tag{3.6}$$

If the equlibrium configuration corresponds to $\epsilon = 0$, then the potential energy functional $E[\epsilon]$ is minimized at this point and we can write

$$\left.\frac{dE[\epsilon]}{d\epsilon}\right|_{\epsilon=0} = \left[\int_\Omega \frac{dW(\text{grady}(\epsilon)}{d\epsilon}da + \frac{dU}{d\epsilon}\right]_{\epsilon=0} \tag{3.7}$$

but

$$\frac{dW}{d\epsilon} = \frac{\partial W}{\partial F_{i\alpha}}\frac{\partial F_{i\alpha}}{d\epsilon} = T_{i\alpha}\frac{dy_{i,\alpha}}{d\epsilon} = T_{i\alpha}\left(\frac{dy_i}{d\epsilon}\right)_{,\alpha}. \tag{3.8}$$

Substituting this into (3.7), the stationarity of E results in

$$\int_\Omega \mathbf{T}\cdot\text{gradu}\quad da + \dot{U} = 0. \tag{3.9}$$

where the superposed dot indicates the value of the derivative at $\epsilon = 0$, $\mathbf{T}(\mathbf{x})$ is the equilibrium Piola stress distribution, $\mathbf{u}(\mathbf{x}) = \dot{\mathbf{y}}$ is the *variation* of $\mathbf{y}$, gradu is its gradient, and the notation $\mathbf{A}\cdot\mathbf{B}$ is used to denote the scalar product, $A_{i\alpha}B_{i\alpha}$, of tensors $\mathbf{A}$, $\mathbf{B}$.

For the type–1 cable attachment ($U = U_1$) we can write from (3.2)

$$\dot{U} = \dot{U}_1 = \left[\frac{d}{d\epsilon}\int_P B(\mathbf{y}')ds\right]_{\epsilon=0} = \left[\int_P \frac{\partial B}{\partial y_i'}\frac{\partial y_i'}{\partial \epsilon}ds\right]_{\epsilon=0} = \int_P \frac{\partial B}{\partial y_i'}u_i'ds \tag{3.10}$$

but from (2.5), $\partial B/\partial y_i' = f(\lambda)t_i$. So it then follows that

$$\dot{U} = \int_P \mathbf{f}\cdot\mathbf{u}'ds, \tag{3.11}$$

where $\mathbf{f} = f(\lambda)\mathbf{t}$ is the force vector in the cable (cf. eqn (2.8)) and $\mathbf{u}(s) = \mathbf{u}(\mathbf{x}(s))$ is the variation of $\mathbf{y}(\mathbf{x})$ evaluated on P. In obtaining eqn (3.11),

we used the fact that $\mathbf{r}(s) = \mathbf{y}(\mathbf{x}(s))$ on P for the class of cable attachment under consideration. The first term of (3.9) can be written as

$$\int_\Omega T_{i\alpha} u_{i,\alpha} da = \int_\Omega [(T_{i\alpha} u_i)_{,\alpha} - T_{i\alpha,\alpha} u_i] da = \int_{\partial\Omega} T_{i\alpha} \nu_\alpha u_i ds$$
$$- \int_\Omega T_{i\alpha,\alpha} u_i da = \int_{\partial\Omega} \mathbf{T}\boldsymbol{\nu} \cdot \mathbf{u} ds - \int_\Omega \mathbf{u} \cdot \mathrm{div}\mathbf{T} da \tag{3.12}$$

in which the Green's theorem (see the next chapter) is used to get the integral over $\partial\Omega$. From (3.11), the second term of (3.9) can be written as

$$\dot{U} = \int_P f_i u_i' ds = \int_P [(f_i u_i)' - (f_i' u_i)] ds = \sum [\mathbf{f} \cdot \mathbf{u}]_{\partial P} - \int_P \mathbf{f}' \cdot \mathbf{u} ds \tag{3.13}$$

where $f_i = f t_i$ and the notation $[\cdot]_{\partial P}$ is used to denote the difference of the enclosed quantity at the endpoints of an arc of P and the sum extends over the individual arcs that comprise P. Substituting these into (3.9) we can write

$$\int_{\partial\Omega \setminus P} \mathbf{T}\boldsymbol{\nu} \cdot \mathbf{u} ds + \sum [\mathbf{f} \cdot \mathbf{u}]_{\partial P} + \int_P (\mathbf{T}\boldsymbol{\nu} - \mathbf{f}') \cdot \mathbf{u} ds -$$
$$\int_\Omega \mathbf{u} \cdot \mathrm{div}\mathbf{T} da = 0. \tag{3.14}$$

Following the standard procedure of calculus of variations, we can conclude that stationarity of E at $\epsilon = 0$ is realized only if eqn (2.22) is satisfied in Ω, only if

$$\mathbf{f} = \mathbf{0} \text{ on } \partial P_f, \tag{3.15}$$

where ∂P_f is an endpoint of P where position is not prescribed, and only if

$$\mathbf{T}\boldsymbol{\nu} = \mathbf{f}'(s) \text{ on } P \tag{3.16}$$

and $\mathbf{T}\boldsymbol{\nu} = \mathbf{0}$ on $\partial\Omega\backslash P$ (on part of the boundary which is traction free). Eqn (3.16) also follows directly from eqn (2.9) on noting that the force per unit reference length, $\mathbf{b}(s)$, transmitted *to* the cable, is opposite to the traction, $\mathbf{T}\boldsymbol{\nu}$, exerted *by* the cable on the surface (Libai and Simmonds, 1998). Although it might be unusual in conventional elasticity, it is a common practice in tension–structure design to allow the reference configuration Ω to consist of disjoint subdomains. In practice, these sub–domains consist of pieces of fabric cut from a roll. These pieces, or *patterns*, are then fastened together, or *sutured*, prior to the erection of the assembled tension structure. In principle it is desirable to arrange the geometries of these patterns so as to achieve an optimal design criteria such as minimum waste material, small stress or strain in the loaded structure that does not cause the fabric to tear, or as close as possible to a desired deformed configuration (which is usually eye pleasing). The problem with these criteria is that they are not often expressed clearly and precisely. Also the present methods of finding these patterns are much more based on practice rather than being backed by science and theory. For these reasons a definitive treatment of the patterning problem has yet to be achieved, despite the considerable effort that has been devoted to its solution. The work of Tabarrok and Qin (1992) is representative of current practice.

For illustrative purposes let's suppose that Ω consists of just two regions Ω_1 and Ω_2. Let $S_1 \subset \partial\Omega_1$ and $S_2 \subset \partial\Omega_2$ be those parts of the boundaries of Ω_1 and Ω_2 that are to be sutured together (Figure 3.3). Also we suppose that $P \subset (\partial\Omega_1\backslash S_1) \cup (\partial\Omega_2\backslash S_2)$. On any part $\partial\Omega_t$ of $\partial\Omega_1\backslash S_1$ or $\partial\Omega_2\backslash S_2$ where position is not assigned, the associated traction vanishes:

$$\mathbf{T}\boldsymbol{\nu} = \mathbf{0} \text{ on } \partial\Omega_t. \tag{3.17}$$

The remaining content of eqn (3.14) is then expressed by the requirement:

$$\int_{S_1} \mathbf{T}_1\boldsymbol{\nu}_1 \cdot \mathbf{u}_1 ds + \int_{S_1} \mathbf{T}_2\boldsymbol{\nu}_2 \cdot \mathbf{u}_2 ds = 0, \tag{3.18}$$

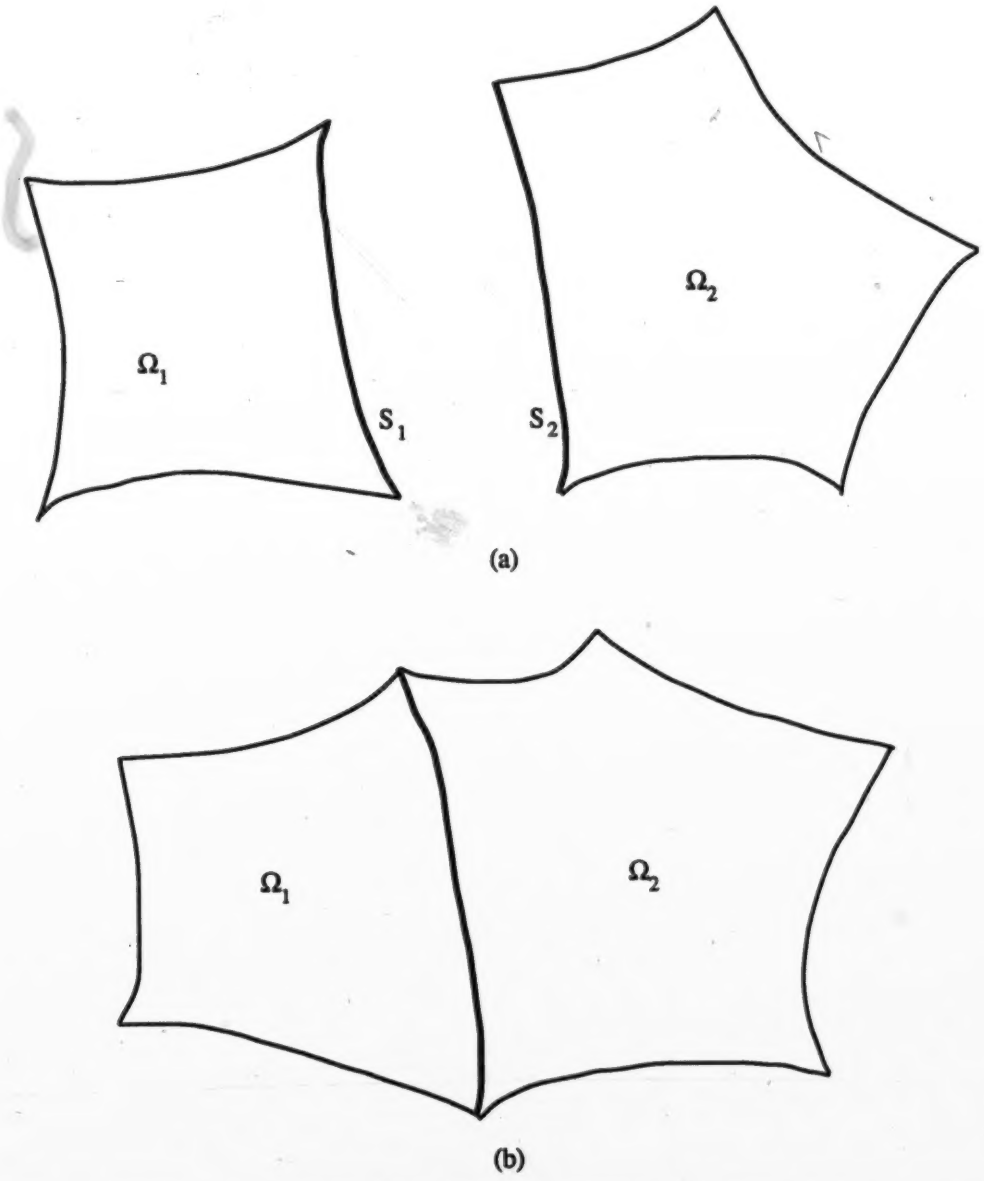

Figure 3.3: Two pieces of membrane sutured together; (a) initial configuration, (b) S_2 is deformed in such a way to coincide with S_1

wherein the subscript 1 or 2 indicates evaluation on S_1 or S_2, respectively.

Now let's assume that S_1 is somehow deformed to coincide S_2. So S_2 can be expressed as $S_2 = d(S_1)$ ($d(\cdot)$ defines the mapping) with local gradient $\alpha(s)$ defined on S_1, i.e. $(ds)_{S_2} = \alpha(s)_{S_1}(ds)_{S_1}$, (this mapping is a matter of choice and before we attempt to solve a problem, we must specify how S_1 and S_2 are connected and in the numerical examples we'll see that this is done by having the same number of nodes on each edge of the suturing line and there is a one two one relation between these nodes). We also assume that the virtual displacement preserves the continuity of sutured structure, so that $\mathbf{u}_2(d(s)) = \mathbf{u}_1(s) \equiv \mathbf{u}(s)$. Then eqn (3.18) reduces to

$$\int_{S_1} (\mathbf{T}_1\boldsymbol{\nu}_1 + \alpha\mathbf{T}_2\boldsymbol{\nu}_2) \cdot \mathbf{u} ds = 0, \tag{3.19}$$

which is true for all kinematically admissible $\mathbf{u}$ and we obtain

$$\mathbf{T}_1\boldsymbol{\nu}_1 = -\alpha\mathbf{T}_2\boldsymbol{\nu}_2 \text{ on } S_1. \tag{3.20}$$

As expected, this implies that for arbitrary arcs $s_1 \subset S_1$ and $s_2 = d(s_1) \subset S_2$, the net force transmitted by Ω_2 to Ω_1 along the suture is opposite to that transmitted by Ω_1 to Ω_2:

$$\int_{s_1} \mathbf{T}_1\boldsymbol{\nu}_1 ds = -\int_{s_2} \mathbf{T}_2\boldsymbol{\nu}_2 ds; \qquad s_1 \subset S_1, s_2 = d(s_1) \subset S_2. \tag{3.21}$$

If $\alpha(s) = 1$, then we have continuity of traction as well as continuity of force across the sutured edge. We see examples of both cases in Chapter 5.

For the case of the type–2 cable attachment, eqn (3.11) is replaced by

$$\dot{U} = \dot{U}_2 = \left[\frac{d}{d\epsilon}\int_L^{l[y(\epsilon)]} f(x/L)dx\right]_{\epsilon=0} \tag{3.22}$$

which can be written as

$$\dot{U} = f(l/L)\dot{l}, \tag{3.23}$$

where

$$\dot{l} = \int_P \dot{g} ds = \int_P \frac{\partial g}{\partial y_i'} u_i' ds = \int_P \frac{y_i'}{|\mathbf{y}'|} u_i' ds = \int_P t_i u_i' ds \tag{3.24}$$

or

$$\dot{l} = \int_P \dot{g} ds = \int_P \mathbf{t} \cdot \mathbf{u}' ds \tag{3.25}$$

where $\mathbf{t}$ is the unit tangent to $\mathbf{y}(P)$. Integrating eqn (3.25) by parts, recalling that ∂P is fixed for the present type of cable attachment and invoking the necessary conditions already derived, we find that eqn (3.14) reduces to

$$\int_P (\mathbf{T}\boldsymbol{\nu} - f\mathbf{t}') \cdot \mathbf{u} ds = 0. \tag{3.26}$$

Thus, eqn (3.16) is replaced by

$$\mathbf{T}\boldsymbol{\nu} = f(l/L)\mathbf{t}'(s) \text{ on } P. \tag{3.27}$$

Since $\mathbf{t} \cdot \mathbf{t}' = 0$ it follows that the cable–membrane interaction is frictionless in the sense that the cable transmits no tangential traction to the membrane.

We remark that if the conditions on ∂P were relaxed to permit $\mathbf{u}$ to be non–zero at one of its points, then the stationarity of E would require that f vanish there, and hence everywhere in the cable. The alternative fixed–end conditions imposed here do not lead to this conclusion. Moreover, they correspond to the conditions that exist in actual tension structures, wherein cable pre-tension is controlled by adjusting the length of cable between the supports.

3.2 Additional necessary conditions

We obtain certain algebraic inequalities that are satisfied by minimizers of the functional (3.1). Among these is the quasiconvexity condition that plays a fundamental role in Ball's existence theorems for nonlinear elasticity (Ball, 1977). Steigmann and Ogden (1997) recently extended Ball's proof of quasiconvexity to account for the presence of surface stress in plane–strain deformations of elastic solids. This extension generates restrictions analogous to quasiconvexity that apply to an elastic boundary, in addition to the condition previously known to apply to the bulk material. Following the perturbation method discussed in Atai and Steigmann (1998), the well known rank–one convexity condition (Ball, 1977) which takes the form

$$W(\mathbf{F}+\mathbf{a}\otimes\mathbf{b})-W(\mathbf{F})\geq\mathbf{T}(\mathbf{F})\cdot\mathbf{a}\otimes\mathbf{b}, \tag{3.28}$$

for all $\mathbf{a}=a_i\mathbf{e}_i$ and $\mathbf{b}=b_\alpha\mathbf{e}_\alpha$ with $\mathbf{F}$ being the deformation gradient corresponding to the equilibrium configuration. This is identical to the condition that Graves suggests for the deformed configuration to be the a strong relative minimizer of the energy $E[\cdot]$ (Graves, 1939). In the limit of small $|\mathbf{a}|$ with $|\mathbf{b}|$ fixed, Taylor expansion of the first term on the left hand side and simplification yields the Legendre–Hadamard inequality:

$$C_{i\alpha j\beta}a_ib_\alpha a_jb_\beta\geq 0, \tag{3.29}$$

where

$$C_{i\alpha j\beta}(\mathbf{F})=\partial^2W/\partial F_{i\alpha}\partial F_{j\beta} \tag{3.30}$$

An interesting consequence of eqn (3.29) is the non–negativity of the 2nd Piola–Kirchhoff stress $\mathbf{S}$ furnished by $\mathbf{F}$ (Steigmann, 1986):

$$\mathbf{b} \cdot \mathbf{S}\mathbf{b} \geq 0, \qquad \forall \mathbf{b} = b_\alpha \mathbf{e}_\alpha. \tag{3.31}$$

For isotropic membranes, this is equivalent to [cf. eqn (2.25)]:

$$w_\alpha \geq 0; \qquad \alpha = 1, 2. \tag{3.32}$$

From $\mathbf{y}(\mathbf{x})$ being the minimizer of the energy E, the inequality for the type–2 cable attachment is found out to be (Atai and Steigmann, 1998)

$$f(l/L)(|\mathbf{y}' + \mathbf{a}| - |\mathbf{y}'| - \mathbf{a} \cdot \mathbf{t}) \geq 0, \qquad \forall \mathbf{a}, \tag{3.33}$$

We decompose $\mathbf{a}$ in the form

$$\mathbf{a} = (\mathbf{a} \cdot \mathbf{t})\mathbf{t} + \mathbf{a}_\perp, \qquad \mathbf{t} \cdot \mathbf{a}_\perp = 0. \tag{3.34}$$

Hence

$$|\mathbf{y}' + \mathbf{a}| = [(|\mathbf{y}'| + \mathbf{a} \cdot \mathbf{t})^2 + |\mathbf{a}_\perp|^2]^{1/2} \geq |\mathbf{y}'| + \mathbf{a} \cdot \mathbf{t}, \tag{3.35}$$

with equality if and only if $\mathbf{a}_\perp = \mathbf{0}$ and $\mathbf{a} \cdot \mathbf{t} \geq -|\mathbf{y}'|$. Thus, eqn (3.33) is equivalent to the requirement that the cable force be tensile (non–compressive) in a minimizing configuration:

$$f(l/L) \geq 0. \tag{3.36}$$

We note that application of the triangle inequality to eqn (3.33) yields no information.

For the type–1 edge reinforcement problem, the equivalent of (3.33) is the Weierstrass condition

$$B(\mathbf{y}' + \mathbf{a}) - B(\mathbf{y}') \geq \mathbf{f} \cdot \mathbf{a}, \qquad \forall \mathbf{a}, \tag{3.37}$$

where $\mathbf{f} = \hat{\mathbf{f}}(\mathbf{y}')$ (cf. eqn (2.3)). This is equivalent to the *two* inequalities (Atai and Steigmann, 1997):

$$f(\lambda) \geq 0, \qquad \hat{B}(\mu) - \hat{B}(\lambda) \geq (\mu - \lambda) f(\lambda), \qquad \forall \mu > 0, \tag{3.38}$$

where $\lambda = |\mathbf{y}'|$ is the local curve stretch in a minimizing configuration. Thus, the cable is under tension and the strain energy $\hat{B}(\cdot)$ is convex at λ. The latter result requires that the tangent modulus be non–negative: $f'(\lambda) \geq 0$.

3.3 Relaxed theory

Strain energy functions typically used in the theories of elastic curves and surfaces do not satisfy the necessary conditions (3.38a) or (3.31), respectively, at all the values of strain. Thus, energy–minimizing configurations generally do not exist for a large class of boundary value problems. Two main approaches to restoring well–posedness have been discussed in the literature. The first, known as *regularization*, is to replace the model by one having additional structure, in which restrictions such as eqns (3.38a) or (3.31) do not arise. In the present context, regularization may be achieved by substituting shell and rod models in place of the simpler membrane and cable theories. The alternative to regularization, known as *relaxation*, is to modify the constitutive equations of the membrane and the cable so that restrictions like eqns (3.31) and (3.38) are automatically satisfied. The task is then to relate the relaxed model to the original model in a way that is physically meaningful.

For example, the relaxed minimization problem for the type–1 cable–membrane model is based on the modified energy functional (Dacarogna, 1989):

$$E_R[\mathbf{y}] = \int_\Omega W_R(\mathbf{F})da + \int_P B_R(\mathbf{y}')ds, \tag{3.39}$$

where $W_R(\mathbf{F})$ is the *quasiconvexification* of $W(\mathbf{F})$:

$$W_R(\mathbf{F}) = \overset{\sup}{\phi}\ \{\phi : \phi(\mathbf{F}) \leq W(\mathbf{F}), \qquad \text{and } \phi \text{ quasiconvex}\}, \tag{3.40}$$

and $B_R(\mathbf{y}')$ is the *convexification* of $B(\mathbf{y}')$:

$$B_R(\mathbf{y}') = \overset{\sup}{\psi}\ \{\psi : \psi(\mathbf{y}') \leq B(\mathbf{y}'), \qquad \text{and } \psi \text{ convex}\}. \tag{3.41}$$

Granted suitable bounds on these functions, it is possible to show that the minimization problem for E_R has a solution in an appropriate function space, and that

$$\min E_R[\mathbf{y}] = \inf E[\mathbf{y}], \tag{3.42}$$

even when $E[\mathbf{y}]$ fails to have a minimizer. In particular, if $\mathbf{y}(\mathbf{x})$ minimizes E_R then it is typically possible to construct a minimizing sequence $\{\mathbf{y}_n\}$ for E, converging (weakly) to $\mathbf{y}(\mathbf{x})$, for which $E[\mathbf{y}_n] \to E_R[\mathbf{y}]$. We refer to Acerbi and Fusco (1984) and Dacarogna (1989) for detailed discussion of these concepts.

If the strain energies $W(\mathbf{F})$ and $B(\mathbf{y}')$ are unequal to their relaxations, then minimizing sequences typically exhibit finer and finer scale discontinuities in the gradients of the $\mathbf{y}_n(\mathbf{x})$ as n increases. In the limit the sequence itself converges to a smooth function, but the limit of the sequence of the gradients is discontinuous everywhere. In the context of membrane and cable theories, this fine scale structure may be interpreted in terms of a continuous distribution of wrinkles of infinitesimal amplitude, spaced an infinitesimal

distance apart (Pipkin, 1986; Atai and Steigmann, 1997). In a real membrane or cable small, but finite, flexural stiffness intervenes to prevent the attainment of an infinitely fine distribution. It is in this sense that the relaxed version of the theory entails a degree of idealization. Despite this limitation, such an approach is far more tractable than regularization, and furnishes a useful model for calculating global features of the response when the original model fails to possess a solution.

We remark that minimizing sequences involving wrinkling have been constructed for membranes and cables separately, but not for the membrane–cable combination considered here. Thus, the attainability of the relaxed energy from the original energy remains an open question in the present context.

3.3.1 Relaxed membrane energy

Kohn and Strang (1986) have observed that W_R is bounded above and below by the *rank-one convexification* and the *convexification* of W, respectively. These are defined as in eqn (3.40), except that ϕ is rank–one or convex as appropriate. The latter functions are defined by algebraic inequalities rather than the integral inequality that defines quasiconvexity. Thus, they are generally easier to compute that W_R.

In membrane theory there are many examples in which the two types of convexification are not easy to compute, but actually coincide. In such cases W_R is obtained directly (Pipkin, 1986). The relaxed strain energy is then convex as a function of $\mathbf{F}$, i.e.

$$W_R(\mathbf{F}+\Delta\mathbf{F}) - W_R(\mathbf{F}) \geq \widehat{\mathbf{T}}\,(\mathbf{F})\cdot\Delta\mathbf{F}, \tag{3.43}$$

where $\widehat{\mathbf{T}}\,(\cdot)$ is the constitutive equation derived from W_R:

$$\widehat{\mathbf{T}}\,(\mathbf{F}) = \widehat{T}_{i\alpha}\,(\mathbf{F})\mathbf{e}_i\otimes\mathbf{e}_\alpha; \qquad \widehat{T}_{i\alpha}\,(\mathbf{F}) = \partial W_R/\partial F_{i\alpha}. \tag{3.44}$$

This property leads to global minimum principles for the potential energy functional and a complementary energy functional to be specified in chapter 4.

Now any rank–one convex function necessarily satisfies the Legendre–Hadamard inequality (3.29), and any convex function satisfies the condition of local convexity obtained by substituting arbitrary $A_{i\alpha}$ in place of $a_i b_\alpha$ in eqn (3.29). Pipkin (1986) has derived inequalities for isotropic elastic membranes that are equivalent to two types of local convexity. In particular, the Legendre–Hadamard inequality is equivalent to inequalities (3.32) and

$$w_{11} \geq 0, \qquad w_{22} \geq 0, \qquad a \geq 0, \tag{3.45}$$

$$(w_{11}w_{22})^{1/2} - w_{12} \geq b - a, \qquad (w_{11}w_{22})^{1/2} + w_{12} \geq -b - a, \tag{3.46}$$

where

$$a = (\lambda_1 w_1 - \lambda_2 w_2)/(\lambda_1^2 - \lambda_2^2), \qquad b = (\lambda_2 w_1 - \lambda_1 w_2)/(\lambda_1^2 - \lambda_2^2) \tag{3.47}$$

with $w_\alpha = \partial w/\partial \lambda_\alpha$ and $w_{\alpha\beta} = \partial^2 w/\partial \lambda_\alpha \partial \lambda_\beta$. For $\lambda_1 = \lambda_2$, the results obtained by applying L'Hôpital's rule to eqns (3.45),(3.46), (3.47) remain valid. Alternatively, the local convexity inequality is equivalent to eqns (3.32) and (3.45), together with

$$w_{11}w_{22} - w_{12}^2 \geq 0, \qquad |a| \geq b \tag{3.48}$$

in place of eqn (3.46) (Pipkin, 1986).

It is frequently the case that inequalities (3.45),(3.46) and (3.48) are satisfied by a given strain energy function $w(\lambda_1, \lambda_2)$. The potential violation of eqn (3.32) is then the only cause of the failure of quasiconvexity. In such

circumstances the relaxed strain energy, expressed as a function of stretches, is the symmetric composite function defined by (Pipkin, 1986):

$$w_R(\lambda_1,\lambda_2) = \begin{array}{lll} w(\lambda_1,\lambda_2); & \lambda_1 \geq v(\lambda_2), & \lambda_2 \geq v(\lambda_1) \\ \hat{w}(\lambda_1); & \lambda_1 > 1, & \lambda_2 \leq v(\lambda_1) \\ \hat{w}(\lambda_2); & \lambda_2 > 1, & \lambda_1 \leq v(\lambda_2) \\ 0; & \lambda_1 \leq 1, \lambda_2 \leq 1 & \end{array} \tag{3.49}$$

provided that $w(1,1) = w_\alpha(1,1) = 0$. Here

$$\hat{w}(x) = w(x, v(x)) = w(v(x), x) \tag{3.50}$$

and $v(x)$ is a solution of

$$w_2(x, v(x)) = w_1(v(x), x) = 0. \tag{3.51}$$

We assume this solution to be unique.

In Pipkin's terminology (Pipkin, 1986), $v(x)$ is called the *natural width in simple tension*. Physically, $v(x)$ is the transverse stretch that nullifies the transverse stress when the longitudinal stretch assumes some value $x > 1$ in uniaxial tension (the relaxed form of the strain energy is actually the model for uniaxial behaviour of the material). Further reduction of the transverse stretch at the same value of X is accomplished by fine scale wrinkling perpendicular to the tensile axis. Wrinkling does not alter the strain energy, which retains the value $\hat{w}(x)$ associated with uniaxial tension. This is the interpretation of the second and third branches of eqn (3.49). The fourth branch corresponds to slack states generated by simultaneous wrinkling along two principal directions. We refer to (Pipkin, 1986) for detailed explanations of these ideas.

The relaxed energy defined by eqn (3.49) is locally convex as a function of $\mathbf{F}$ for all $\lambda_1, \lambda_2 \geq 0$, and thus in all of $\mathbf{F}$–space. Since the latter region is

convex, it follows that the global convexity inequality (3.43) is also satisfied, as discussed previously (We remark that the unilateral constraint on the determinant of the deformation gradient in conventional elasticity has no counterpart here as the determinant of **F** in eqn (2.12) is not defined).

In this work we use several membrane strain energy functions whose relaxations meet the foregoing conditions. Each of these involves a material constant μ with dimensions of force/length (or energy/area). This constant may be interpreted as the bulk shear modulus of the material at infinitesimal strain, multiplied by the uniform initial thickness of the membrane. For example, the relaxation of the neo–Hookian strain energy is defined by eqns (3.49) and (3.50) with (Pipkin, 1986):

$$\begin{aligned} w(\lambda_1,\lambda_2) &= \tfrac{1}{2}\mu(\lambda_1^2+\lambda_2^2+\lambda_1^{-2}\lambda_2^{-2}-3), \\ \hat{w}(x) &= \tfrac{1}{2}\mu(x^2+2x^{-1}-3), \quad v(x)=x^{-1/2}, \end{aligned} \tag{3.52}$$

and the relaxed form of the Varga strain energy (Varga, 1966) is given by (Haseganu and Streigmann, 1994b):

$$\begin{aligned} w(\lambda_1,\lambda_2) &= 2\mu(\lambda_1+\lambda_2+\lambda_1^{-1}\lambda_2^{-1}-3), \\ \hat{w}(x) &= 2\mu(x+2x^{-1/2}-3), \quad v(x)=x^{-1/2}. \end{aligned} \tag{3.53}$$

We also study harmonic materials (Varley and Cumberbatch, 1980). For these the (unrelaxed) strain energy is of the form

$$w(\lambda_1,\lambda_2) = 2\mu[F(I)-J]; \qquad I=\lambda_1+\lambda_2, \qquad J=\lambda_1\lambda_2 \tag{3.54}$$

for some function $F(\cdot)$. In this work, we consider two special cases. The first one is the case of *standard linear solid* (Wu, 1979):

$$F(I) = \frac{\bar{\lambda}+2\mu}{4\mu}I^2 + \frac{\bar{\lambda}+\mu}{\mu}(1-I), \tag{3.55}$$

where $\bar{\lambda}$ and μ are the usual Lamé moduli times the membrane thickness, the overbar being used so as not to confuse the modulus with the cable stretch. The second case investigated by Varley and Comberbatch (1980) and Ru (1998) shows interesting results (as we see in Chapter 5) and it's given by

$$F(I) = \frac{1}{4\alpha}(I + \sqrt{I^2 - 16\alpha\beta}), \tag{3.56}$$

where α and β are material constants. On the first branch of eqn (3.49) where $w_a > 0$, it follows by adding the expression for w_a obtained from eqn (3.54) that $F(I) > I/2$. According to eqn (3.55) this corresponds to the region defined by $I > 2$ in the (λ_1, λ_2)–plane. Elsewhere the remaining branches of eqn (3.49) are used, with

$$\hat{w}(x) = 2\mu[F(x + v(x)) - xv(x)], \qquad v(x) = \frac{2(\bar{\lambda} + \mu)}{\bar{\lambda} + 2\mu} - \frac{\bar{\lambda}}{\bar{\lambda} + 2\mu}x. \tag{3.57}$$

We note that values of x for which $v(x) < 0$ lie outside the range in which eqn (3.55) furnishes reasonable agreement with data on real materials. If we exclude such values then it is straightforward to show that the relaxed energy defined by eqns (3.49) and eqns (3.57), satisfies eqn (3.32) and the convexity conditions (3.45) and (3.48) provide that

$$\mu > 0, \qquad \bar{\lambda} + \mu > 0. \tag{3.58}$$

Another material that is worth mentioning is based on Ogden's three–term strain energy function, which models rubber over a wide range of strains (Ogden, 1984) as compared to neo–Hookian material which is a model for rubber for a lower range of strains (we model the behaviour of a kind of rubber for a strain range of 0 to 0.60 with the neo–Hookian model in Chapter 6). Ogden material is behaving in such a way under large strains that existence of solutions with finite energy even in the presence of strong singularities can

be expected (see example 5.3). Li and Steigmann (1995) discuss examples of this kind for which alternative strain energies yield non–existence. The unrelaxed Ogden strain energy function is given by

$$w(\lambda_1, \lambda_2) = \mu \sum_{r=1}^{3} \beta_r [\lambda_1^{\alpha_r} + \lambda_2^{\alpha_r} + (\lambda_1 \lambda_2)^{-\alpha_r} - 3]/\alpha_r, \tag{3.59}$$

where

$$\begin{aligned} &\alpha_1 = 1.3,\ \alpha_2 = 5.0,\ \alpha_3 = -2.0; \\ &\beta_1 = 1.491,\ \beta_2 = 0.003,\ \beta_3 = -0.0237. \end{aligned} \tag{3.60}$$

Following the procedure described in Section 3.3, the relaxed form of this strain energy will be (Li and Steigmann, 1995):

$$\hat{w}(x) = \mu \sum_{r=1}^{3} \beta_r (x^{\alpha_r} + 2x^{-\alpha_r/2} - 3)/\alpha_r, \quad v(x) = x^{-1/2}. \tag{3.61}$$

It should be noted that the solution for $v(x)$ is not unique in this case but it furnishes the optimal version of eqn (3.49) for the problems considered (Atai and Steigmann, 1998).

Strain energies that were considered so far, are for isotropic materials. But in a practical structure, the fabric is actually made of families of fibers that carry the most part of the loading plus a cover–up material that is used for protection and has some shear resistance. If we neglect the resistance of the material to shear, a very simple model of such a material would be two identical families of fibers which are perpendicular to each other. The fibers behave linearly to strain and this model can also be thought of a cable net made up of orthogonal grids with linear elastic cables. The strain energy for such a material would be

$$w(\lambda_1, \lambda_2) = \frac{1}{2}\mu[(\lambda_1 - 1)^2 + (\lambda_2 - 1)^2]. \tag{3.62}$$

It can be easily seen that

$$v(x) = 1, \quad \hat{w}(x) = \frac{1}{2}\mu(x-1)^2. \tag{3.63}$$

Stability inequality (3.32) also holds for this kind of material but now stretches are along the fibers (this is equivalent to having the force in the cable to be non-negative if the material is thought of as a cable net). We can easily see that the material shows a symmetric behaviour that repeats itself every 90 degrees (see example 5.3). We could have selected two different families of linear elastic behaviour in which case two different constants would appear in front of parentheses in (3.62) and the material showed a symmetry with a repetition of 180 degrees. Although this is a very basic model for actual fabrics used in structures, but it shows a more realistic behaviour of structure as compared to the isotropic ones.

3.3.2 Relaxed cable energy

The construction of the relaxed cable strain energy function is far simpler. We assume that $\hat{B}(\lambda) = B(\mathbf{y}')$ is a convex function of the stretch with an isolated minimum at $\lambda = 1$. Then eqn (3.38b) is satisfied for all positive λ and $f = \hat{B}'(\lambda)$ violates eqn (3.38a) if and only if $\lambda < 1$. The relaxed energy $B_R(\mathbf{y}')$ is the function of $\lambda = |\mathbf{y}'|$ defined by (Atai and Steigmann, 1997):

$$\hat{B}_R(\lambda) = \begin{array}{ll} \hat{B}(\lambda), & \lambda \geq 1 \\ 0, & 0 \leq \lambda < 1 \end{array} \tag{3.64}$$

Here, too, the second branch may be interpreted in terms of a continuous distribution of wrinkles. The associated constitutive relation is

$$\mathbf{f} = \hat{\mathbf{f}}_R(\mathbf{y}') = f_R(|\mathbf{y}'|)\mathbf{y}'/|\mathbf{y}'|, \tag{3.65}$$

where

$$f_R(\lambda) = \begin{array}{ll} f(\lambda), & \lambda \geq 1 \\ 0, & 0 \leq \lambda < 1. \end{array} \tag{3.66}$$

The function $B_R(\mathbf{y}')$ thus defined is convex, since it satisfies eqn (3.38a,b), and hence eqn (3.37), for all values of its argument.

In this work we use a simple strain energy that conforms to the foregoing requirements:

$$\hat{B}(\lambda) = \frac{1}{2}E(\lambda - 1)^2; \qquad f(\lambda) = E(\lambda - 1), \tag{3.67}$$

where E is a positive constant with dimensions of force.

For the type–2 cable–membrane problem, inequalities (3.38a,b) are replaced by the single inequality (3.36). Strictly speaking, this need only apply at stretches associated with minimizing configurations. Thus the *function* $G(\cdot)$ in eqn (3.3) need not be convex. More precisely, our methods do not yield convexity as a necessary condition in this case. However, it is natural to impose the requirement that $f(l/L)$ be a non–decreasing function, in accordance with eqn (3.38b). Thus we assume that $G(\cdot)$ is convex on $(0, \infty)$ with an isolated minimum at $l = L$, and define its relaxation by

$$G_R(l) = \begin{array}{ll} G(l), & l \geq L \\ 0, & 0 \leq l < L, \end{array} \tag{3.68}$$

where L is the unstretched length of the cable. The associated force–extension relation is $f_R(l/L) = G'_R(l)$. This is equivalent to eqn (3.66) with $f(\lambda)$ replaced by $G'(l)$, and the relaxed potential energy is now given by

$$E_R[\mathbf{y}] = \int_\Omega W_R(\mathbf{F})da + G_R(l[\mathbf{y}]). \tag{3.69}$$

The remainder of this work is based on the relaxed energies (3.39) and (3.69). Thus, we drop the subscript R in the subsequent development.

Chapter 4

Discretization and numerical solution

Since it is not feasible for us to satisfy equilibrium equation (2.22) at every point of Ω, we discretize the domain as described below and use a numerical technique to solve equilibrium equations, which are the finite difference approximates of the continuous ones, at some specific points.

4.1 Discretization

We discretize the region Ω into quadrilateral regions called *zones* that are surrounded by 4 nodes (Figure 4.1). Nodes are identified by a pair of integer superscripts like (i, j) while zone centers, shown by circles, are identified by a pair of half integer ones, such as $(i+1/2, j+1/2)$; x_α^{ij} are the coordinates of the node (i, j) in the reference configuration and y_k^{ij} are its coordinates in the deformed configuration. We consider quantities such as displacements and internal and external forces at the nodes while quantities like deformation gradient, strain, stretches, and stress are averaged at the zone centers. One useful theorem that helps us calculate the deformation gradient and internal nodal forces by relating the derivatives of a quantity to its value is the Green's theorem. It states that

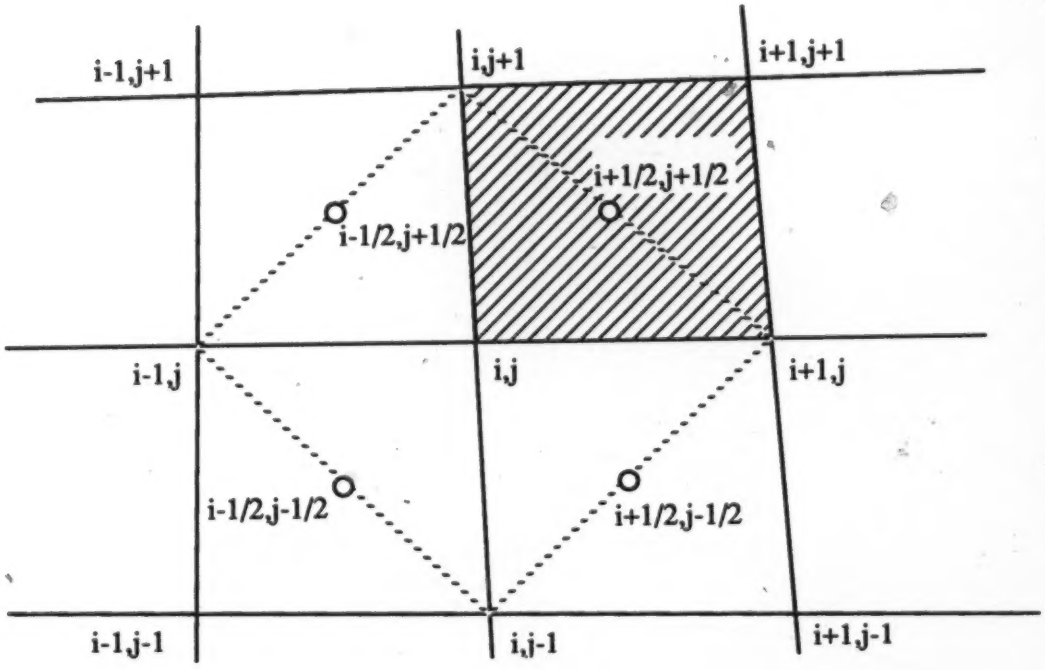

Figure 4.1: Discretized regions for finite-difference approximation of equations of equilibrium.

$$\int\int_{\Omega} \phi_{,\alpha} da = e_{\alpha\beta} \oint_{\partial\Omega} \phi dx_\beta \tag{4.1}$$

where $\phi(\mathbf{x})$ is any piecewise differentiable field in the plane, $e_{\alpha\beta}$ is the unit alternator ($e_{12} = -e_{21} = 1, \quad e_{11} = e_{22} = 0$), and $\partial\Omega$ is the piecewise smooth boundary of Ω. Haseganu and Steigmann (1994a) have fully discussed the application of Green's theorem to a membrane. Upon replacing ϕ with y_k in (4.1), the integrand on the left hand side becomes the $k\alpha$ component of the deformation gradient. If we consider the quadrilateral with the zone center $(i+1/2, j+1/2)$ for example, and replace $y_{k,\alpha}$ with $F_{k\alpha}^{i+1/2,j+1/2}$ (which is considered to be constant over the corresponding quadrilateral region), replacing y_k on the right hand side with the average value at the edges of the quadrilateral results in the average deformation gradient components for the shaded region in Figure 4.1 (Silling, 1988b)

$$\begin{aligned} F_{k\alpha}^{i+1/2,j+1/2} &= (2A^{i+1/2,j+1/2})^{-1} e_{\alpha\beta}[(x_\beta^{i,j+1} - x_\beta^{i+1,j})(y_k^{i+1,j+1} - y_k^{i,j}) - \\ &\quad (x_\beta^{i+1,j+1} - x_\beta^{i,j})(y_k^{i,j+1} - y_k^{i+1,j})], \end{aligned} \tag{4.2}$$

where

$$\begin{aligned} A^{i+1/2,j+1/2} &= \frac{1}{2}[(x_2^{i,j+1} - x_2^{i+1,j})(x_1^{i+1,j+1} - x_1^{i,j}) - \\ &\quad (x_1^{i,j+1} - x_1^{i+1,j})(x_2^{i+1,j+1} - x_2^{i,j})] \end{aligned} \tag{4.3}$$

is the area of the shaded region. We can then use (2.13) to calculate the Cauchy-Green strain tensor and the Piola stress can be calculated from (2.20) at the zone center. We do this for each zone center on the dashed contour and using Green's theorem replacing ϕ by $T_{k\alpha}$, the discretized equation of equilibrium for the node at the center of the dashed contour can be written as

$$
\begin{aligned}
P_k^{ij} &= 2A^{ij}(T_{k\alpha,\alpha}) \\
&= e_{\alpha\beta}[T_{k\alpha}^{i+1/2,j+1/2}(x_\beta^{ij+1} - x_\beta^{i+1,j}) + T_{k\alpha}^{i-1/2,j+1/2}(x_\beta^{i-1,j} - x_\beta^{ij+1}) \\
&\quad + T_{k\alpha}^{i-1/2,j-1/2}(x_\beta^{ij-1} - x_\beta^{i-1,j}) \\
&\quad + T_{k\alpha}^{i+1/2,j-1/2}(x_\beta^{i+1,j} - x_\beta^{ij-1})] = 0
\end{aligned} \tag{4.4}
$$

where A^{ij} is half of the area of the dashed contour

$$
\begin{aligned}
A^{ij} = \frac{1}{4}[& (x_2^{i-1,j} - x_2^{i+1,j})(x_1^{ij+1} - x_1^{ij-1}) - \\
& (x_1^{i-1,j} - x_1^{i+1,j})(x_2^{ij+1} - x_2^{ij-1})].
\end{aligned} \tag{4.5}
$$

Once again, the average value of the Piola stress on the sides of the contour is used on the right hand side of (4.1). Equation (4.4) gives the kth component of the sum of the internal forces at the node (i, j). The truncation errors related to (4.4) and (4.2) are discussed in Silling (1988b) and Herrmann and Bertholf (1983). They state that the error is of the order of mesh size times the mesh distortion parameters. The distortion parameters are minimized if the shape of the zone is as close to a rectangle as possible. This is the reason why we try to use the orthogonal curvilinear coordinate system discussed in Appendix A to generate the meshes for the examples in the next chapter.

In order to simulate traction–free boundaries, we still consider a dashed contour surrounding each node on the boundary at a time by assuming *ghost* quadrilateral regions exterior to the domain and we then set the Piola stress corresponding to the zone centers of these ghost zones to zero in (4.4) and collapse the zone–centers exterior to the boundary on to it (thus reducing the area of the ghost zone to zero). A similar procedure may be used to simulate suturing. Let's consider two edges s_1 and s_2 of two pieces of membrane that are to be sutured together (Fig. 4.2). We know that if we consider each piece separately after the suturing is done, there is going to be a traction

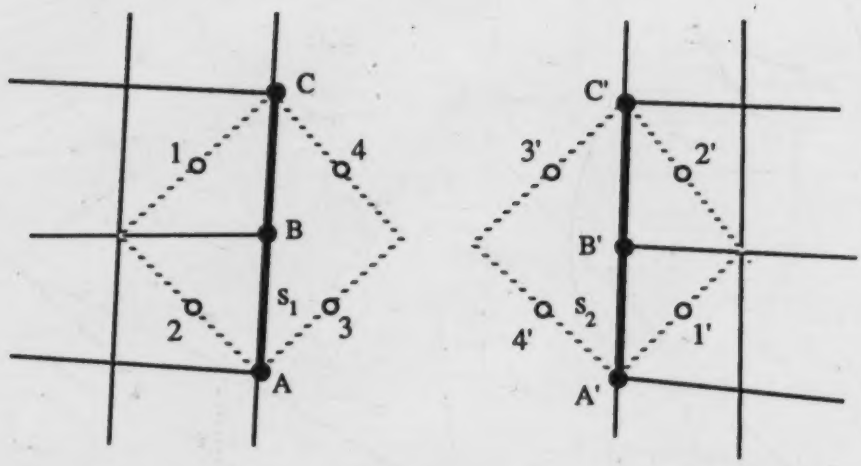

Figure 4.2: Green integration path for two pieces that are to be sutured.

distribution on the edge on one piece exerted by the other piece. Integration of the traction distribution along each edge gives us the force exerted from one piece to the other piece [Cf. (3.21)]. We approximate this force by approximating the traction integration with the integration of traction on those edges of the dashed contour that are exterior to the domain

$$\int_{s_1} \mathbf{T}\nu ds \approx \int_3 \mathbf{T}\nu ds + \int_4 \mathbf{T}\nu ds, \quad \int_{s_2} \mathbf{T}\nu ds \approx \int_{3'} \mathbf{T}\nu ds + \int_{4'} \mathbf{T}\nu ds \quad (4.6)$$

where subscripts 3(3′) and 4(4′) refer to the two dashed segments exterior to the left– (right–)hand part of the membrane shown in the figure. Equation (3.21) is approximated by requiring that the sum of the above two integrals be zero. Considering this in mind and writing the equation of equilibrium (4.4) point B and its matching point B' and adding them together, We arrive at

$$\int_{\Omega_L} div\mathbf{T}da + \int_{\Omega_R} div\mathbf{T}da \approx \sum_{i=1}^{2} \int_i \mathbf{T}\nu ds + \sum_{i'=1}^{2} \int_{i'} \mathbf{T}\nu ds, \quad (4.7)$$

where Ω_L and Ω_R are the regions enclosed by the left and right contours, respectively. We then collapse the zone–centers exterior to the regions on to the boundaries reducing Ω_L and Ω_R to the regions enclosed by the interior dashed lines and the boundaries. This is the same as considering the regions enclosed by the boundaries and the dashed interior segments that remain, as the dashed contour for both points B and B'. The area–weighted average of $div\mathbf{T}$ formed by the two contours is equal to the left hand side of eqn (4.7) divided by $A_L + A_R$, the total area of the region $\Omega_L \cup \Omega_R$. This average value is assigned to each member of the pair of opposing nodes along the two edges to be sutured. The resulting difference formula is identical to (4.4) (apart from labeling) with the stresses on the right–hand side of the second equality evaluated at the interior zone–centered points along segments 1,2,1' and 2',

with 2A on the left–hand side of that equality replaced by $A_L + A_R$. With this interpretation of $div\mathbf{T}$, the first equality in eqn (4.4) furnishes the net force on the common deformed node. To maintain displacement continuity for the nodes on the sutured edges, we assign the same deformed position $\mathbf{y}$ to each pair.

Cable–membrane interaction may be approximated in a similar manner. Thus let's assume that a cable is attached to the boundary of the left–hand region in Figure 4.2. The net force on the boundary node B of the membrane is again given by

$$\mathbf{P} = \int_{\Omega_L} div\mathbf{T}da = \sum_{i=1}^{4} \int_i \mathbf{T}\nu ds. \tag{4.8}$$

The sum of the integrals over segments 3 and 4 approximates the integral of the traction applied to the membrane from point A to point C along the edge. According to the coupling condition (3.16) between cable and membrane, this is equal to $\mathbf{f}_C - \mathbf{f}_A$, where $\mathbf{f}_{A(C)}$ is the force in the part AB (resp. BC) of the cable, evaluated at node A (resp. C). Therefore, the sum of the forces at node B can be approximated by

$$\mathbf{P} \approx \sum_{i=1}^{2} \int_i \mathbf{T}\nu ds + \mathbf{f}_C - \mathbf{f}_A. \tag{4.9}$$

The traction integrals over the segments 1,2 in the interior of the membrane are estimated by replacing the stresses with their values at the zone–centered points, as in eqn (4.4). It should be noted that for a cable reinforcement in the interior, the force due to the cable $\mathbf{f}_C - \mathbf{f}_A$ is added to the right hand side of (4.4). This can also be considered as having the suturing and cable reinforcement along the same edge together. To obtain the cable forces we consider the cable to be *connected* to the membrane only at the nodes (the word connection means that at the nodes, the cable follows the displacement

of the membrane. For the type–1 cable, a point of the cable is attached to a point of membrane at the nodes at all time but for the type–2 one, it's not a fixed connection type and after equilibrium, a point on the cable coincides with a point on the membrane at the nodes). The actual curve of the cable is thus replaced by a connected sequence of cables. For a sufficiently fine mesh, this approximates the continuous attachment condition. So the local response of the cables can be considered as though the distributed loads acting upon them vanished. Equations (2.8) and (2.9) then imply that the deformed cables are straight and uniformly stressed between successive nodes (the mass of the cable is neglected). For the type–1 problem, this leads to the approximations

$$\mathbf{f}_C = f(\lambda_{BC})\mathbf{t}_{BC}, \quad \mathbf{f}_A = f(\lambda_{AB})\mathbf{t}_{AB} \tag{4.10}$$

where $f(\cdot)$ is the force–stretch relation of the actual cable, presumed to be elastically uniform,

$$\mathbf{t}_{BC} = (\mathbf{y}_C - \mathbf{y}_B)/|\mathbf{y}_C - \mathbf{y}_B| \text{ and } \mathbf{t}_{AB} = (\mathbf{y}_B - \mathbf{y}_A)/|\mathbf{y}_B - \mathbf{y}_A| \tag{4.11}$$

are the directions of the segments between the deformed nodes, $\mathbf{y}_{A,B,C}$ are the nodal positions, and

$$\lambda_{BC} = |\mathbf{y}_C - \mathbf{y}_B|/|\mathbf{x}_C - \mathbf{x}_B|, \quad \lambda_{AB} = |\mathbf{y}_B - \mathbf{y}_A|/|\mathbf{x}_B - \mathbf{x}_A| \tag{4.12}$$

are the stretches. The type–2 problem is handled in the same way except that the stretches are now taken to be equal to the total arclength of the deformed cable divided by the total reference arclength:

$$\lambda_{AB} = \lambda_{BC} = l/L, \tag{4.13}$$

where l and L are estimated as the sums of the straight–line distances between successive nodes on the cable, in the deformed and reference configurations, respectively. It might be interesting to note that we can model a cable with variable modulus as a type–1 cable with each cable segment (between two successive nodes) having a constant modulus but the same cable with a type–2 attachment is very hard to model because the relative position of cable and membrane is changing during the analysis. We'll see an interesting application of the first case when we talk about elliptic neutral holes in the next chapter.

We remark that preliminary calculations for some examples discussed in the next chapter exhibited zero–energy modes (the zones are distorted severely without any change in the strain energy), or *hourglassing* , which typically results in serious degradation of the solution. Special measures to suppress hourglassing have been described by Flanagan and Belytschko (1981) and Silling (1988b). Rather than adopting such measures here, we have instead used hourglassing to assess the suitability of a particular mesh topology for the problem under investigation. We'll see in the next chapter how choosing a mesh that is not consistent with the geometry of the deformation can cause hourglassing and collapse of the mesh. We've then redesigned the mesh and repeated the calculations and as we'll see, the hourglassing problem is eliminated.

4.2 Numerical method

Equilibrium of free node (i,j) requires that $\mathbf{P}^{ij} = \mathbf{0}$ (by free nodes, we mean nodes that are not fixed or under prescribed displacement). Let's see how the unknown position vector $\mathbf{y}^{ij}$ appears in this expression. It first appears in the deformation gradient (4.2), then the Cauchy–Green strain tensor (2.13) is calculated which is quadratic in unknown position vector components. The principal stretches and principal vectors of this tensor will

have a higher degree on nonlinearity in terms of $y_k^{i,j}$. Then the material non–linearity comes into play and w_a's are calculated. Then the Piola stress is calculated from (2.20). So as we see, the Piola stress components that enter into discretized equilibrium equations (4.4) are highly non–linear in terms of unknown nodal coordinates. So if we try to solve the equilibrium equations by methods that directly depend on the stiffness matrix (or the Jacobian), such as Newton–Raphson, first of all we are facing a big complication in calculating the elements of that matrix in terms of unknown coordinates due to the extremely high non–linearity present in the problem. Secondly, we need a high computational time and a large memory storage for the stiffness matrix. And thirdly, even if we can overcome those obstacles, we must invert the stiffness matrix. This is not an easy task from the computational point of view and other than this, a very important fact is when we are dealing with problems that include slack and/or wrinkled regions, the stiffness matrix will become ill–conditioned and the results obtained for these problems based on these kinds of stiffness matrices is not the true numerical solution.

Here, we're using a numerical method that does not make use of the stiffness matrix (at least not directly), needs small memory storage because it only deals with vector quantities instead of matrices, and no matrix inversions are involved. This method is called *dynamic relaxation*. The method is similar to the artificial viscosity schemes used by Silling (1987; 1988a,b; 1989), Swart and Holmes (1992), and Klouček and Luskin (1994). These authors didn't use relaxed strain energies in their computations since they were mainly interested in simulating the dynamic evolution and asymptotic behavior of fine scale features similar to those associated with minimizing sequences in the corresponding variational theories. Haseganu and Steigmann (1994a, 1996) used this method in application to membrane theory as a tool to overcome the ill-conditioning of conventional stiffness–based formulations derived from eqn (3.49).

In this method, the equilibrium equations are replaced by the artificial

dynamical problem

$$\text{div}\mathbf{T}(\mathbf{x},t) = \rho(\mathbf{x})\partial\mathbf{v}(\mathbf{x},t)/\partial t + c\rho(\mathbf{x})\mathbf{v}(\mathbf{x},t); \quad \mathbf{v}(\mathbf{x},t) = \partial\mathbf{y}(\mathbf{x},t)\partial t \quad (4.14)$$

subject to the *kinematically admissible* initial conditions

$$\mathbf{y}(\mathbf{x},0) = \mathbf{Y}(\mathbf{x}), \qquad \mathbf{v}(\mathbf{x},0) = \mathbf{0}. \quad (4.15)$$

where $\rho(\mathbf{x})$ is the mass per unit area of the reference plane, c is a positive damping coefficient, t is the time, and $\mathbf{Y}(\mathbf{x})$ is the initial guess for the deformed configuration (which we usually take to be the undeformed configuration). If we choose the mass and damping properly, hopefully the velocity and acceleration terms in (4.14) go to zero and the steady state response will be the solution to the equilibrium equations (4.4). A 1D analog of this would be the problem of finding the displacement at the end of a spring when a force is applied to it. An alternative for solving this problem is to add acceleration and velocity terms with proper mass and damping constants to the equation of equilibrium and thus making it a dynamical problem. From classical vibration, we know that the steady state response for the dynamic problem is the solution of static one (what we were after from the beginning). The discrete form of the dynamic equations of motion thus would be

$$M^{i,j}\ddot{\mathbf{y}}^{i,j,n} + cM^{i,j}\dot{\mathbf{y}}^{i,j,n} = \mathbf{P}^{i,j,n}, \quad (4.16)$$

where the subscript n identifies the time value t_n (or the iteration number with n=0 corresponding to the initiation of the process),

$$M^{i,j} = 2A^{i,j}\rho(\mathbf{x}^{i,j}) \quad (4.17)$$

is the nodal mass, and superposed dot represents the time derivative. The time derivatives are replaced by the central differences

$$\begin{aligned}\dot{\mathbf{y}}^n &= \tfrac{1}{2}(\dot{\mathbf{y}}^{n+1/2} + \dot{\mathbf{y}}^{n-1/2}),\\ \ddot{\mathbf{y}}^n &= \tfrac{1}{h}(\dot{\mathbf{y}}^{n+1/2} - \dot{\mathbf{y}}^{n-1/2}),\\ \dot{\mathbf{y}}^{n-1/2} &= \tfrac{1}{h}(\mathbf{y}^n - \mathbf{y}^{n-1}),\end{aligned} \tag{4.18}$$

where h is the time increment and the node label (i, j) has been suppressed. These are accurate to order $O(h)$. On substituting them into eqn (4.16) we obtain the explicit decoupled system in terms of velocities at half time step (Underwood, 1983; Haseganu and Steigmann, 1994a):

$$\begin{aligned}(h^{-1} + c/2)M^{i,j}\dot{\mathbf{y}}^{i,j,n+1/2} &= (h^{-1} - c/2)M^{i,j}\dot{\mathbf{y}}^{i,j,n-1/2} + \mathbf{P}^{i,j,n}\\ \mathbf{y}^{i,j,n+1} &= \mathbf{y}^{i,j,n} + h\dot{\mathbf{y}}^{i,j,n+1/2},\end{aligned} \tag{4.19}$$

which is used to advance the solution in time node by node. The first expression in the above equation holds for $n > 0$. For $n = 0$, since we have $\mathbf{y}^{i,j,0} = \mathbf{Y}(\mathbf{x}^{i,j})$ and $\dot{\mathbf{y}}^{i,j,0} = \mathbf{0}$ [Cf. (4.15)], it follows from eqns (4.19) and (4.19) that

$$(2/h)M^{i,j}\dot{\mathbf{y}}^{i,j,1/2} = \mathbf{P}^{i,j,0}, \tag{4.20}$$

wherein the right-hand side is determined by $\mathbf{Y}(\mathbf{x})$.

Although the automation of dynamic relaxation in order to calculate the proper values for mass and damping is well documented (e.g. Papadrakakis, 1981: Underwood, 1983), we've made no attempt to optimize this method and rather, in the algorithm described below, we pick the mass and damping coefficients to be constant both in time and space. In the examples that we've considered in the next chapter, the number of iterations for an error tolerance of 10^{-5} for the equations of equilibrium haven't exceeded 2000.

Here is the step by step description of the algorithm used to solve the equations of equilibrium:

- Pick an initial guess $\mathbf{Y}$ for the deformed configuration which is consistent with prescribed displacements. Set initial velocities $\dot{\mathbf{y}}^{i,j,0}$ to zero. Set $n = 0$. Pick the values for mass and damping.
- Calculate the deformation gradient at zone centers from (4.2).
- Calculate the Cauchy–Green strain tensor from (2.13).
- For isotropic materials, calculate the ppl. stretches λ_α as the square root of the eigenvalues of $\mathbf{C}$ and the ppl. vectors $\mathbf{u}_\alpha$ as the eigenvectors. For orthotropic materials, $\mathbf{u}_\alpha$ are the unit vectors along the two families of the fibers and the stretches along them are calculated from $\lambda_\alpha^2 = \mathbf{u}_\alpha \cdot \mathbf{C}\mathbf{u}_\alpha$.
- Calculate the Piola stress at the zone centers from (2.20) using (2.24).
- Calculate the total force at each free (unconstrained) node from: (4.4) for ordinary nodes; (4.9) for nodes along cable reinforcements; (4.7) for nodes along the sutured edge. We call this the residual.
- If residual is close enough to zero, stop. Otherwise, continue.
- Calculate the velocity at the free nodes at a half time step later from $(4.19)_1$ or (4.20), whichever applicable.
- Calculate the unknown position vectors at a time step later from $(4.19)_2$.
- n=n+1
- Go To the second step.

Chapter 5

Numerical Examples

In this section, the results obtained by applying the dynamic relaxation procedure to some problems are discussed. Wherever possible (e.g. Carrol, 1988), analytical results are presented and comparison is made. We've tried to cover the areas of suturing and cable reinforcement by providing different examples. In all examples, trial of different initial guesses for the deformed configuration has resulted in solutions that can not be distinguished.

5.1 Examples involving plane deformation of membranes

For a general plane deformation, the deformation gradient is a square matrix and its determinant is well defined. Applying the two–dimensional polar decomposition theorem we obtain

$$\mathbf{F} = \lambda_1 \mathbf{v}_1 \otimes \mathbf{u}_1 + \lambda_2 \mathbf{v}_2 \otimes \mathbf{u}_2 \tag{5.1}$$

where, for an isotropic material, λ_1, λ_2 are the principal stretches, $\mathbf{u}_1$, $\mathbf{u}_2$ are the orthonormal principal vectors of $\mathbf{F}^T\mathbf{F}$ [cf. eqn(2.14)], and $\mathbf{v}_1$, $\mathbf{v}_2$ are the orthonormal principal vectors of $\mathbf{F}\mathbf{F}^T$. The determinant of $\mathbf{F}$ is $J = \lambda_1\lambda_2$ [cf. eqn(3.54)]. Then, from eqns (2.20) and (2.24) it follows that

$$\mathbf{T} = w_1 \mathbf{v}_1 \otimes \mathbf{u}_1 + w_2 \mathbf{v}_2 \otimes \mathbf{u}_2. \tag{5.2}$$

Since the relations $(3.54)_{2,3}$ defining I and J in terms of λ_1 and λ_2 are invertible, the strain energy may be represented as $W(I, J)$, and

$$w_1 = W_I + \lambda_2 W_J, \qquad w_2 = W_I + \lambda_1 W_J. \tag{5.3}$$

Substituting this into (5.2) we get

$$\begin{aligned} \mathbf{T} &= (W_I + \lambda_2 W_J)\mathbf{v}_1 \otimes \mathbf{u}_1 + (W_I + \lambda_1 W_J)\mathbf{v}_2 \otimes \mathbf{u}_2 \\ &= W_I(\mathbf{v}_1 \otimes \mathbf{u}_1 + \mathbf{v}_2 \otimes \mathbf{u}_2) + W_J(\lambda_2 \mathbf{v}_1 \otimes \mathbf{u}_1 + \lambda_1 \mathbf{v}_2 \otimes \mathbf{u}_2). \end{aligned} \tag{5.4}$$

Setting

$$\mathbf{F}^* = \lambda_2 \mathbf{v}_1 \otimes \mathbf{u}_1 + \lambda_1 \mathbf{v}_2 \otimes \mathbf{u}_2 = J\mathbf{F}^{-T} \tag{5.5}$$

as the *adjugate* of $\mathbf{F}$, eqn (5.4) can be written as

$$\mathbf{T} = I^{-1} W_I(\mathbf{F} + \mathbf{F}^*) + W_J \mathbf{F}^*. \tag{5.6}$$

The identity $\mathrm{div}\mathbf{F}^* = \mathbf{0}$ makes eqn (5.6) attractive for the analysis of the equilibrium equation (this identity can be easily proved by writing the deformation gradient $\mathbf{F}$ for a general 2D deformation in Cartesian coordinates and calculating $\mathbf{F}^*$ from the last expression in (5.5) and writing the divergence vector components using $(\mathrm{div}\mathbf{F}^*)_\alpha = \mathbf{F}^*_{\alpha\beta,\beta}$).

Now let's consider the class of axisymmetric radial plane deformations

$$\mathbf{x} = r\mathbf{e}_r(\theta) \to \mathbf{y} = \rho(r)\mathbf{e}_r(\theta), \tag{5.7}$$

where (r, θ) are the polar coordinates in the plane and $\mathbf{e}_r(\theta)$ is the unit vector in radial direction. Thus

$$\begin{aligned} d\mathbf{x} &= dr\mathbf{e}_r(\theta) + rd[\mathbf{e}_r(\theta)] = dr\mathbf{e}_r + rd\theta\mathbf{e}_\theta, \\ d\mathbf{y} &= d[\rho(r)]\mathbf{e}_r(\theta) + \rho(r)d[\mathbf{e}_r(\theta)] = \rho' dr\mathbf{e}_r + \rho d\theta\mathbf{e}_\theta, \end{aligned} \tag{5.8}$$

and from $d\mathbf{y} = \mathbf{F}d\mathbf{x}$, the deformation gradient is

$$\mathbf{F} = \rho'(r)\mathbf{e}_r \otimes \mathbf{e}_r + (\rho/r)\mathbf{e}_\theta \otimes \mathbf{e}_\theta. \tag{5.9}$$

Comparing this with (5.1), the radial stretch is $\lambda_1 = \rho'(r)$ and the hoop stretch is $\lambda_2 = \rho/r$ and the requirement of $J > 0$ for a physical deformation yields $\rho' > 0$. The adjugate is

$$\mathbf{F}^* = (\rho/r)\mathbf{e}_r \otimes \mathbf{e}_r + \rho'(r)\mathbf{e}_\theta \otimes \mathbf{e}_\theta, \tag{5.10}$$

and it can be easily seen that

$$\mathbf{F} + \mathbf{F}^* = I\mathbf{\Delta}; \qquad I = \rho' + \rho/r, \tag{5.11}$$

where $\mathbf{\Delta}$ is the two–dimensional unit tensor. Then eqn (5.6) reduces to

$$\mathbf{T} = W_I\mathbf{\Delta} + W_J\mathbf{F}^* \tag{5.12}$$

for axisymmetric radial deformations. The equation of equilibrium thus is

$$\begin{aligned} \mathrm{div}\mathbf{T} &= \mathrm{div}(W_I\mathbf{\Delta} + W_J\mathbf{F}^*) = \mathrm{div}(W_I\mathbf{\Delta}) + \mathrm{div}(W_J\mathbf{F}^*) \\ &= \mathbf{\Delta}\mathrm{grad}(W_I) + \mathbf{F}^*\mathrm{grad}(W_J) = \mathbf{0}. \end{aligned} \tag{5.13}$$

If in addition, an elastically uniform cable is attached to the membrane along its inner edge $r = r_i$, its stretch is $\lambda = \lambda_2(r_i)$ and its direction is $\mathbf{t}(s) = -\mathbf{e}_\theta(\theta)$, where $\theta = -s/r_i$ (the negative sign is there because s is measured in accordance with Green's theorem; it runs clockwise along the inner boundary of the annulus). Therefore, the force transmitted by the cable is

$$\mathbf{f}(s) = -f(\lambda_2(r_i))\mathbf{e}_\theta. \tag{5.14}$$

Because of the symmetry in the deformation, the cable has no shear interaction with the membrane and thus the above expression is true for both types of cable attachment. Substituting (5.14) into (3.16) [or (3.27)] with $\boldsymbol{\tau} = -\mathbf{e}_r$ and invoking eqns (5.10)-(5.12), the coupling condition between membrane and cable would be

$$f/r_i = [W_I + (\rho/r)W_J]_{r=r_i}. \tag{5.15}$$

We also prescribe the displacement on the outer boundary $r = r_o$

$$\rho(r_o) = \rho_o(> r_o). \tag{5.16}$$

Then having the strain energy functions for membrane and cable, we can solve the ordinary differential equation (5.13) with boundary conditions (5.15) and (5.16) to obtain $\rho(r)$ and hence the analytical solution to the equilibrium equation. We consider a few material models here.

5.1.1 Varga material

We assume that the condition (5.16) generates biaxial tension everywhere in the membrane and therefore the stretches belong to the first branch of the relaxed Varga strain energy defined by eqns (3.49) and (3.53). We also

assume that the cable stretch is greater than zero """ and these assumptions are verified when we obtain the solution. Based on the definition of Varga strain energy [Cf. eqn (3.49)]

$$W_I = 2\mu(= const.), \qquad W_J = -2\mu J^{-2}. \tag{5.17}$$

So the equilibrium equation (5.13) reduces to (Varga, 1966)

$$-4\mu J^{-3}\mathbf{F}^*\text{grad}J = 0 \qquad \rightarrow \qquad J = \frac{\rho\rho'}{r} = \text{Const.}, \tag{5.18}$$

which applying the boundary condition (5.16) yields

$$\rho(r) = [\rho_o^2 - J(r_o^2 - r^2)]^{1/2}. \tag{5.19}$$

We use the coupling condition (5.15) to calculate J

$$f(\lambda_2(r_i))/r_i = 2\mu(1 - \lambda_2(r_i)/J^2) \tag{5.20}$$

but from (5.19)

$$\lambda_2(r_i) = \frac{\rho(r_i)}{r_i} = \left\{\left(\frac{\rho_o}{r_i}\right)^2 - J\left[\left(\frac{r_o}{r_i}\right)^2 - 1\right]\right\}^{1/2}. \tag{5.21}$$

Assuming a linear elastic force–stretch relation for the cable given by eqn (3.67), we can solve eqn (5.20) to get $\lambda_2(r_i)$ as

$$\lambda_2(r_i) = \left(1 + \frac{E}{2\mu r_i}\right) / \left(J^{-2} + \frac{E}{2\mu r_i}\right). \tag{5.22}$$

We can then equate this to (5.21) and get a non–linear equation in J which can be solved by Newton's method, for example. Knowing J, we have the complete solution from (5.19).

In order to make a comparison between the analytical and numerical solutions, we consider the case

$$r_i/r_o = 0.5, \qquad \rho_o/r_o = 1.2. \tag{5.23}$$

Figure 5.1 shows the meshed initial configuration used for computations. It consists of 10 divisions radially and 72 equally spaced divisions circumferentially. Without imposing any symmetry on the free nodes, the outer boundary is displaced radially as specified and Figure 5.2 shows the deformed configuration for the case of no cable ($E = 0$) along the inner boundary. As we can see, there is axisymmetry in the solution as expected. Figure 5.3 shows the comparison of distribution of analytical and numerical radial and hoop stretches versus radius for this case. The solid curves show the analytical results while the circles and triangles show the numerical values for the hoop and radial stretch respectively. The numerical values for the stretches are considered to be at zone centers. As it is seen, there is a very good match between analytical and numerical results. Figure 5.4 shows the stretch distribution for the case of cable reinforcement along the inner boundary with a cable stiffness of $E/2\mu r_i = 2.0$. Again the numerical and analytical solutions coincide and we can see by comparing this to the previous case that the primary effect of adding the cable reinforcement is to reduce the high stretch gradients along the inner boundary. For both the above cases, the stretches fall in in the range for which Varga material shows good agreement with biaxial data on rubber (Varga, 1966). As it was said before, the assumptions that were made about the stretches in the beginning are now verified.

5.1.2 Harmonic materials

Let's consider the same boundary value problem for the class of Harmonic materials. Making the same assumption about the stretches, we can use the unrelaxed strain energy function for harmonic materials given by (3.55).

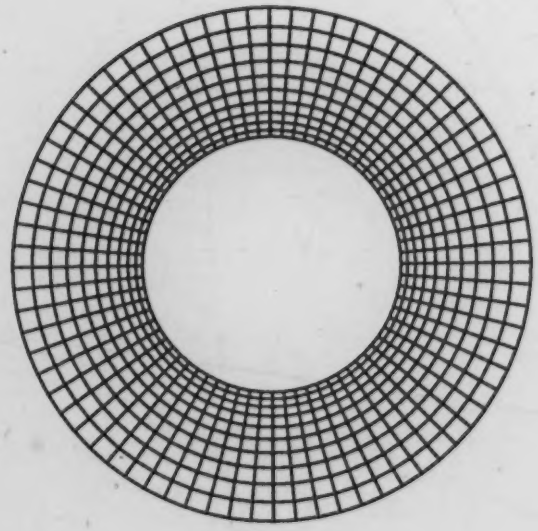

Figure 5.1: Meshed reference configuration of an annular membrane with $r_I/r_O=0.5$

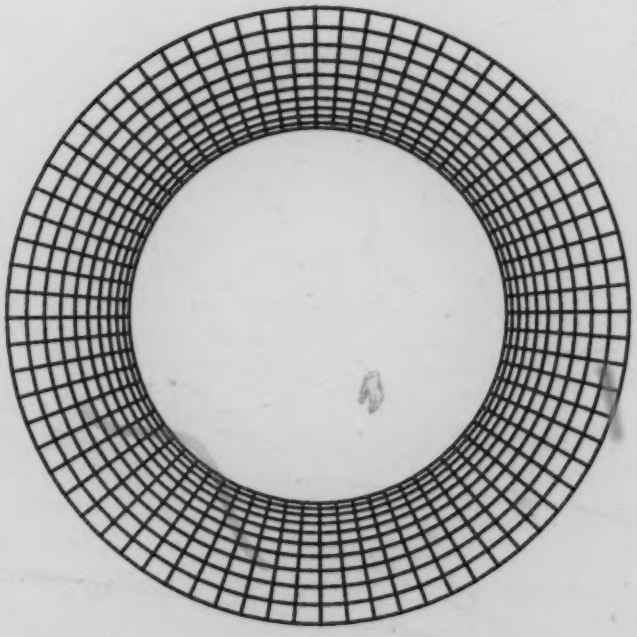

Figure 5.2: Deformed configuration with $\rho_o=1.2r_o$. Varga material. No cable reinforcement

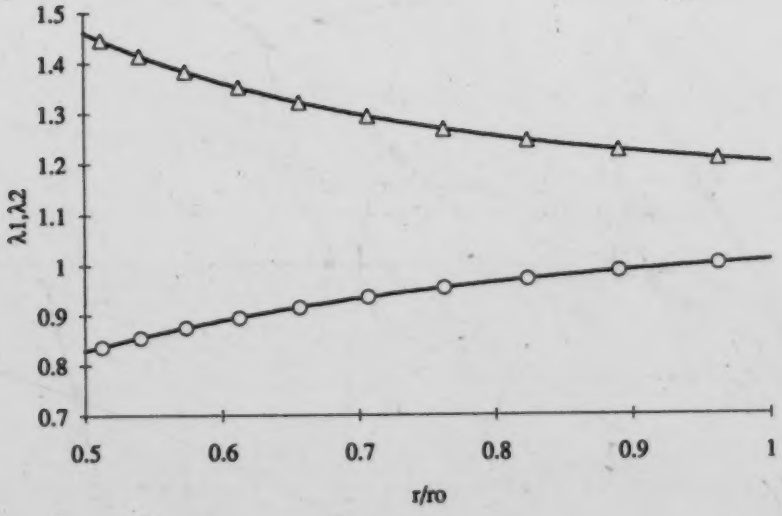

Figure 5.3: Distribution of stretches vs. radius for Varga material with no cable reinforcement; (Δ) numerical hoop stretch, (O) numerical radial stretch. Solid lines show the analytical results.

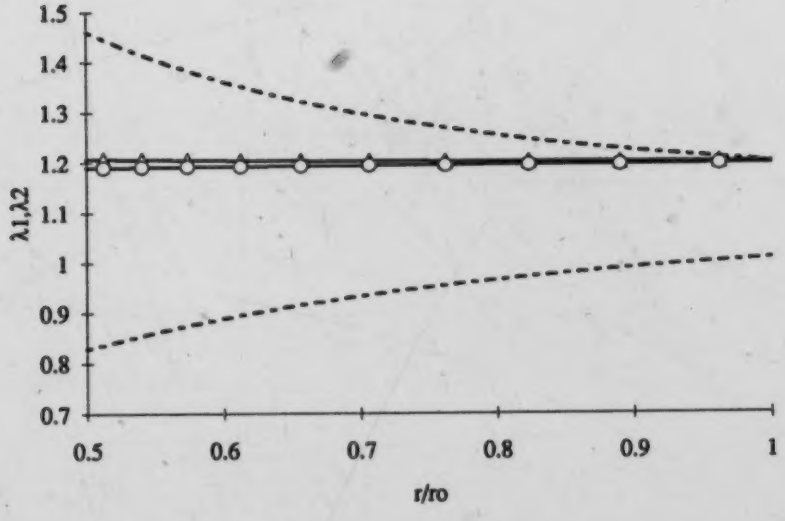

Figure 5.4: Distribution of stretches vs. radius for Varga material. Cable reinforcement with $E/2\mu r_i=2.0$; (Δ) numerical hoop stretch, (O) numerical radial stretch. Solid and dashed lines show the analytical results for this case and previous one respectively.

Therefore

$$W_I = 2\mu F'(I) = 2\mu\left(\frac{\bar{\lambda}+2\mu}{2\mu}I - \frac{\bar{\lambda}+\mu}{\mu}\right) = (\bar{\lambda}+2\mu)I - 2(\bar{\lambda}+\mu),$$
$$W_J = -2\mu(= const.). \tag{5.24}$$

and the equilibrium equation (5.13) reduces to

$$(\bar{\lambda}+2\mu)\Delta \mathrm{grad} I = 0 \qquad \rightarrow \qquad I = \rho' + \rho/r = const. \tag{5.25}$$

and when subjected to (5.16) it yields

$$\rho(r) = \frac{I}{2}(r - r_o^2/r) + \rho_o r_o/r. \tag{5.26}$$

The coupling condition (5.15) reduces to

$$(\bar{\lambda}+2\mu)I - 2(\bar{\lambda}+\mu) = (2\mu + E/r_i)\lambda_2(r_i) - E/r_i, \tag{5.27}$$

with

$$\lambda_2(r_i) = \frac{I}{2}(1 - r_o^2/r_i^2) + \rho_o r_o/r_i^2. \tag{5.28}$$

Substituting this into (5.27) and solving for I (this is a linear equation in I), the solution (5.26) becomes

$$\rho(r) = \frac{(\frac{\bar{\lambda}}{\mu}+1) + (1+\frac{E}{2\mu r_i})\frac{\rho_o r_o}{r_i^2} - \frac{E}{2\mu r_i}}{(\frac{\bar{\lambda}}{\mu}+2) - (1+\frac{E}{2\mu r_i})(1 - r_o^2/r_i^2)}(r - r_o^2/r) + \rho_o r_o/r. \tag{5.29}$$

For illustrative purposes, we use the data in (5.23) and set $\bar{\lambda}/\mu = 2.0$. Figure 5.5 shows the stretch distribution for the case of $E = 0$ (no cable) using the mesh in Figure 5.1. The results for the case of a cable reinforcement with $E/2\mu r_i = 2.0$ is shown in Figure 5.6. Both figures show excellent agreement between numerical and analytical results.

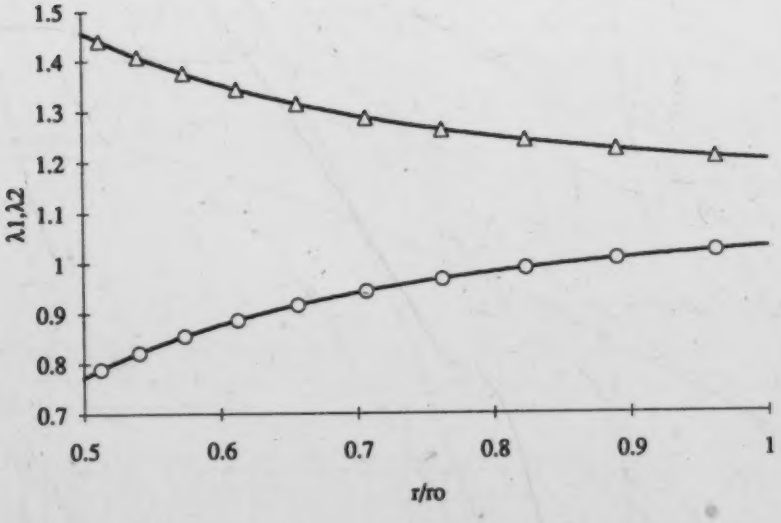

Figure 5.5: Distribution of stretches vs. radius for standard harmonic material ($\bar{\lambda}/\mu = 2.0$) with no cable reinforcement; (Δ) numerical hoop stretch, (O) numerical radial stretch. Solid lines show the analytical results.

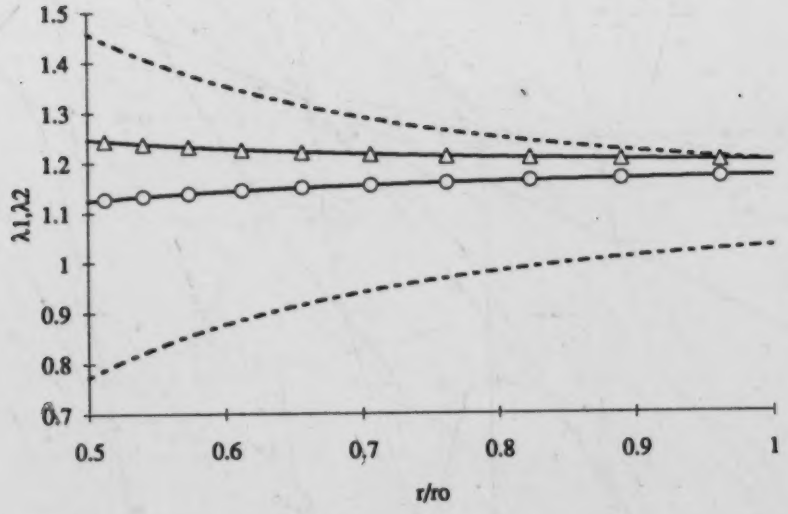

Figure 5.6: Distribution of stretches vs. radius for standard harmonic material ($\bar{\lambda}/\mu = 2.0$). Cable reinforcement with $E/2\mu r_i$=2.0; (Δ) numerical hoop stretch, (O) numerical radial stretch. Solid and dashed lines show the analytical results for this case and previous one respectively.

5.1.3 Neo-Hookian material

Using the relaxed strain energy function for this material defined by (3.52), we get

$$W_I = \mu I, \qquad W_J = -\mu(1 + J^{-3}) \tag{5.30}$$

and the equations of equilibrium are

$$\mu \mathrm{grad} I \boldsymbol{\Delta} + 3\mu J^{-4} \mathrm{grad} J \mathbf{F}^* = \mathbf{0}. \tag{5.31}$$

Having the definitions for I and J and knowing that the stretches only depend on r, we can write

$$\begin{aligned} \mathrm{grad} I &= \mathrm{grad}(\rho/r + \rho') = (\tfrac{r\rho' - \rho}{r^2} + \rho'')\mathbf{e}_r, \\ \mathrm{grad} J &= \mathrm{grad}(\rho\rho'/r) = (\tfrac{r\rho' - \rho}{r^2}\rho' + \rho\rho''/r)\mathbf{e}_r, \\ \boldsymbol{\Delta} &= \mathbf{e}_r \otimes \mathbf{e}_r + \mathbf{e}_\theta \otimes \mathbf{e}_\theta, \\ \mathbf{F}^* &= \rho/r \mathbf{e}_r \otimes \mathbf{e}_r + \rho' \mathbf{e}_\theta \otimes \mathbf{e}_\theta. \end{aligned} \tag{5.32}$$

Substituting these into (5.31) and simplifying we get

$$\frac{r\rho' - \rho}{r^2} + \rho'' + 3(\rho\rho'/r)^{-4}(\rho/r)\left(\frac{r\rho' - \rho}{r^2}\rho' + \rho\rho''/r\right) = 0. \tag{5.33}$$

This is a non–linear ODE that has to be solved numerically subject to boundary conditions (5.16) and the coupling condition between cable and membrane which for a cable corresponding to (3.67) yields

$$\frac{E}{\mu r_i} = \frac{(\rho_i/r_i + \rho_i') - \frac{\rho_i}{r_i}[1 + (\rho_i'\rho_i/r_i)^{-3}]}{\frac{\rho_i}{r_i} - 1} \tag{5.34}$$

where $\rho_i = \rho(r_i)$ and $\rho'_i = \rho'(r_i)$. We use the *shooting method* [see Press, (1992) for example] to solve (5.33) numerically to get the analytical solution. For the data set given in (5.23), Figures 5.7 and 5.8 show the distribution of stretches for the cases of $E = 0$ (no cable) and $E/\mu r_i = 2.0$ respectively. Once again, we see a good agreement between numerical and analytical results.

Now let's consider another axisymmetric problem with wrinkling involved. We take the same annulus membrane made up of neo-Hookian material but this time subject to the following boundary conditions

$$\rho(r_o) = \rho_o = r_o, \text{ Applied traction } \mathbf{t} = -\mathbf{e}_r \text{ at } r = r_i. \tag{5.35}$$

With these conditions, we expect to have some wrinkling near the inner boundary because of the shrinkage of membrane due to the applied inward traction. Solving the numerical problem using the same mesh as before verifies our expectation. Figure 5.9 shows the deformed configuration for this problem and as we can see, a ring around the inner boundary is wrinkled (shown by the zones with straight lines at the center where these lines show the tensile trajectories which are in the radial directions as expected). In order to get the analytical solution, we first need to find out how the Piola stress $\mathbf{T}$ changes for a wrinkled region. Since we expect the membrane to be tense radially and slack circumferentially in the wrinkled region, the membrane strain energy for this case would be [Cf. (3.50)]

$$\hat{w}(\lambda_1) = w(\lambda_1, v(\lambda_1)) \tag{5.36}$$

and the Piola stress would be [Cf. (3.44)]

$$\hat{\mathbf{T}} = \hat{w}_1 \mathbf{e}_r \otimes \mathbf{e}_r \tag{5.37}$$

where $\hat{w}_1 = d\hat{w}/d\lambda_1$. The equation of equilibrium in the wrinkled region then is

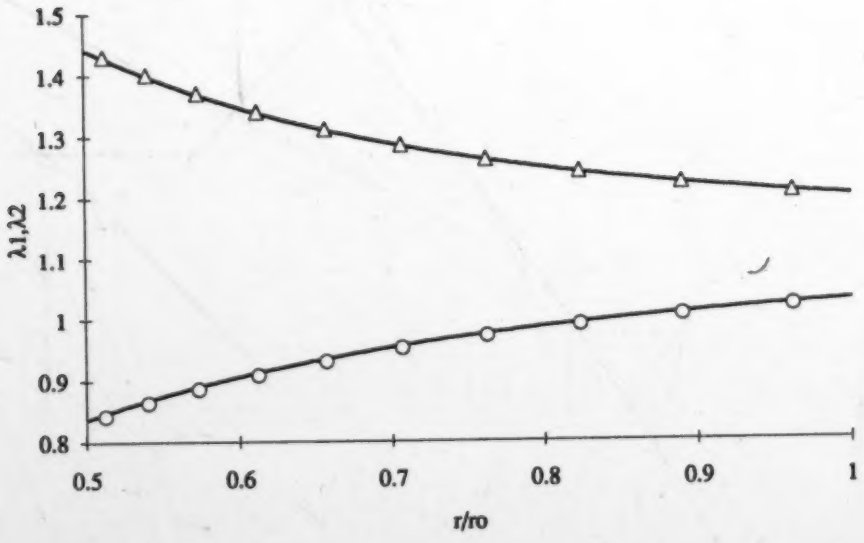

Figure 5.7: Distribution of stretches vs. radius for neo-Hookian material with no cable reinforcement; (Δ) numerical hoop stretch, (O) numerical radial stretch. Solid lines show the analytical results.

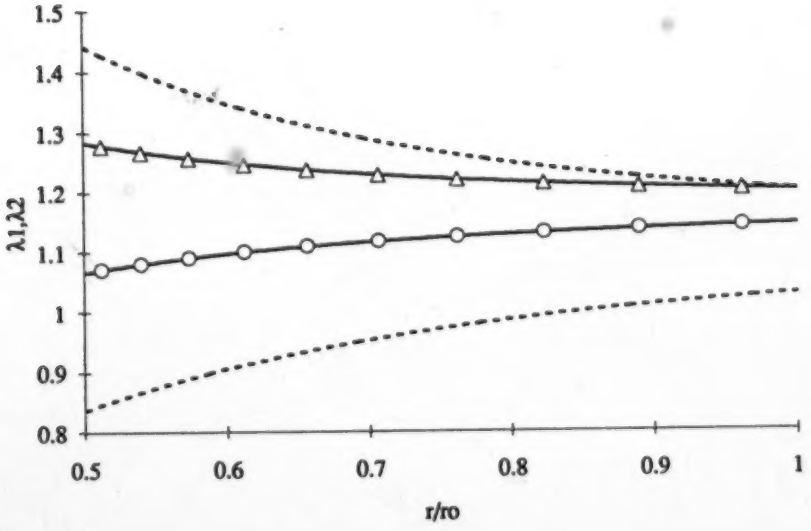

Figure 5.8: Distribution of stretches vs. radius for neo-Hookian material. Cable reinforcement with $E/\mu r_i=2.0$; (Δ) numerical hoop stretch, (O) numerical radial stretch. Solid and dashed lines show the analytical results for this case and previous one respectively.

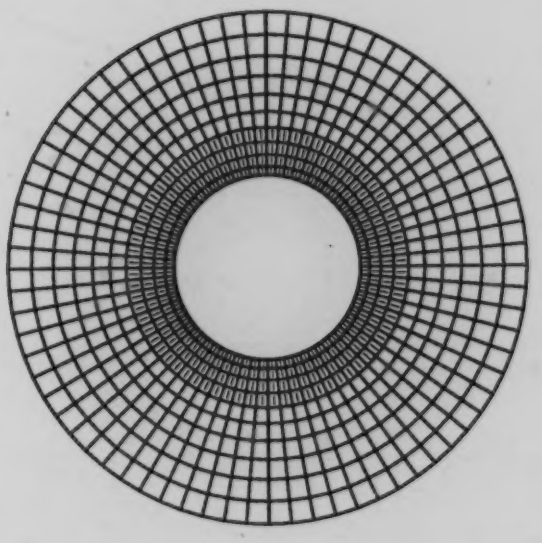

Figure 5.9: Deformed configuration with $\rho_o=r_o$ and applied radial traction of $t=-e_r$ on the inner boundary. Neo-Hookian material. No cable reinforcement

$$\text{div}\hat{\mathbf{T}} = \mathbf{0} \rightarrow d\hat{w}_1/dr + \hat{w}_1/r = 0. \tag{5.38}$$

Now let's denote the radius in the undeformed configuration corresponding to the boundary between wrinkled and tense region by $\bar{r}$ with $r_i \leq \bar{r} \leq r_o$. Then the relation between principal stretches at that location would be [Cf. (3.51)]

$$\lambda_2 = v(\lambda_1) \qquad \text{at } r = \bar{r} \qquad \text{or} \qquad \rho(\bar{r})/\bar{r} = \rho'(\bar{r}). \tag{5.39}$$

From eqn (2.21), the boundary condition at $r = r_i$ can be rewritten as

$$\hat{\mathbf{T}}\boldsymbol{\nu} = \mathbf{t} = -\mathbf{e}_r \rightarrow \hat{w}_1 = 1 \qquad \text{at } r = r_i. \tag{5.40}$$

So, in order to get the analytical solution for this problem, we must solve the following differential equation system

$$\begin{aligned} &\text{eqn (5.13) for } \bar{r} \leq r \leq r_o \\ &\text{eqn (5.38) for } r_i \leq r \leq \bar{r} \end{aligned} \tag{5.41}$$

subject to boundary conditions (5.35) with $\bar{r}$ derived from (5.39). It should be noted that the solution for the interval $\bar{r} \leq r \leq r_o$ is the same as the ones obtained for (5.13) for different materials. Figure 5.10 shows the analytical and numerical distribution of stretches vs. radius for neo-Hookian material.

5.2 Neutral holes

In this section, we discuss how the application of proper cable reinforcement around the boundary of the hole in the membrane subject to biaxial stretch, can produce such a stretch distribution inside the membrane as if the hole

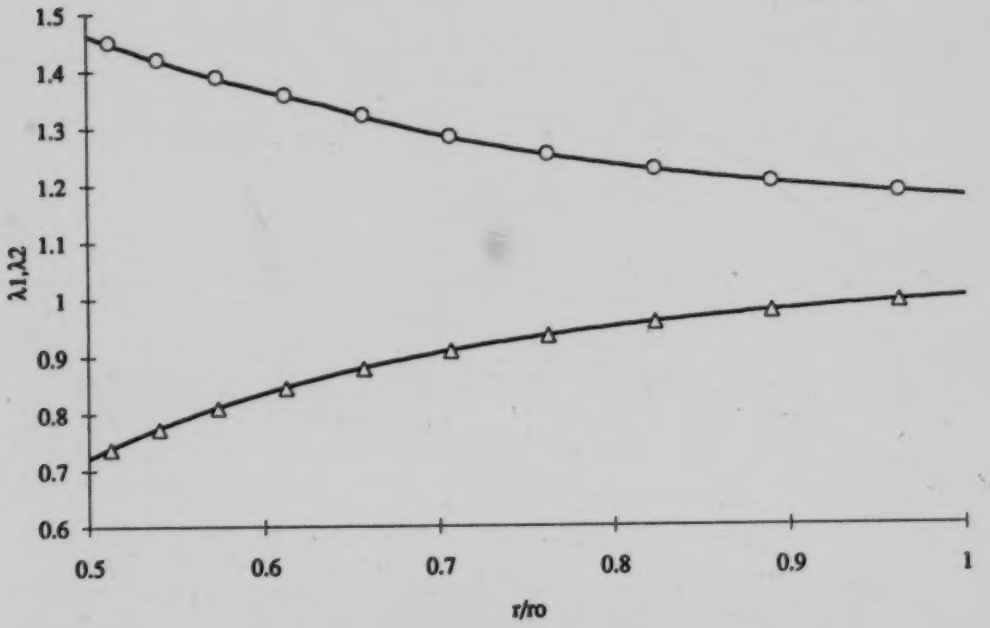

Figure 5.10: Distribution of stretches vs. radius for neo-Hookian material with no cable reinforcement and applied radial traction ; (Δ) numerical hoop stretch, (O) numerical radial stretch. Solid lines show the analytical results.

wasn't there at all(neutral hole effect). Mansfield (1953) has discussed this issue for infinitesimal displacements in the class of linear elastic theory but we present cases of finite displacements. We present two cases for which we can formulate analytical solutions and compare with numerical ones.

5.2.1 Circular hole

Following the cases discussed in the previous section, one might have this expectation that it is possible to choose the cable modulus such that the hole behaves neutrally (for example, if we consider the limiting case of a cable with modulus at infinity, the hole does not expand under deformation and thus we have a hoop stretch of one at the hole boundary increasing to a value greater than one at the outer boundary and increasing hoop stretch corresponds to a decreasing radial stretch. But in the previous cases, we had a decreasing hoop stretch and an increasing radial stretch. So there should be a point that the curves corresponding to the stretches have crossed or even lied on top of each other). Following the energy and stability discussions in Atai and Steigmann (1998), we take the deformation gradient for the case of applied equibiaxial stretch to be

$$\mathbf{F}(\mathbf{x}) = \lambda \mathbf{\Delta}; \qquad \lambda = \rho_o / r_o (> 1). \tag{5.42}$$

Then from (5.5) $\mathbf{F}^* = \mathbf{F}$ and (5.12) reduces to

$$\mathbf{T} = T(\lambda)\mathbf{\Delta}, \qquad T(\lambda) = W_I + \lambda W_J \tag{5.43}$$

with $I = 2\lambda$ and $J = \lambda^2$. Since λ is constant, the equation of equilibrium (5.13) is satisfied inside the domain and the boundary condition at the hole is

$$f(\lambda)/r_i = T(\lambda) = W_I + \lambda W_J. \tag{5.44}$$

Having the strain energy function for the membrane and assuming a linear elastic cable, this can be re–written as

$$E(\lambda - 1)/r_i = W_I + \lambda W_J. \tag{5.45}$$

For example, for Varga material, $W_I = 2\mu$ and $W_J = -2\mu J^{-2} = -2\mu\lambda^{-4}$ and the above boundary condition reduces to

$$E/2\mu r_i = (1 - \lambda^{-3})/(\lambda - 1) = (\lambda^2 + \lambda + 1)/\lambda^{-3}. \tag{5.46}$$

Following the same procedure, the boundary condition reduces to

$$E/\mu r_i = (\lambda^2 + 1)(\lambda + 1)/\lambda^3 \tag{5.47}$$

for neo–Hookian material and

$$\frac{E}{2(\bar{\lambda} + \mu)r_i} = 1 \tag{5.48}$$

for standard harmonic material. It is interesting to note that for the latter case, the cable modulus for neutral hole case does not depend on the amount of stretch $\lambda = \rho_o/r_o$ meaning that if we choose this value for the modulus, the hole remains neutral no matter what is the value of the equibiaxial stretch applied on the outer boundary which makes this more flexible and suitable for applications as opposed to the other two cases where the cable modulus depends on the amount of the stretch applied on the outer boundary. But for small stretches ($\lambda \approx 1$), we can always linearize the right hand side of the above boundary conditions to get a cable modulus for the neutral hole case that does the job for a small range of stretches close to 1. Figure 5.11 shows the comparison of numerical and analytical stretch distributions for standard harmonic materials with $\bar{\lambda}/\mu = 2.0$ which yields $E/2\mu r_i = 3.0$.

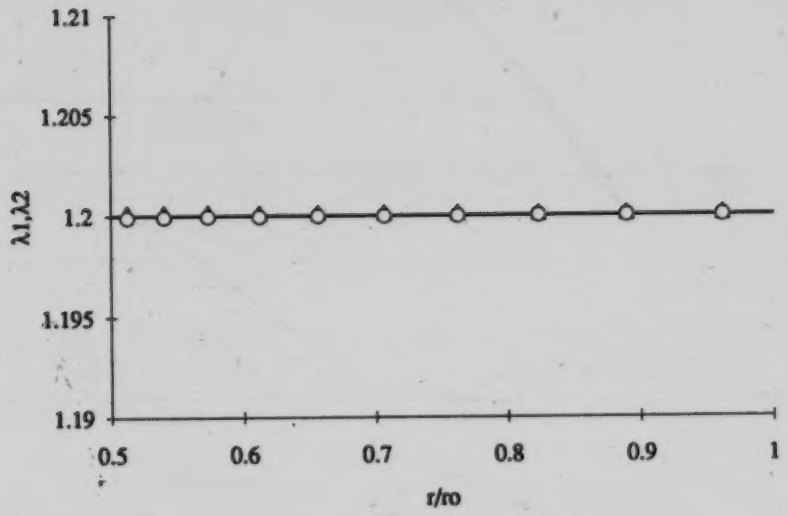

Figure 5.11: Distribution of stretches vs. radius for standard harmonic material ($\bar{\lambda}/\mu = 2.0$). Cable reinforcement with $E/2\mu r_i$=3.0; (Δ) numerical hoop stretch, (O) numerical radial stretch. Solid lines show the analytical results.

5.2.2 Elliptic neutral hole

Let's consider a membrane in x_1–x_2 plane with an elliptic hole with axes along x_1 and x_2 subject to a biaxial stretch along those axes with the deformation gradient

$$\mathbf{F} = \lambda_1 \mathbf{e}_1 \otimes \mathbf{e}_1 + \lambda_2 \mathbf{e}_2 \otimes \mathbf{e}_2 \tag{5.49}$$

where $\lambda_1 > 1$ and $\lambda_2 > 1$ are the applied stretches (not to be confused with principal stretches derived from Cauchy–Green strain tensor) along x_1 and x_2 axes with unit vectors $\mathbf{e}_1$ and $\mathbf{e}_2$ respectively and the assumption is made that the hole is neutralized with the use of proper cable reinforcement. The Piola stress will then be

$$\mathbf{T} = (W_I + \lambda_2 W_J)\mathbf{e}_1 \otimes \mathbf{e}_1 + (W_I + \lambda_1 W_J)\mathbf{e}_2 \otimes \mathbf{e}_2 \tag{5.50}$$

with $I = \lambda_1 + \lambda_2$ and $J = \lambda_1 \lambda_2$. It can be readily seen that the equation of equilibrium is satisfied inside the membrane. In order to examine the boundary condition (3.16) at the hole, let's consider the geometry of the hole before and after deformation (Figure 5.12). So a and b are the semi–axes of the ellipse before deformation and $\lambda_1 a$ and $\lambda_2 b$ are their deformed lengths. From the geometry of the ellipse in the undeformed configuration, we can write

$$\mathbf{t} = \frac{a \sin\theta \mathbf{e}_1 - b \cos\theta \mathbf{e}_2}{(a^2 \sin^2\theta + b^2 \cos^2\theta)^{1/2}}, \quad \boldsymbol{\nu} = -\frac{b \cos\theta \mathbf{e}_1 + a \sin\theta \mathbf{e}_2}{(a^2 \sin^2\theta + b^2 \sin^2\theta)^{1/2}} \tag{5.51}$$

where $\mathbf{t}$ is the unit tangent to the boundary and $\boldsymbol{\nu}$ is the rightward normal to it and θ is the parametrization of the boundary that defines the coordinates of each point on it as

$$x_1 = a \cos\theta, \qquad x_2 = b \sin\theta. \tag{5.52}$$

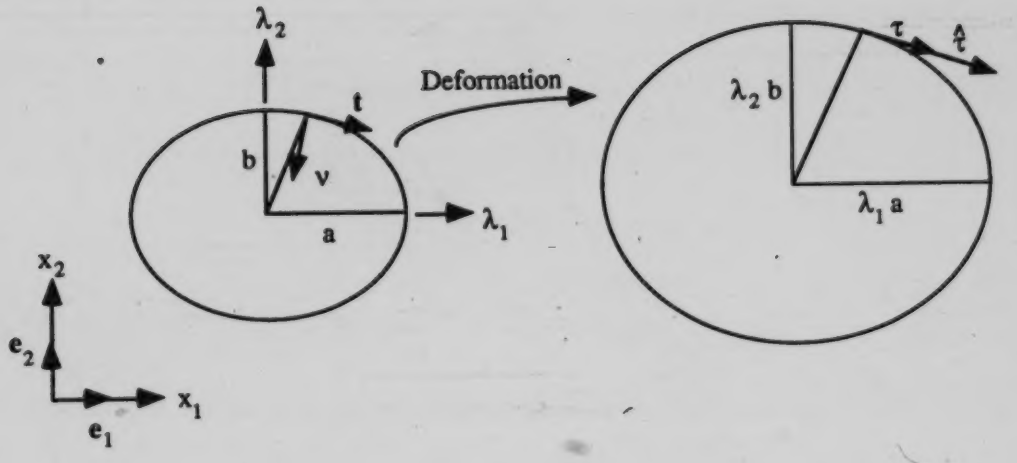

Figure 5.12: Geometry of the elliptic hole before and after deformation

In order to write down the force vector in the cable, we need the unit tangent vector to the deformed boundary. This can be derived by finding the deformed state of $\mathbf{t}$ as

$$\hat{\boldsymbol{\tau}} = \mathbf{F}\mathbf{t} = \frac{a\lambda_1 \sin\theta \mathbf{e}_1 - b\lambda_2 \cos\theta \mathbf{e}_2}{(a^2 \sin^2\theta + b^2 \cos^2\theta)^{1/2}} \tag{5.53}$$

and normalizing it to get

$$\boldsymbol{\tau} = \hat{\boldsymbol{\tau}}/|\hat{\boldsymbol{\tau}}| = \frac{a\lambda_1 \sin\theta \mathbf{e}_1 + b\lambda_2 \cos\theta \mathbf{e}_2}{(a^2\lambda_1^2 \sin^2\theta + b^2\lambda_2^2 \cos^2\theta)^{1/2}}. \tag{5.54}$$

The boundary condition at the hole is $\mathbf{T}\boldsymbol{\nu} = \mathbf{f}'(s)$. From (5.50) and (5.51), the left hand side of this can be written as

$$\mathbf{T}\boldsymbol{\nu} = -\frac{b\cos\theta(W_I + \lambda_2 W_J)\mathbf{e}_1 + a\sin\theta(W_I + \lambda_1 W_J)\mathbf{e}_2}{(a^2 \sin^2\theta + b^2 \cos^2\theta)^{1/2}}. \tag{5.55}$$

For the right hand side we can write

$$\mathbf{f}(s) = f(s)\boldsymbol{\tau} \rightarrow \mathbf{f}'(s) = f'(s)\boldsymbol{\tau} + f d\boldsymbol{\tau}/ds = f'(s)\boldsymbol{\tau} + f\frac{d\theta}{ds}\frac{d\boldsymbol{\tau}}{d\theta}. \tag{5.56}$$

Substituting for $\boldsymbol{\tau}$ from (5.54) and for $d\theta/ds$ from

$$ds = (dx_1^2 + dx_2^2) \rightarrow d\theta/ds = \frac{-1}{(a^2 \sin^2\theta + b^2 \cos^2\theta)^{1/2}} \tag{5.57}$$

into (5.56) and equating it with (5.55), we get expressions for f and f' which won't be mentioned here because of complications. Upon taking the arclength derivative of f and comparing it with f', we arrive at the following constraint (Atai, 1997)

$$\frac{a}{b} = \left(\frac{\lambda_2(W_I + \lambda_2 W_J)}{\lambda_1(W_I + \lambda_1 W_J)}\right)^{1/2}. \tag{5.58}$$

This condition states that having the elliptic hole geometry, the biaxial stretches that must be applied as one of the necessary conditions to obtain neutral hole state are not independent of each other. There might even be cases that certain choices of λ_1 or λ_2 does not yield a real value for the other stretch. It can be seen that setting $a = b$ (circular hole) results in the equibiaxial stretch case of $\lambda_1 = \lambda_2 = \lambda$ as the trivial case. The other necessary condition is the magnitude of the force f given by

$$f = b(W_I + \lambda_2 W_J)\left(\frac{\lambda_2^2 b^2}{\lambda_1^2 a^2}\cos^2\theta + \sin^2\theta\right)^{1/2}. \tag{5.59}$$

Since θ is varying along the hole boundary, the modulus of the cable E must also vary according to this expression. This might not be feasible for practical purposes as opposed to the circular hole case where the modulus is constant along the cable. The second point is that because of the symmetry in the problem in the previous case, application of a type–1 or type–2 cable reinforcement didn't make any difference. However, for the present case, since the modulus of the cable has to be a certain value at a certain point, the cable and membrane cannot slide with respect to each other and hence a type–1 cable reinforcement must be applied here. Setting $a = b = r_i$ and $\lambda_1 = \lambda_2 = \lambda$ reduces this to (5.15) for the circular hole case.

We present an example here discussed in Atai (1997). We use the mesh shown in Figure 5.13 for computational purposes. We use a hole geometry of $a = 1.25b = 0.5r_o$ and specifying a stretch of $\lambda_2 = 2.5$ along the x_2 axis and a Varga type material, the stretch along x_1 is calculated from (5.58) to be $\lambda_1 = 1.4596$. Although according to (5.59), the modulus of the cable should vary continuously along the boundary, for numerical purposes we've calculated the modulus for the center points of the edges of the zones around the boundary and kept it constant for the length of that edge. Hence, instead of being continuous, the modulus is jumping step by step along the boundary. Figure 5.14 shows the distribution of stretches along the x_1 axis and the

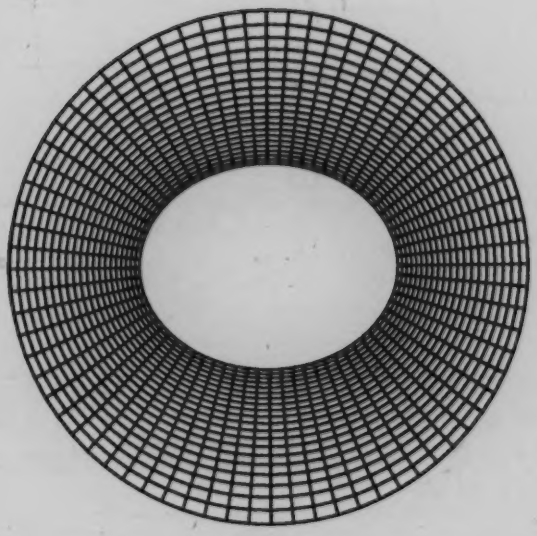

Figure 5.13: Elliptic hole with dimensions a=2.5b=r_o/2 inside a circular domain of radius r_o.

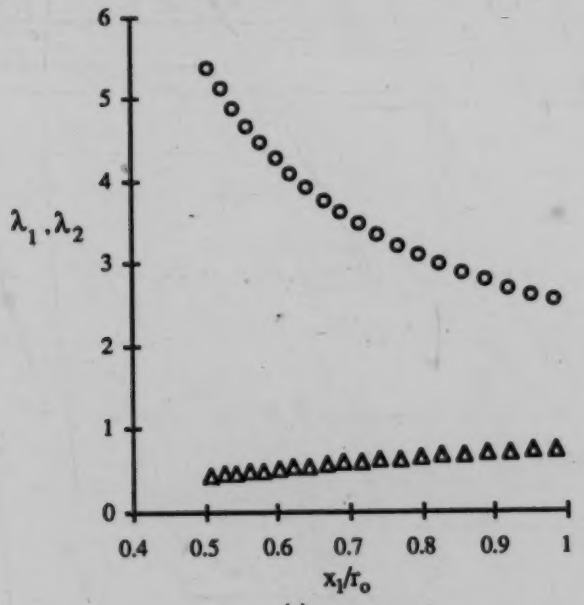

(a)

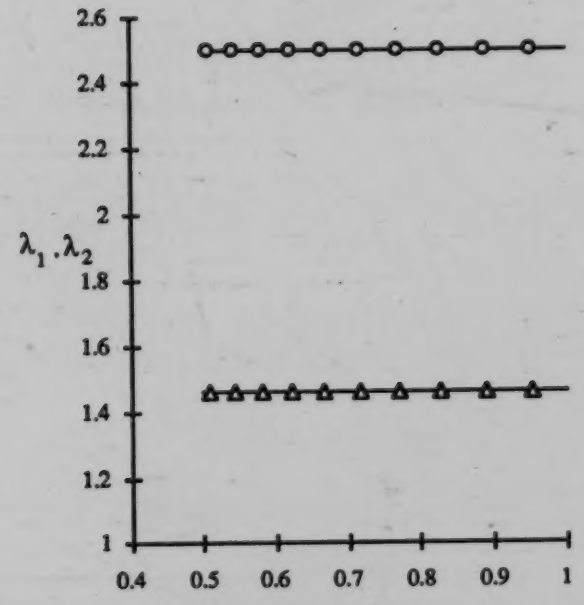

(b)

Figure 5.14: Distribution of stretches vs. horizontal axis for an elliptic hole of $a=2.5b=r_o/2$ in a circular domain of radius r_o. Varga material. Applied stretches of $\lambda_1=1.46$ and $\lambda_2=2.5$ on the outside. (Δ) horizontal stretch, (O) vertical stretch;(a) No cable reinforcement, (b) Cable reinforcement corresponding to the neutral hole case

numerical results correspond to the centers of the zones closest to the x_1 axis. The distribution of stretches for the case of no cable reinforcement from the numerical results are also presented to once again, emphasize on the stretch gradient reduction effect of cable reinforcement. Although the modulus of the cable is approximated for the numerical results, once again we see a good agreement between analytical and numerical results.

5.3 Planar deformation of membrane with orthotropic material

We present an example here that shows the behaviour of the linear orthotropic material defined by (3.62). We take an annulus membrane as shown in Figure 5.1 with the fibers parallel to horizontal and vertical directions. we hold the outer boundary fixed while we twist the inner circle inside the plane of mesh by 20 degrees counter–clockwise. Figure 5.15 shows the deformed configuration. Because of the symmetry in the deformation and in the material, we see a pattern that repeats itself every 90 degrees as it was suggested in Chapter 3. Zones with the straight lines in them show the wrinkled regions. They can be justified in this way: because of the twist of the inner boundary, the horizontal fibers become loose in some places while the vertical fibers are stretched and vice versa. It is interesting to know that the same deformation with the same initial configuration but with an isotropic material shows a wrinkled ring around the hole. Now let's introduce a disturbance in the initial configuration by having a slit along the right–hand side horizontal radial line and repeat the deformation. Figure 5.16 shows the deformed configuration. It can be seen that in the area near the slit, the state of stress in the zones has completely changed but far from the disturbance (opposite side of the slit), the deformation is to a good extent similar to the previous case (St. Venant principal). An isotropic material also shows a similar behaviour.

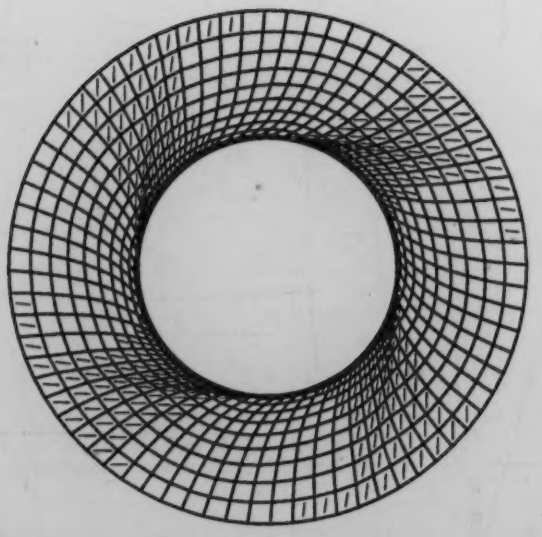

Figure 5.15: Deformed configuration of an annular membrane with r_i/r_o=0.5. Twist of inner boundary by 20° ccw. Linear orthotropic material.

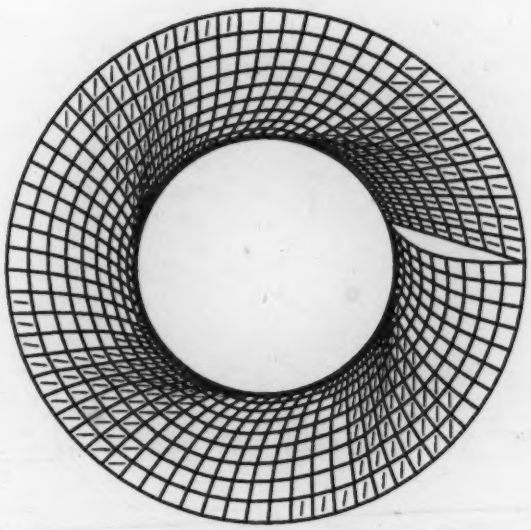

Figure 5.16: Deformed configuration of an annular membrane with r_i/r_o=0.5 with a slit along the horizontal radial line. Twist of inner boundary by 20° ccw. Linear orthotropic material.

5.4 Plane deformation of a square sheet

In this section, we deal with an example that clearly shows the effect of cable–reinforcement. The aim is to take a square sheet and move the corners diagonally out and compare the deformations with and without cable reinforcement along the edges. Since we anticipate high stretch gradients at the corners, we choose the Ogden's three–term strain energy function [Cf. (3.59)]. But before we present the actual mesh and actual deformation we intend, we use a very simple mesh with very small diagonal deformations at the corners just to show that because of singularities at the corners, the mesh will degenerate if it is not consistent with the deformation. Figure 5.17 shows a 10 by 10 square mesh with side L that is used for this purpose. There are no cable reinforcements and the deformation consists of moving the corners diagonally out such that after deformation, each two neighboring corners are 1.05L apart. Figure 5.18 is found as the converged deformed configuration and in order to show the zones edges clearly, we haven't used any means to distinguish between different stress states for the zones. As it is clearly seen, the mesh is severely deteriorated due to unsuitable topology of the mesh even though the deformation is small. As it was mentioned in the previous chapter, we redesign the mesh such that it takes care of the singularities. In our work, whenever a point load or displacement is encountered, we use a mesh that fans out from that point. That's what we have done here as it is shown in Figure 5.19 as the undeformed configuration. It consists of 861 nodes and without imposing any symmetries, the mesh is deformed such that the corner nodes are moved diagonally out and each two neighboring corners are $1.5L$ apart with L being the side of the square. Figure 5.20 shows the deformed configuration corresponding to the case of no cable reinforcement. We see that the topology of the selected mesh is consistent with the deformation and no degradation is happening. But what is significant is that the deformation seems to be happening mostly at the corners and the inside has remained almost undeformd. The stretches for this case go from a value as high as

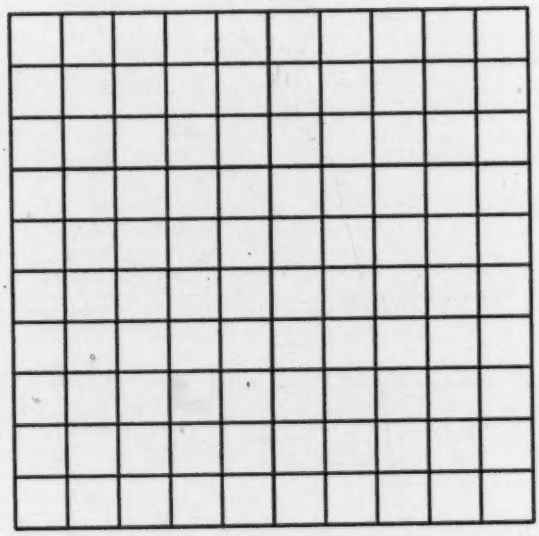

Figure 5.17: A 10 by 10 square mesh representing the initial configuration of a square with side L.

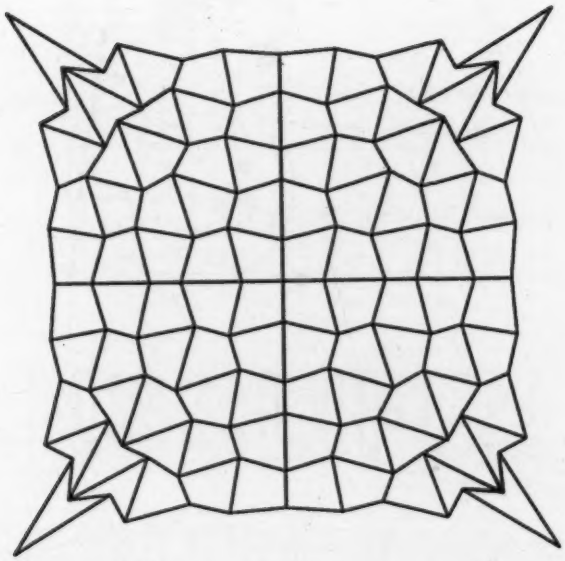

Figure 5.18: Spurious deformed configuration with corner nodes pulled out diagonally by 0.025L in the horizontal and vertical directions. Ogden material.

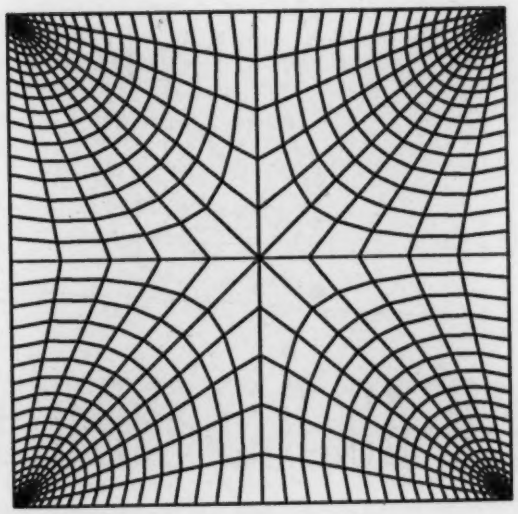

Figure 5.19: Initial configuration of a square with side L.

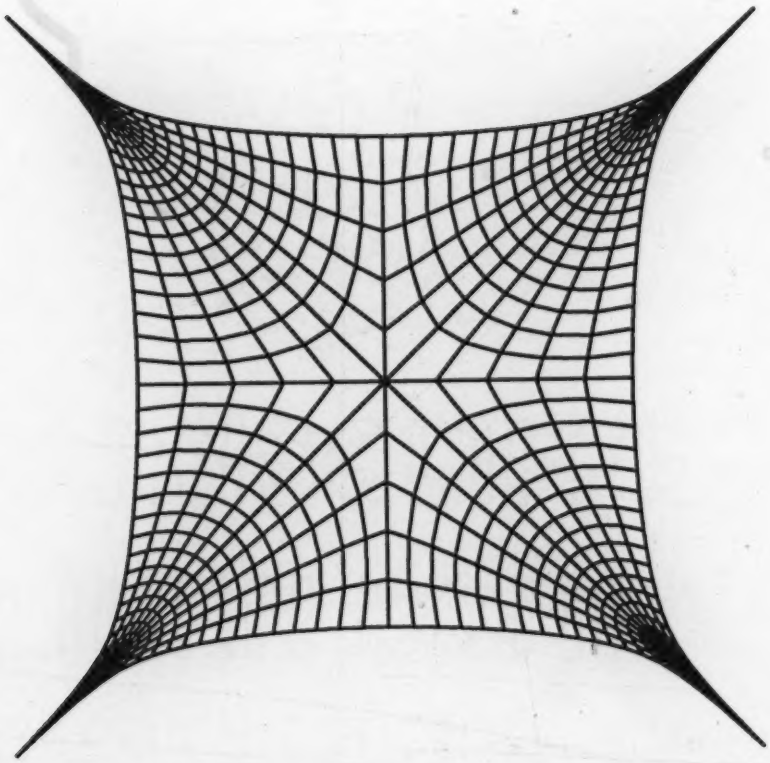

Figure 5.20: Deformed configuration. Corner nodes pulled out diagonally by 0.25L along horizontal and verical directions. Ogden material.

8.10 near the corners to a low of 1.04 near the center. Even though the deformation is small, all zones are in a tense stress state. Now if we reinforce the edges with a type–1 cable attachment with a modulus of $E/\mu L = 10.0$, and apply the same deformation, we end up with a deformed configuration that is shown in Figure 5.21. This figure shows that the deformation is now distributed to all over the domain and it's not just localized at the corners and the numbers confirm that. The highest stretch is now 1.67 at the corners and the lowest is 1.44 near the center. We see a significant drop in the sharp gradient of stretch near the corners and that's all because of the presence of cable reinforcement. If we replace this cable with a type–2 one with the same modulus, the highest and lowest values of stretch will be 2.47 and 1.42 respectively at the same locations. The reason for a larger highest stretch for this case is that in this case, there is a weaker interaction between cable and membrane. Figure 5.22 shows the deformed configuration for this case. Although the stretches are somewhat different for cable reinforcement cases, the deformed configurations look almost the same. All the zones for both cases have a tense stress state.

5.5 Inclusion

Atai and Ru (1998) have shown that in the class of harmonic materials defined by (3.54) and (3.56), if a region S_2 is embedded within another region S_1 (we call the first region *inclusion*) with a perfect bound between the two regions (so that the displacement and traction are continuous along the common boundary) and the structure is subject to uniform remote stress (at infinity), then the stress state inside the inclusion is uniform if the inclusion is an ellipse. Other shapes of the inclusion do not show such an interesting result. It can be shown (Atai and Ru, 1998) that the analytical values of the uniform stretches inside the elliptic inclusion can be found from

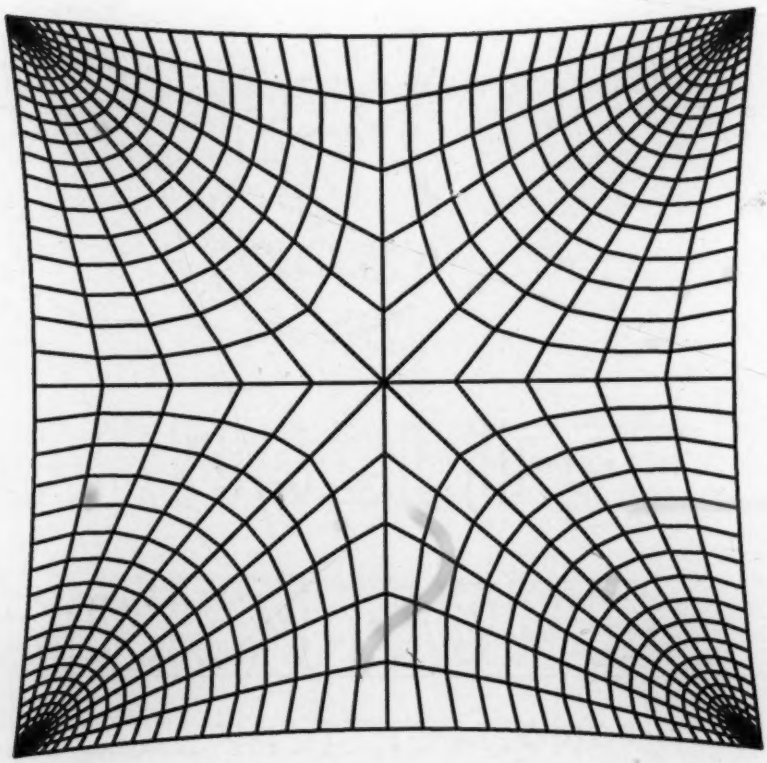

Figure 5.21: Deformed configuration. Corner nodes pulled out diagonally by 0.25L along horizontal and verical directions. Attached cable on the edges with E/μL=10. Ogden material.

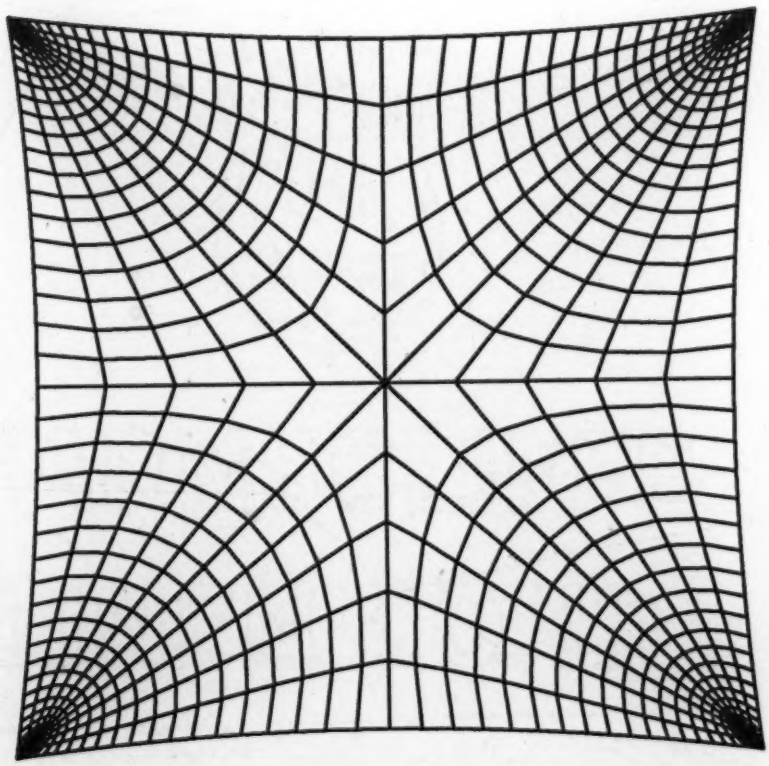

Figure 5.22: Deformed configuration. Corner nodes pulled out diagonally by 0.25L along horizontal and verical directions. Shearless cable on the edges with E/μL=10. Ogden material.

$$I = \lambda_1 + \lambda_2 = 2\frac{\alpha_2 C^2 + \beta_2}{C}$$
$$J = \lambda_1\lambda_2 = (\alpha_2 C + \frac{\beta_2}{C})^2 - D^2 \qquad (5.60)$$

where

$$C = \frac{-\hat{b} + \sqrt{\hat{b}^2 - 4\hat{\xi}\hat{\eta}}}{2\hat{\xi}} \qquad D = (A - \hat{\mu}C - \hat{\alpha}C - \frac{\hat{\beta}}{C})\frac{\hat{\lambda}}{\bar{\lambda}\hat{\gamma}}$$
$$A = \frac{t + \sqrt{t^2 + 16\mu_1^2\beta_1(1-\alpha_1)}}{4\mu_1(1-\alpha_1)} \qquad \hat{b} = A\hat{\rho} + \frac{\hat{\zeta}}{A}$$
$$\hat{\xi} = (\hat{\alpha} + \hat{\mu})[\alpha_1\bar{\lambda}(1 - \frac{\hat{\lambda}^2}{\bar{\lambda}^2}) + \frac{\hat{\lambda}^2}{\bar{\lambda}\hat{\gamma}}] - \alpha_2\bar{\lambda} \qquad \hat{\rho} = (\alpha_1\hat{\gamma} - 1)\frac{\hat{\lambda}^2}{\bar{\lambda}\hat{\gamma}}, \quad (5.61)$$
$$\hat{\eta} = \beta_2\bar{\lambda}(\alpha_1\hat{\gamma} - 1)(1 - \frac{\hat{\lambda}^2}{\bar{\lambda}^2}) \qquad \hat{\zeta} = \beta_1\bar{\lambda}$$
$$\hat{\mu} = \frac{\mu_2}{\mu_1} \quad \hat{\gamma} = 1 - \hat{\mu} \quad \hat{\alpha} = \hat{\gamma}\alpha_2 \quad \hat{\beta} = \hat{\gamma}\beta_2 \quad \hat{\lambda} = \frac{a+b}{2} \quad \bar{\lambda} = \frac{a-b}{2}$$

a and b are the semi- major and minor axes of the ellipse (the semi-major axis is assumed to be along horizontal line), t is the magnitude of the tensile stress (or traction) at infinity,and μ, α, β are the material constants with subscript 2 refering to the inclusion and subscript 1 to the surrounding media.

In this example, we try to investigate this result numerically. Figure 5.23 shows the grid corresponding to a square with side L and an elliptic region embeded in that with dimensions $a = 2b = 0.05L$ where a and b are semi-major and minor axes of the ellipse respectively (we've tried to make the dimensions of ellipse as small as possible as compared to the size of the square so that the concept of uniform stress at infinity is simulated to a good extent). We've used the orthogonal grid mapping technique to generate the mesh for the ellipse and for the square with the elliptic hole at the center. We consider different material constants for the inclusion and the square (for simplicity, we just use different μ's and α and β are taken to be 1/2 for both regions).

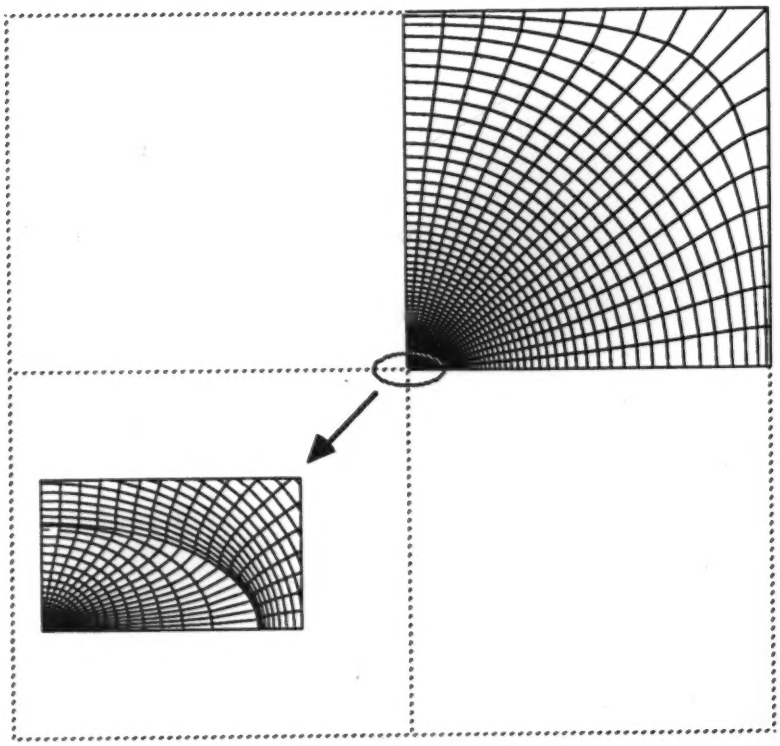

Figure 5.23: Initial configuration of a square with Side L with an elliptic inclusion of dimensions a=2b=0.05L (dotted lines show the boundary of the square and inclusion and the lines of symmetry). The area near the inclusion is enlarged to show the details of the mesh

Next, we apply an equibiaxial traction of magnitude $t = \mu_1/2$ normal to the sides of the square and we analyze the structure under such a loading. The stretches inside the inclusion turn out to be uniform as suggested analytically. Table 5.1 shows the comparison of the analytical and numerical values of the stretches inside the inclusion for several cases of material constants. The first column shows the ratio of the material constant in the inclusion to that of the surrounding media. The next four columns show the maximum and minimum values of the horizontal and vertical stretches inside the inclusion resulted from the numerical computations and the last two columns show the analytical values for those stretches. As it is seen, there is a very good agreement between numerical and analytical results.

μ_2/μ_1	Numerical				Analytical	
	λ_{1min}	λ_{1max}	λ_{2min}	λ_{2max}	λ_1	λ_2
5.0	1.00525	1.00548	0.99774	0.99798	1.00511	0.99811
3.0	1.00895	1.00904	0.99958	0.99971	1.00900	0.99967
1/3	1.16509	1.17072	1.07803	1.08183	1.16411	1.07839
1/5	1.25287	1.25389	1.10126	1.10149	1.25238	1.10129
1/10	1.36139	1.36265	1.12467	1.12492	1.35985	1.12480

Table 5.1: Comparison of numerical and analytical stretches for elliptic inclusion

In order to investigate other shapes of the inclusion. We replace the ellipse with an extended circle (a shape made up of two semicircles facing each other and two lines parallel to the center lines joining the semicircles together). Figure 5.24 shows the grid resulted from orthogonal mappinf technique for this case. The size of the extended circle is $l/2 = r = .025L$ where l is the length of the connecting lines and r is the radius of semicircles. Once again, we apply an equibiaxial traction of magnitude $t = \mu_1/2$ normal to the edges of square and analyze the structure. Table 5.2 shows the maximum and minumum values of the principal stretches inside the inclusion. Although for

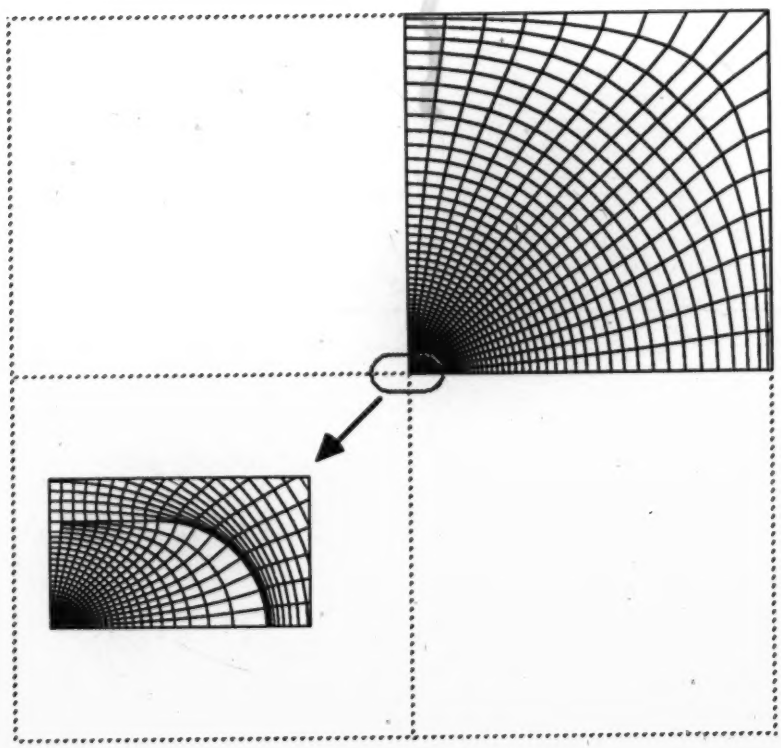

Figure 5.24: Initial configuration of a square with Side L with an extended circle inclusion of dimensions r=l/2=0.025L (dotted lines show the boundary of the square and inclusion and the lines of symmetry). The area near the inclusion is enlarged to show the details of the mesh

inclusions stiffer than the square the results might seem uniform, but that's because there hasn't been much deformation inside the inclusion and cases of softer inclusion clearly show that the state of stress is not uniform inside the inclusion and that's once again according to the analytical expectations.

μ_2/μ_1	Numerical			
	λ_{1min}	λ_{1max}	λ_{2min}	λ_{2max}
5.0	1.00376	1.00693	0.99636	0.99939
3.0	1.00695	1.01110	0.99762	1.00157
1/3	1.14112	1.17972	1.06555	1.09848
1/5	1.20682	1.28388	1.08095	1.13475
1/10	1.28673	1.41347	1.09531	1.17397

Table 5.2: Numerical stretches for extended circle inclusion

5.6 Suturing

In this section, we present some examples in which the undeformed configuration consists of two or more pieces that are to be sutured according to the procedure described in the previous chapter. Due to the incompatibility between the edges to be sutured, in general, we anticipate wrinkling to occur as it will be seen in the following examples. The first example shows two symmetric chevron–shaped pieces of membrane each consisting of 121 nodes (Figure 5.25). The distance between vertical edges is $10L$, horizontal edges of each piece are $4L$ apart, and the distance between the vertex of each piece and its vertical edge is $4L$, where L is the length scale. The material is neo–Hookian and without imposing any symmetry conditions, the deformation consists of holding the vertical edges fixed while the facing oblique edges are to be sutured together. As it was mentioned in the previous chapter, because the edges to be sutured are of the same length and are connected together such that each point matches its mirror image, we have continuity of

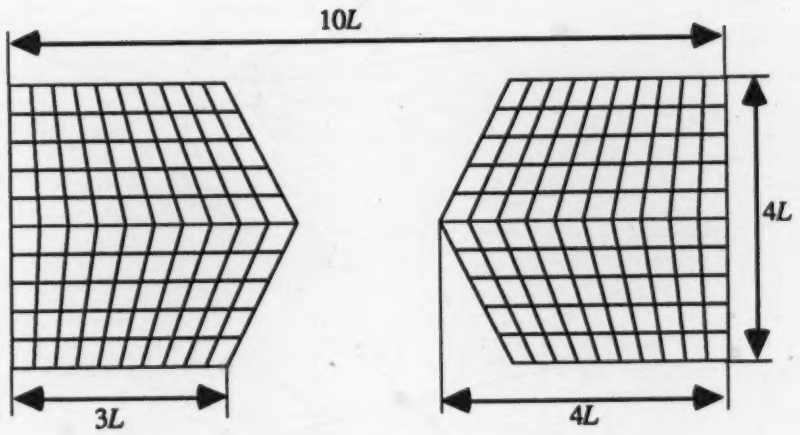

Figure 5.25: Undeformed configuration of two chevron shaped pieces fixed at the vertical edges. Facing edges are to be sutured.

traction as well as continuity of force along the sutured edge. Figure 5.26 shows the deformed configuration. The straight lines in some zones show the tensile trajectories in the wrinkled regions. As expected, the deformed configuration is symmetric (both vertically and horizontally as is the undeformed configuration and the applied deformation) and in the wrinkled regions, the tense direction is almost parallel to the direction of stretching the two pieces in order to suture them together. The maximum computed stretch is about 2.06 and it occurs near the top and bottom of sutured edges. As a second example, we replace one of the above two pieces by a square of side $4L$ such that the distance between the vertex of the other piece and the closest vertical edge of the new piece is the same as the distance between the vertexes of the old two pieces!!!! (Figure 5.27). Applying the same deformation as before, we get figure 5.28 as the deformed configuration. This time, we see only symmetry about the horizontal middle line and since the length of the sutured edges are not identical, we only have continuity of force across the sutured edge. Again we see some wrinkling with tensile trajectories almost parallel to the stretch direction as expected. The largest stretch computed is now about 1.61 at the zone centers of the regions at the upper and lower right–hand corners of the square and the reason for decrease of the maximum stretch is that in this case, the corresponding points on the top and bottom of the suturing edges are closer as compared to the previous case.

5.7 Three dimensional tents

As a final set of examples, we present two practical analyzes of fabric tension structures. In the first one, which is a six pole tent, 16 pieces of membrane are sutured together to form the tent (Figure 5.29). The base of the tent is $60'$ by $100'$ and the height of the poles is $17'$. The undeformed configuration shows the pieces that are laid on top of each other and we can see pieces overlapping. These 16 pieces actually consist of 4 sets of 4 different pieces;

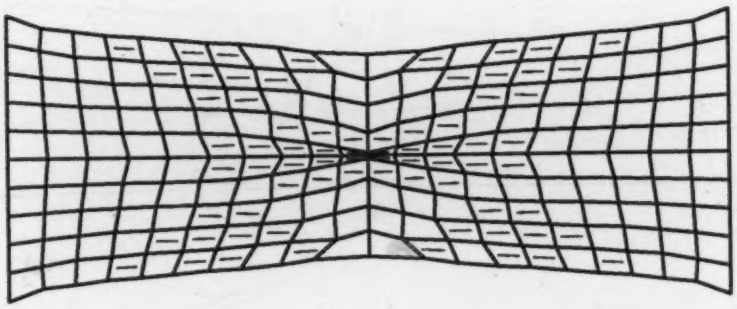

Figure 5.26: Deformed configuration of two chevron shaped pieces fixed at the vertical edges. Facing edges are sutured. Neo-Hookian material

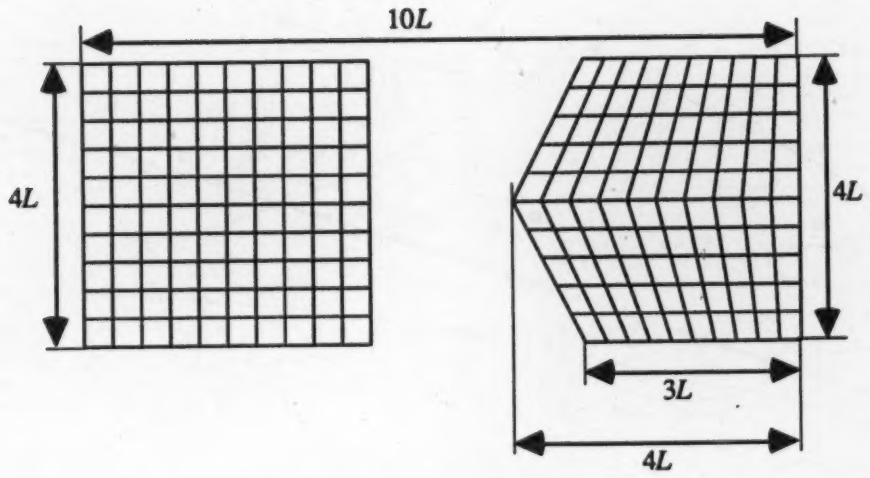

Figure 5.27: Undeformed configuration of a chevron shaped piece and a square one fixed at the outer vertical edges. Facing edges are to be sutured.

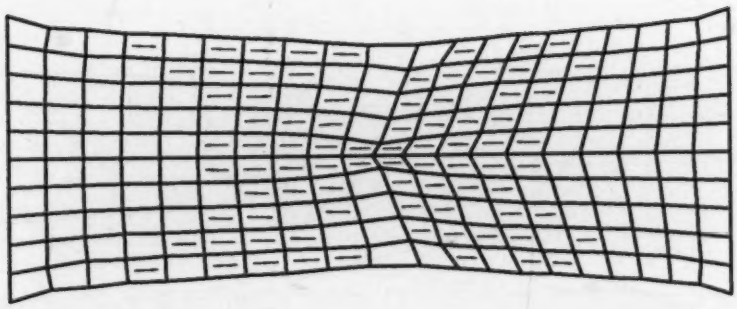

Figure 5.28: Deformed configuration of a chevron shaped piece and a square one fixed at the outer vertical edges. Facing edges are sutured. Neo-Hookian material.

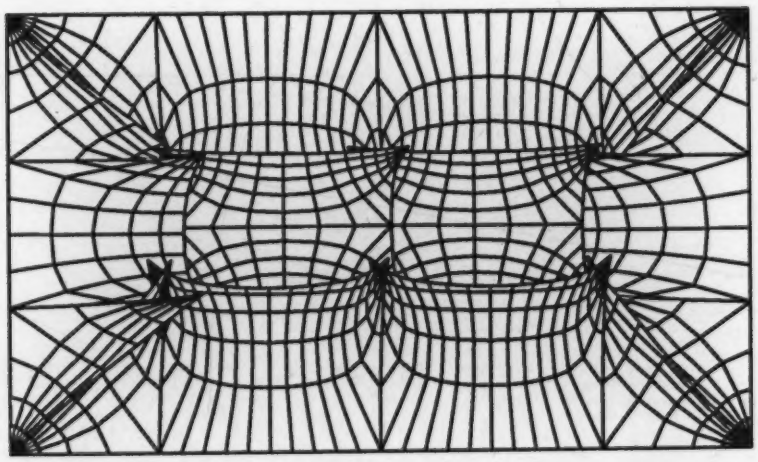

Figure 5.29: Undeformed configuration of a 6-pole tent. 16 pieces of membrane are to be sutured together to form a tent with a base of 60 by 100 and a height of 17 at the pole tips.

one triangular piece at the corner, and three rectangular pieces surrounding it. The middle pieces can be added to make the tent 8 pole, 10 pole, etc. These pieces are derived from patterning a deformed membrane that was initially rectangular and flat and was raised at 6 points where the poles are and the method for patterning is the one described by Tabbarok and Qin (1992). The mesh is then added to the pieces and it's in such a way that after suturing and erecting, mesh lines fan out from the pole points (singular points). The deformation consists of holding the rectangular boundary fixed, suturing the pieces together and raising the nodes at the position of the poles which have a projected distance of 20′ from each other and the edges. The material used is neo-Hookian. Figure 5.30 shows the deformed configuration in an angle view and in order to keep things clear, we haven't distinguished between different states of stress for the zones but because the patterns are obtained in a way to minimize the strain in the structure after the erection, we anticipate some wrinkling and that is the case. The maximum stretch is about 1.04 happening at the position of the poles. As the second and final example, we consider a single pole tent that shows the effect of cable reinforcement and patterning. If we take a square sheet and fix it at the corners and raise the center point out of the plane of the sheet, we expect a high stress gradient at the position of the pole (from computational data and an Ogden material, raising the center point by half the side of the square results in a high stretch of 3.0 at the point of raise). So if we divide the square into 8 equal triangles with a common point at the center and extend them near that point, we anticipate a lesser stretch at the center point (position of the pole) and that's what we are going to show here. Figure 5.31 shows the undeformed configuration of two overlapping triangles (these are extension of the triangles we talked about). The reference configuration actually consists of repetition of these extended triangles by rotating each pair by 90 degrees to get the next pair (as it is suggested by the dotted lines in Figure 5.31). But because of the existing symmetry in the problem, we need to analyze

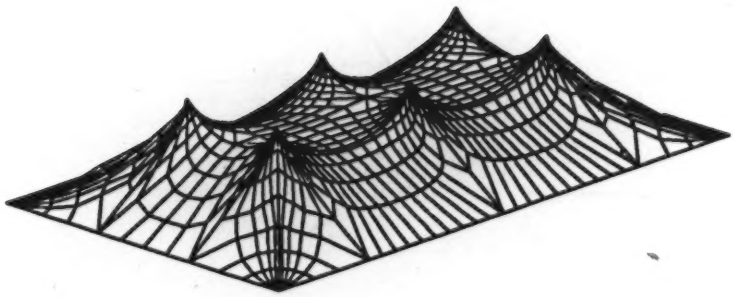

Figure 5.30: Angle-view of the deformed configuration of the 6-pole tent. Ogden material.

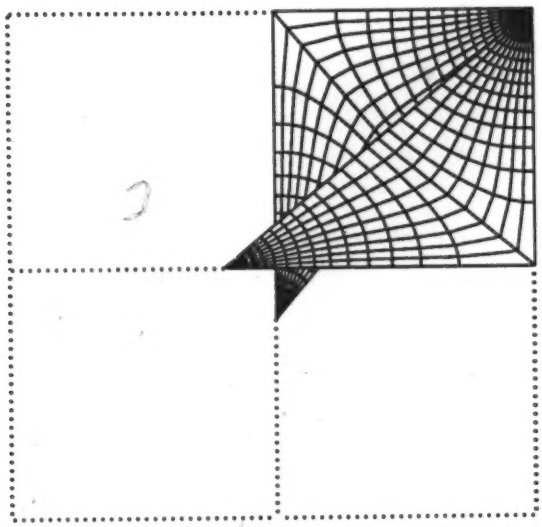

Figure 5.31: Overlapping meshes of two extended triangles which are to be sutured and form a quarter of a single-pole tent with a square base. Dots show the lines of symmetry.

only the shown pair provided that symmetry constraints are observed at the edges that are to be connected to the other pairs (edges along x_1 and x_2). These conditions are imposed by requiring the x_2 components of the nodes on the edge along x_1 and the x_1 components of the nodes on the edge along x_2 to remain constant throughout the numerical analysis. The remaining components of the points on these two edges are obtained by requiring the corresponding components of the force vector at those nodes to vanish (If we had considered the whole reference configuration, the total force components for these nodes was actually twice what we considered here due to the symmetry but if f_{x_1} vanishes for example, $2f_{x_1}$ vanishes too). Choosing an Ogden material, the deformation consists of holding the common point of the extended triangles (corner of the tent) fixed, suturing the triangles along the oblique edge, and raising their vertices directly above the center of the dotted square by half of the side of that, and thus creating a single pole tent. Figure 5.32 shows the side view of the deformed configuration with traction free edges. The white regions show the tense ones while the gray and black ones show the wrinkled and slack ones respectively. The maximum stretch is about 2.69 occurring near the corners. It is interesting to notice how a very rough pattern could reduce the maximum stretch to this extent and it shows the importance of the patterning issue. Figure 5.33 shows the side view of the deformed configuration for a type–1 cable reinforcement with a modulus of $E/\mu L = 0.5$ (L is the side of the square) applied at the edges. We can see that the wrinkled region (shaded zones) has become smaller and slack regions are eliminated. The maximum stretch is about 2.60 but it's now happening near the apex. If we replace this cable with a type–2 one with the same modulus, we get a maximum stretch of 2.30 near the corners and the zones around the corners are in a tense state but in the previous case they were wrinkled. Figure 5.34 shows the side view of the deformed configuration for this case. These two latter cases show the importance of application of cable reinforcement and its role in eliminating the unwanted wrinkling.

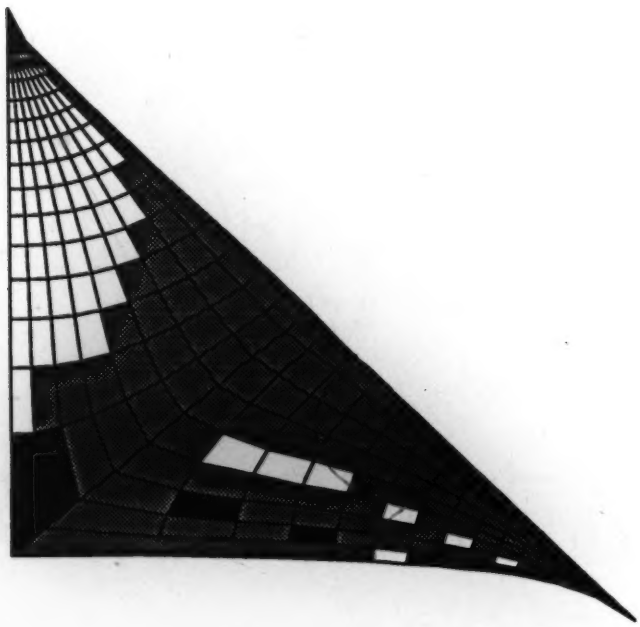

Figure 5.32: Side-view of the deformed configuration for single-pole tent with no cable reinforcement. Ogden material.

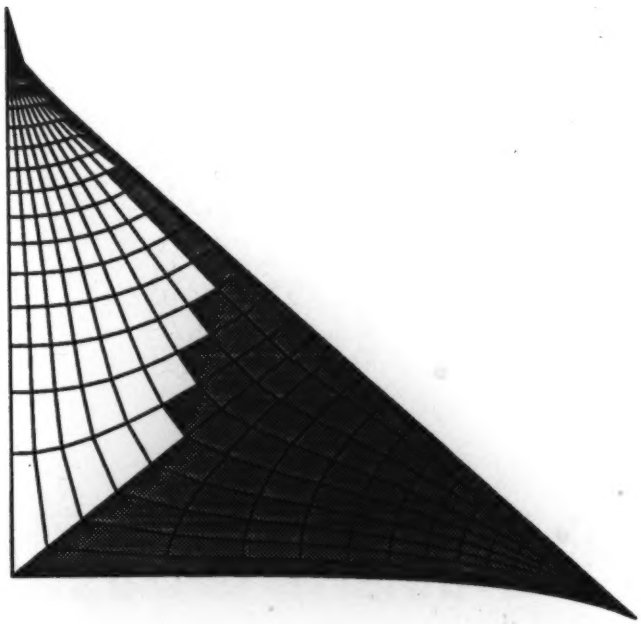

Figure 5.33: Side-view of the deformed configuration for single-pole tent with attached cable reinforcement of $E/\mu L$=0.5 on the edges. Ogden material.

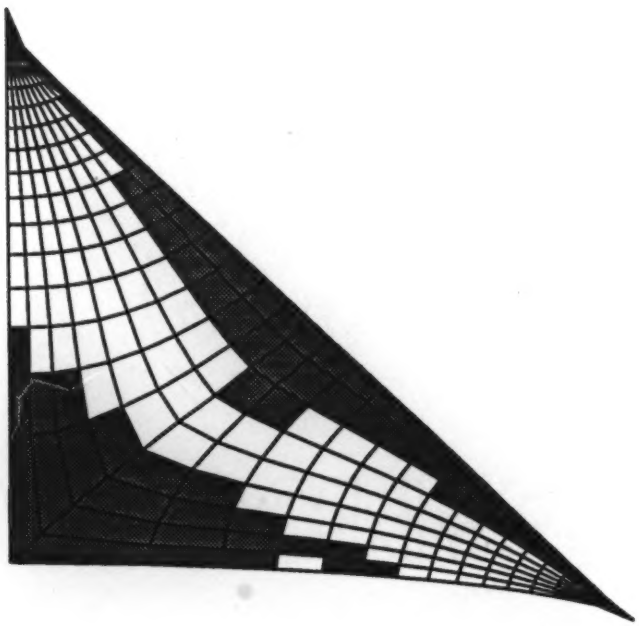

Figure 5.34: Side-view of the deformed configuration for single-pole tent with shearless cable reinforcement of $E/\mu L$=0.5 on the edges. Ogden material.

Chapter 6

Experimental results

In this section, we intend to experiment with the axisymmetric annulus problem with and without cable reinforcement discussed in the previous chapter and compare the results with numerical and analytical ones. We take a natural rubber sheet with a thickness of $\frac{1}{16}''$ and the first step is to find out which material model best describes the behavior of this rubber. Since the uniaxial response of the material can be regarded as the *relaxed* 2D response, we perform a uniaxial test on the rubber fitting the data with the relaxed form of a material model, we can then use the unrelaxed strain energy as the model for the response under biaxial stretch. To ensure isotropy of the rubber, we cut two strips of rubber in two different directions and check to see if their test results are more or less the same (isotropy) or not (anisotropy). We base our testing procedure including the preparation of the specimens mainly on the DIN standard for testing rubber (ASTM D412, 1997). The dimension of strips is $11'' \times 0.56''$ and in order to measure the strain in the rubber in an area where it is uniform to a good degree, we draw two parallel lines (benchmarks) across the width of the strip and symmetric about the middle line of the strip with a distance of $2''$. Figure 6.1 shows the setup for uniaxial test schematically. One end of the strip is connected to a fixed load cell and the other end to a movable grip which can be given a specific displacement (although we are not using this specific displacement in our calculations).

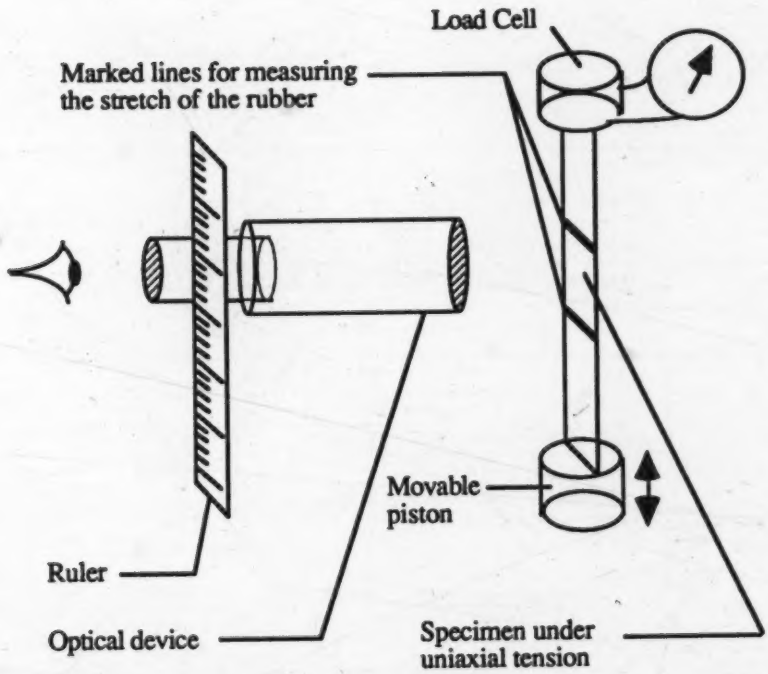

Figure 6.1: Schematic of setup for the tensile test of the rubber

To get a datapoint, we displace the grip and hold it there. Then we read the signal from the load cell which is proportional to the force at the ends of the strip and using an optic device, we measure the distance between the benchmarks and from that the stretch (strain) in the rubber is calculated. We repeat this procedure to cover a strain range of 0 to .60 which is sufficient for the experiments that we want to perform. Figure 6.2 shows the non-dimensionalized datapoint from this test (which turned out to be quite the same for both strips). It also shows the uniaxial force-stretch relation for the neo-Hookian material fitted to those points as the best model for the behaviour of the rubber over the specified range of strain. The stress-stretch relation for this material is given by

$$\sigma = G(\lambda - \lambda^{-2}) \tag{6.1}$$

where σ is the stress, λ is the stretch and G is the shear modulus of the rubber. This relation could also be derived by taking the derivative of the relaxed strain energy for the neo-Hookian material [Cf. $(3.53)_2$]. Doing so and comparing it with (6.1), we can write $\mu = Gh$ where h is the thickness of the sheet and thus we can calculate the material constant for the rubber. The load f in Figure 6.2 is divided by the shear modulus G, the rubber thickness h, and the width of the strip w to make it nondimentional. Now that we have the material strain energy and constants, we start the experiments. First of all, we take the rubber sheet and draw a mesh on that as shown in Figure 6.3. It shows circles starting with a radius of 3.75″ and ending with a radius of 7.5″ and with a radius increment of 0.75″. It also shows radial lines with an angle of 45 degrees between them. This is the grid that we are using in our calculation of experimental stretches. In order to apply the equibiaxial stretches, we use two wooden frames (one on each side of the rubber sheet) with a circular hole of radius 9.25″ and stretch the sheet by hands gradually so that the biggest circle of the grid coincides with the edge of the circular hole on the frames and then we clamp the frames to hold the sheet stretched.

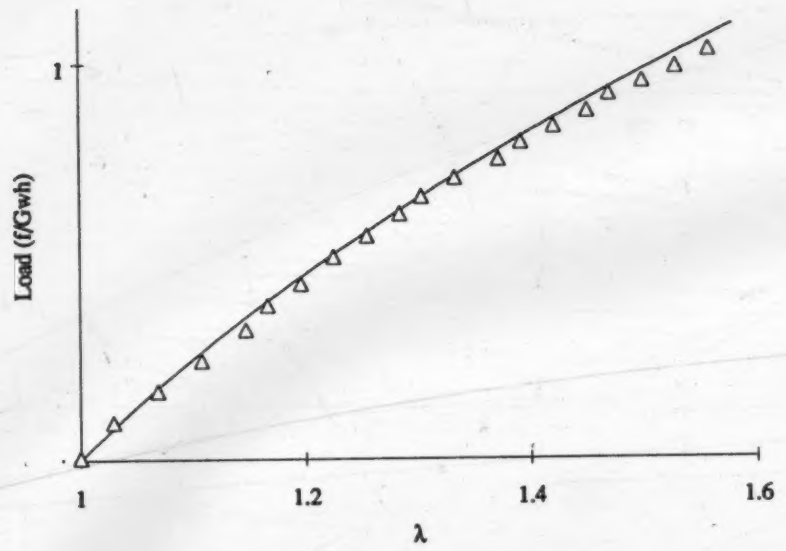

Figure 6.2: Results of uniaxial tensile test on rubber; (Δ) datapoints,(——) fitted curve.

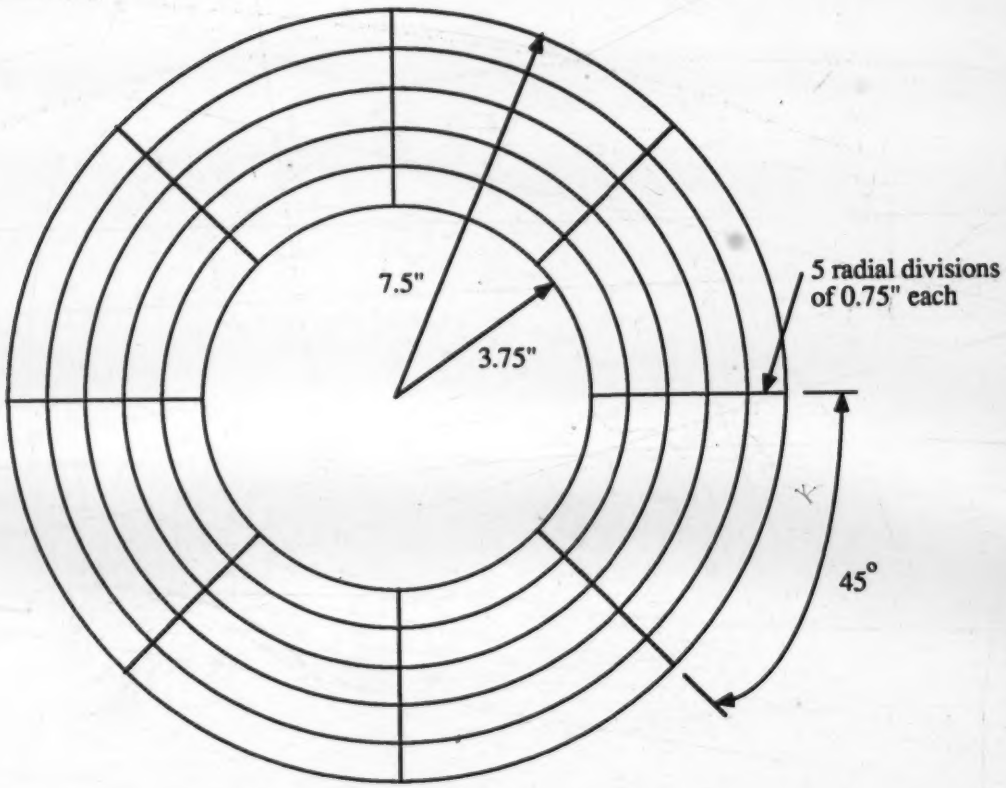

Figure 6.3: Grid used for stretch calculations

As a very simple experiment, we stretch the sheet without any holes or reinforcements as described above. We expect to have a uniform stretch of $\frac{9.25}{7.5} \approx 1.233$ everywhere. Figure 6.4 shows the distribution of the measured stretches vs. radius in the undeformed configuration. It can be seen that the hoop stretch very well matches the expected value but the radial stretch fluctuates around that. The reason is that the hoop stretch is calculated from $\lambda_2 = \rho/r$ and thus it's just a matter of measuring the undeformed and deformed radii at the nodes which is an easy and fairly accurate task, but the radial stretch is calculated from $\lambda_1 = \rho'$ and since the mesh drawn in Figure 6.3 is very coarse, the value of the derivative which is approximated by finite difference is not very accurate. We will see this inaccuracy in the radial stretch for the rest of the experiments. Now we cut a hole with a radius of 3.75″ (along the smallest circle of the mesh on the rubber) and we repeat the stretching experiment. Figures 6.5 and 6.6 show the deformed configuration and distribution of stretches vs. radius respectively. As it can be seen, there is a very good match between experimental, numerical and analytical results for the hoop stretch. To simulate the cable reinforcement, we cut a ring with an inner and outer radius of 3.75″ and 4.25″ respectively from another rubber sheet made up of the same material and using a rubber contact cement, we glue it to the rubber sheet with the hole such that the boundary of the hole and the inner boundary of the ring coincide (Figure 6.7). We stretch the reinforced rubber and measure the stretches. Figure 6.8 shows the comparison of stretches for the experimental, numerical and analytical methods. It should be noted that a neo-Hookian cable model is used for analytical and numerical data, so the force magnitude f used in (5.14) is calculated from $f = \sigma wh$ where w is the width of the ring (0.5″) and σ is calculated from (6.1) with λ being the hoop stretch at the hole boundary. Thus the non–dimensionalized cable modulus [Cf. (5.34)] would be $E/\mu r_i = (Gwh)/(Ghr_i) = w/r_i = 0.5/3.75$. It can be seen from the graph that the hoop stretch (which is assumed to be more accurate than the radial stretch)

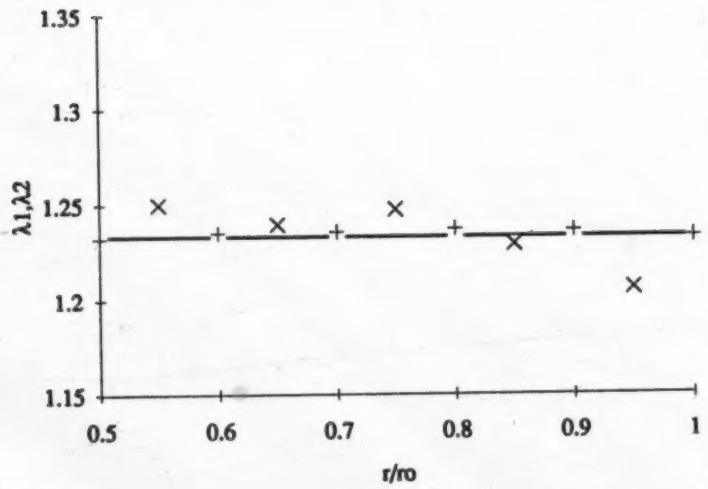

Figure 6.4: Distribution of stretches vs. radius for the rubber; (×) experimental radial stretch, (+) experimental hoop stretch, (——) analytical result

Figure 6.5: Deformed configuration for the rubber sheet with a hole and no reinforcement

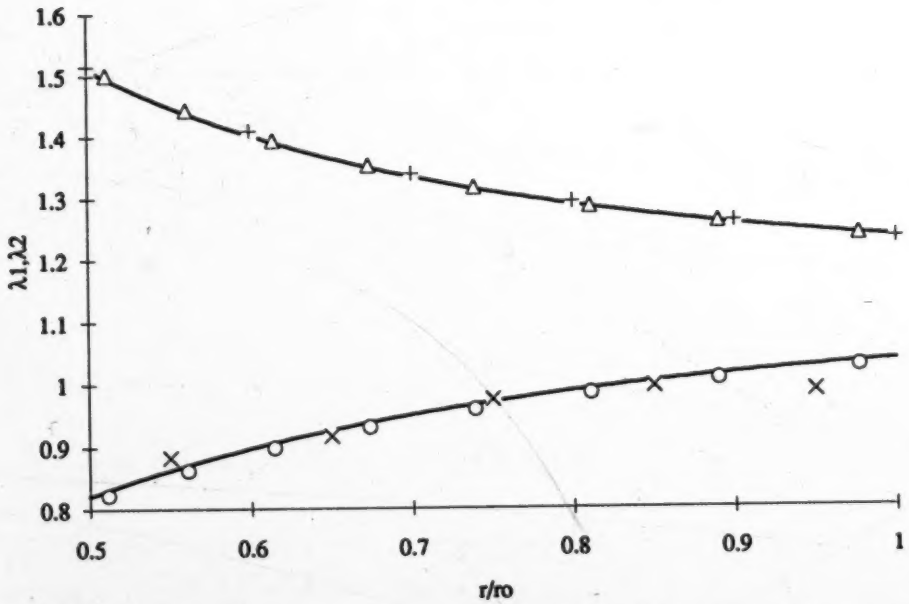

Figure 6.6: Distribution of stretches vs. radius for rubber; (Δ) numerical hoop stretch, (O) numerical radial stretch, (+) experimental hoop stretch, (×) experimental radial stretch, (——) analytical results

Figure 6.7: Undeformed configuration for the rubber sheet with a hole and a reinforcement ring around the hole

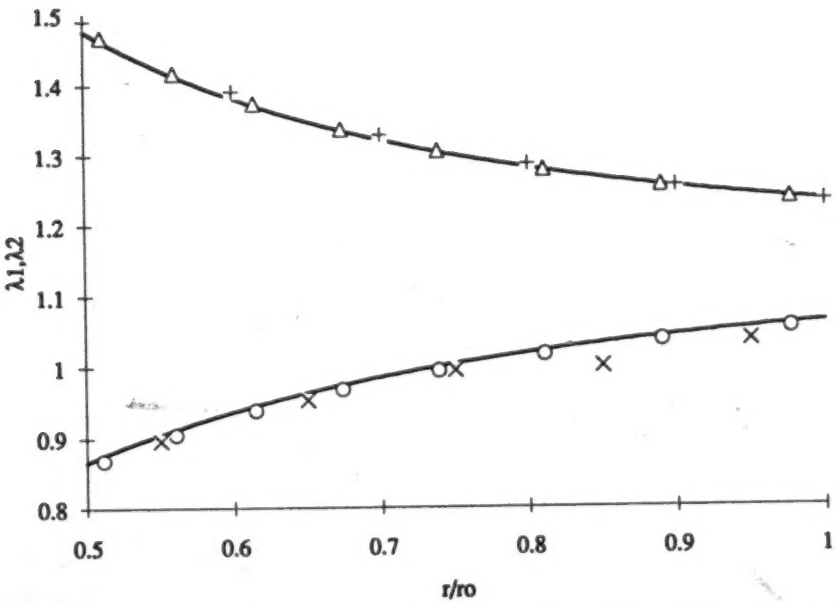

Figure 6.8: Distribution of stretches vs. radius for rubber; (Δ) numerical hoop stretch, (O) numerical radial stretch, (+) experimental hoop stretch, (×) experimental radial stretch, (——) analytical results

is higher in the experiment near the hole and it gets closer to the other two results as the radius increases. The reason could be that in the analytical and numerical cases, it is assumed that the reinforcement is concentrated at the hole boundary but it is obvious from the experiment that the reinforcement is actually distributed across the width of the ring. Since for the case of no reinforcement, the hoop stretch is decreasing with the increase of the radius, adding a distributed reinforcement along the hole boundary is almost equivalent to having a less stiff cable concentrated at the hole boundary and that's why the experiment shows a higher hoop stretch near the hole. A more accurate model for this case would be a rubber sheet which has a ring in the center made up of a material twice as stiff as the rest of the sheet (the analytical result for this case is hard to get). Finally, another ring with the same dimensions is glued to the other side of the already reinforced rubber sheet and the experiment is repeated. Figures 6.9 and 6.10 show the deformed configuration and distribution of stretches respectively. Same behaviour of stretches are seen as compared to the one–ring case. Although our goal was to reproduce the neutral hole case experimentally, we couldn't accomplish that because it required having a stiffer rubber as the cable reinforcement, testing it to get the material constants, calculating the required width of the ring for reinforcement. And still the ring had to be narrow enough so that the reinforcement could be regarded as concentrated along the hole boundary. Despite all these, the present experiment showed a fairly good agreement with analytical and numerical results and showed the behaviour of the cable reinforcement qualitatively. The neutral hole case can be left as a future work.

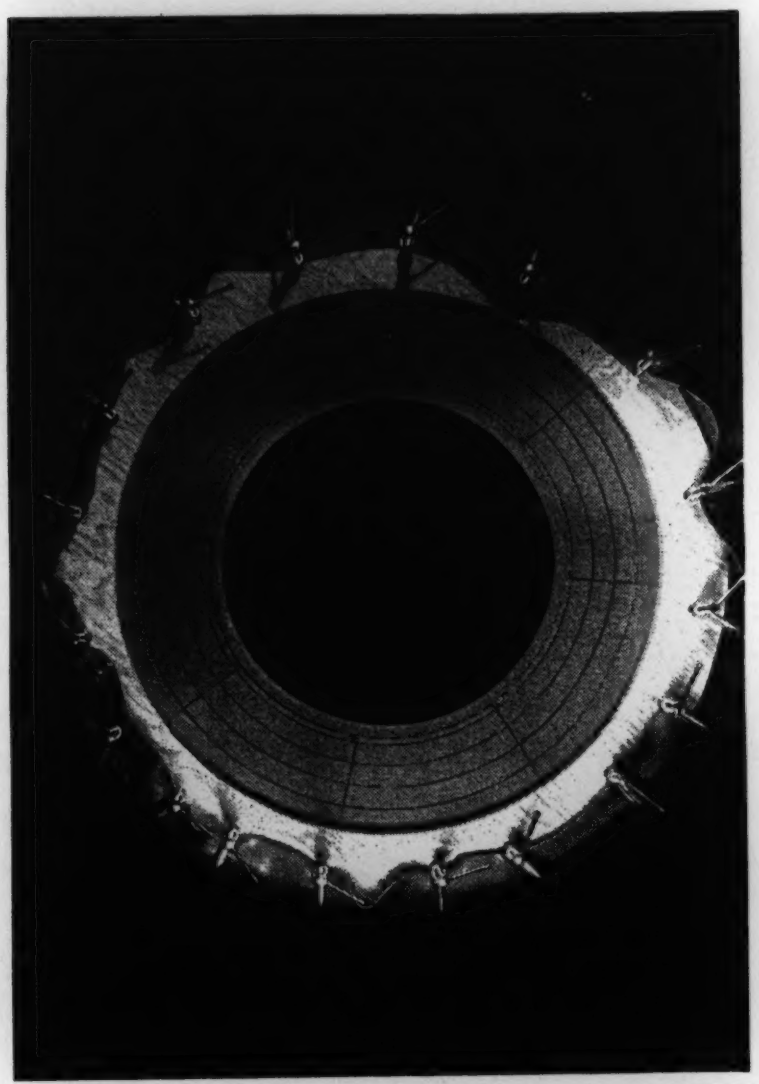

Figure 6.9: Deformed configuration for the rubber sheet with a hole and two reinforcement rings around the hole

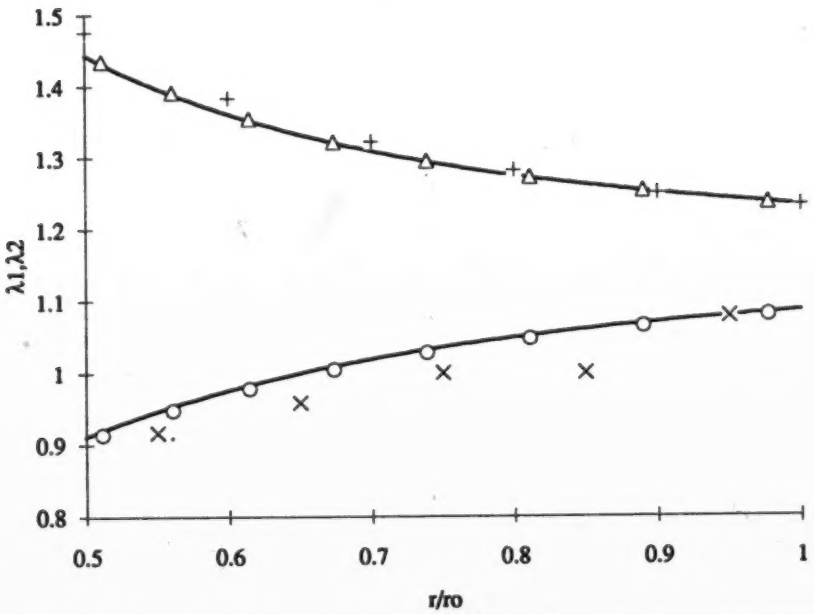

Figure 6.10: Distribution of stretches vs. radius for rubber; (Δ) numerical hoop stretch, (O) numerical radial stretch, (+) experimental hoop stretch, (×) experimental radial stretch, (——) analytical results

Chapter 7

Conclusion and Summary

In this work, a discussion of perfectly flexible elastic curves (cables) and surfaces (membranes) based on earlier works is presented. The equations of equilibrium for a cable–membrane system are derived using variational theory. Two types of cable attachments which are practical are considered: attached and shearless. The coupling conditions between membrane and each type of cable attachment are discussed. These coupling conditions relate the change of the force vector along the cable with the traction at the boundary. To model a common practice in structural design, the undeformed configuration is allowed to consist of several disjoint pieces and then these pieces are sutured together and the resulting structure is analyzed under applied loading. The relation between sutured pieces, which is derived as a consequence of variational procedure, is interpreted as the continuity of force across the sutured edge and as the continuity of traction if the mapping that puts one edge on top of the other one has a deformation gradient of unit tensor. The necessary conditions for stability of the equilibrium configuration are derived for both membrane and the cable. For the membrane, these conditions state that $\partial w/\partial \lambda_\alpha = w_\alpha$ be non–negative. This is for an isotropic membrane but if an orthotropic one is thought of as a cable network, the same conditions apply to that but in that case, λ_α's are the stretches along the fibers. For the type–1 cable attachment, the cable force and its modulus should be non–negative

but for the type–2 cable attachment, this only reduces to a non–negative cable force. The strain energies for the membrane and cable are then *relaxed* to take those conditions into account automatically. The Green's theorem is used to find the finite difference form of the equations of equilibrium for a discretized domain. A numerical method called *dynamic relaxation* is used to solve those equations. This method considers the problem as a damped dynamic one and the solution to the equilibrium equation is the steady state response of the dynamic system. The method has the advantage of not making direct use of stiffness matrix and needs less memory requirement because it only deals with vectors rather than matrices. These features makes it a preferable choice over methods that need the calculation of in this case a very complicated stiffness matrix such as Newton–Raphson. Since the errors in the approximations are minimized if the zones are as close to rectangles as possible, a boundary–fitted orthogonal coordinate generating method is used to generate the mesh for numerical calculations. Wherever the analytical results are available, the numerical ones show a very good agreement with them. The circular and elliptic neutral holes are very interesting examples of this case. The effect of cable reinforcement in reducing the sharp gradient of stretches specially near the singularities is shown by some numerical examples. The qualitative behavior of the cable–membrane system is illustrated by an experiment and the results show close agreement with analytical and numerical results. Although it was intended to simulate the circular neutral hole with the experiment, some difficulties didn't allow for that and this part can be done in the future. Also there is a need to model fabric materials which are mostly orthotropic with shear resistance in order to investigate the behavior of structures as close to the real case as possible. Another important issue that needs attention is *patterning*. Current methods are mainly practical and lack the theoretical background and the clear definition of the optimization criterion. This also could be a potential for future work.

Bibliography

Acerbi, E. and Fusco, N. (1984) Semicontinuity problems in the calculus of variations. *Archive for Rational Mechanics and Analysis* **86**, 125-145.

ASTM D412 (1997) Standard test methods for vulcanized rubber and thermoplastic rubbers and thermoplastic elastomers - Tension *ASTM Standards* bf D412 41–53

Atai, A. (1997) Numerical analysis of membrane structures. *Proceedings of the IASS International Symposium 97 on Shell and Spatial Structures, November. 97, Singapore* 163–172

Atai, A. and Ru, C.Q. (1998) Complete solution of elliptic inclusion in a harmonic material (in progress)

Atai, A. and Steigmann D.J. (1997) On the non–linear mechanics of discrete networks. *Archive of Applied Mechanics* **67**, 303-319.

Atai, A. and Steigmann D.J. (1998) Coupled deformations of elastic curves and surfaces. *International Journal of Solids and Structures* **35**, 1915–1952.

Ball, J.M. (1977) Convexity conditions and existence theorems in nonlinear elasticity. *Archive for Rational Mechanics and Analysis* **63**, 337-403.

Bufler, H. and Schneider, H. (1994) Large strain analysis of rubber–like membranes under dead weight, gas pressure, and hydrostatic loading.*Computational Mechanics* **14**, 165–188.

Carroll, M.M. (1988) Finite strain solutions in compressible elasticity. *Journal of Elasticity* **20,** 65–92.

Como, M. and Grimaldi, A. (1995) *Theory of Stability of Continuous Elastic Structures.* CRC Press, Boca Raton, FL.

Dacarogna, B. (1989) *Direct Methods in the Calculus of Variations.* Springer, Berlin.

Fisher, D. (1988) Configuration dependent pressure potentials. *Journal of Elasticity* **19,** 77–84.

Flanagan, D.P. and Belytschko, T. (1981) A uniform strain hexahedron and quadrilateral with orthogonal hourglass control. *International Journal for Numerical Methods in Engineering* **17,** 679–706.

Graves, L.E. (1939) The Weirstrass condition for multiple integral variation problems. *Duke Mathematical Journal* **5,** 656–660.

Haseganu, E.M. and Steigmann, D.J. (1994a) Analysis of partly wrinkled membranes by the method of dynamic relaxation. *Computational Mechanics* **14,** 596–614.

Haseganu, E.M. and Steigmann, D.J. (1994b) Theoretical flexural response of a pressurized cylindrical membrane. *International Journal of Solids and Structures* **31,** 27–50.

Haseganu, E.M. and Steigmann, D.J. (1996) Equilibrium analysis of finitely deformed elastic networks. *Computational Mechanics* **17,** 359–373.

Hermann, W. and Bertholf, L.D. (1983) Explicit Lagrangian finite–difference methods. *Computational Methods for Transient Analysis,* eds T. Belytschko and T.J.R. Hughes, pp. 361–416. Elsevier, Amsterdam.

Klouček, P. and Luskin, M. (1994) The computation of the dynamics of the martensitic transformation. *Continuum Mechanics and Thermodynamics* **6**, 209–240.

Knops, R.J. and Wilkes, E.W. (1973) Theory of elastic stability. *Handbuch der physik*, Vol. VIa/3, ed. S. Flügge, p. 125. Springer, Berlin.

Kohn, R.V. and Strang, G. (1986) Optimal design and relaxation of variational problems. *Communications on Pure and Applied Mathematics* **39**, 1–25 (Part I), 139–182 (Part II) and 353–377 (Part III).

Li, X. and Steigmann, D.J. (1995) Point loads on a hemispherical elastic membrane. *International Journal of Non-Linear Mechanics* **30**, 569–581.

Libai, A. and Simmonds, J.G. (1998) *The Nonlinear Theory of Elastic Shells*, 2nd edn. Cambridge University Press.

Mansfield, E. (1953) Neutral holes in plane sheet–reinforced holes which are elastically equivalent to the uncut sheet. *Quarterly Journal of Mechanics and Applied Mathematics* **6**, 370–378.

Naghdi, P.M. and Tang, P.Y. (1977) Large deformation possible in every isotropic elastic membrane. *Philosophical Transactions of the Royal Society of London* **A287**, 145–187.

Ogden, R.W. (1984) *Non-linear Elastic Deformations*. Ellis–Horwood, Chichester.

Papadrakakis, M. (1981) A method for the automatic evaluation of dynamic relaxation parameters. *Computational Methods in Applied Mechanics and Engineering* **25**, 35–48.

Pipkin, A.C. (1986) The relaxed energy density for isotropic elastic membranes. *IMA Journal of Applied Mathematics* **36**, 85–99.

Podio-Guidugli, P. (1988) A variational approach for live loadings in finite elasticity. *Journal of Elasticity* **19,** 25–36.

Press, W.H. *et al.*(1992) *Numerical Recipes in FORTRAN,* Cambridge University Press, England.

Ru, C.Q. (1998) A complete solution for interface crack in finite elastostatics (in preparation)

Ryskin, G, and Leal, L.G. (1983) Orthogonal mapping. *Journal of Computational Physics* **50,** 71–100

Silling, S.A. (1987) Incompressibility in dynamic relaxation. *ASME Journal of Applied Mechanics* **54,** 539–544.

Silling, S.A. (1988a) Numerical studies of loss of ellipticity near singularities in an elastic material. *Journal of Elasticity* **19,** 213–239.

Silling, S.A. (1988b) Finite difference modeling of phase changes and localization in elasticity. *Computational Methods in Applied Mechanics and Engineering* **70,** 251–273.

Silling, S.A. (1989) Phase changes induced by deformation in isothermal elastic crystals. *Journal of the Mechanics and Physics of Solids* **37,** 293–316.

Steigmann, D.J. (1986) Proof of a conjecture in elastic membrane theory. *ASME Journal of Applied Mechanics* **53,** 595–596.

Steigmann, D.J. (1991) A note on pressure potentials. *Journal of Elasticity* **26,** 87–93.

Steigmann, D.J. and Li, D. (1995) Energy-minimizing states of capillary systems with bulk, surface, and line phases. *IMA Journal of Applied Mathematics* **55,** 1–17.

Steigmann, D.J. and Ogden, R.W. (1997) Plane deformations of elastic solids with intrinsic boundary elasticity. *Proceedings of the Royal Society of London* **A453,** 853–877.

Swart, P.J. and Holmes, P.J. (1992) Energy minimization and the formation of microstructure in dynamic antiplane shear. *Archive for Rational Mechanics and Analysis* **121,** 37–85.

Tabarrok, B. and Qin, Z. (1992) Nonlinear analysis of tension structures. *Computers and Structures* **45,** 973–984.

Underwood, P. (1983) Dynamic relaxation. *Computational Methods for Transient Analysis,* eds T. Belytschko and T.J.R. Hughes, pp. 245–265. Elsevier, Amsterdam.

Varga, O.H. (1966) *Stress Strain Behavior of Elastic Materials.* Wiley, New York.

Varley, E. and Cumberbatch, E. (1980) Finite deformations of elastic materials surrounding sylindrical holes. *Journal of Elasticity* **10,** 341–405.

Wu, C.H. (1979) Large finite strain membrane problems. *Quarterly of Applied Mathematics* 347–359.

Appendix A

Boundary-Fitted Orthonormal Grids

In this section, we discuss the procedure that leads to generation of orthonormal grid for a domain with arbitrary boundary. As it was mentioned earlier, having a mesh with orthogonal grids reduces the error in approximation of the equilibrium equations. The method for grid generation discussed here is developed by Ryskin and Leal (1983).

If we consider the Cartesian coordinates x_α in the physical plane, it is obvious that these coordinates are a linear function of position. Therefore, their gradients are constant valued vector fields and we can write

$$\text{div}(\text{grad}(x_\alpha)) = \nabla^2 x_\alpha = 0, \quad \alpha \in 1,2 \tag{A.1}$$

where ∇^2 is the Laplacian operator. The above expression is true no matter in which coordinate system the Laplacian is written. Now let us consider a coordinate system (which is curvilinear in general) with components ξ_α, $\alpha \in 1,2$ (in a fictitious plane). We consider the boundary(s) in the physical plane as a coordinate line in this new system and impose the orthogonality conditions such that when a square grid in the ξ_1–ξ_2 plane is mapped onto the x_1–x_2 plane, it generates a mesh with orthogonal grids. Let's consider

the metric tensor $g_{\alpha\beta}$ which defines the arclength element ds in the physical plane in terms of the coordinate element sin the fictitious plane as

$$ds^2 = g_{\alpha\beta} d\xi_\alpha d\xi_\beta. \tag{A.2}$$

The $\alpha\beta$ component of the metric tensor can be obtained by the scalar product of the unit vectors tangent to the coordinate lines ξ_α and ξ_β in the physical plane (See any book on differential geometry). These unit vectors are defined by $\epsilon_\alpha = \partial x_\beta / \partial \xi_\alpha \mathbf{e}_\beta$. If the grid lines in the physical plane are to be orthogonal, we must have $g_{\alpha\beta} = 0, \quad \alpha \neq \beta$. The well–known formula for covariant Laplace operator is given by (Ryskin and Leal, 1983)

$$\nabla^2 = \frac{1}{h_{\xi_1} h_{\xi_2}} [\frac{\partial}{\partial \xi_1} (\frac{h_{\xi_2}}{h_{\xi_1}} \frac{\partial}{\partial \xi_1}) + \frac{\partial}{\partial \xi_2} (\frac{h_{\xi_1}}{h_{\xi_2}} \frac{\partial}{\partial \xi_2})] \tag{A.3}$$

where h_{ξ_α} are called scale factors (representing how much the sides of a rectangle of the grid in the physical plane have been scaled as compared to the sides of the corresponding square in the fictitious plane which is 1) and can be calculated from

$$h_{\xi_1}^2 = g_{11} = (\frac{\partial x_1}{\partial \xi_1})^2 + \frac{\partial x_2}{\partial \xi_1})^2, \quad h_{\xi_2}^2 = g_{22} = (\frac{\partial x_1}{\partial \xi_2})^2 + \frac{\partial x_2}{\partial \xi_2})^2. \tag{A.4}$$

So (A.1) can be written as

$$\frac{\partial}{\partial \xi_1} [f(\xi_1, \xi_2) \frac{\partial x_\alpha}{\partial \xi_1}] + \frac{\partial}{\partial \xi_2} [\frac{1}{f(\xi_1, \xi_2)} \frac{\partial x_\alpha}{\partial \xi_2}] = 0 \tag{A.5}$$

or

$$f \frac{\partial^2 x_\alpha}{\partial \xi_1^2} + \frac{1}{f} \frac{\partial^2 x_\alpha}{\partial \xi_2^2} + \frac{\partial f}{\partial \xi_1} \frac{\partial x_\alpha}{\partial \xi_1} - \frac{1}{f^2} \frac{\partial f}{\partial \xi_2} \frac{\partial x_\alpha}{\partial \xi_2} = 0 \tag{A.6}$$

where $f(\xi_1, \xi_2) = h_{\xi_2}/h_{\xi_1}$ (or f) is called the distortion function (it shows the aspect ratio of a rectangular zone in the grid in the physical plane). Using a central difference approximation, the derivatives in (A.6) can be written as

$$\begin{aligned} \frac{\partial x_\alpha}{\partial \xi_1} &\approx \frac{x_\alpha^{i+1,j} - x_\alpha^{i-1,j}}{2\Delta\xi_1} & \frac{\partial x_\alpha}{\partial \xi_2} &\approx \frac{x_\alpha^{i,j+1} - x_\alpha^{i,j-1}}{2\Delta\xi_2} \\ \frac{\partial^2 x_\alpha}{\partial \xi_1^2} &\approx \frac{x_\alpha^{i+1,j} - 2x_\alpha^{i,j} + x_\alpha^{i-1,j}}{(2\Delta\xi_1)^2} & \frac{\partial^2 x_\alpha}{\partial \xi_2^2} &\approx \frac{x_\alpha^{i,j+1} - 2x_\alpha^{i,j} + x_\alpha^{i,j-1}}{(2\Delta\xi_2)^2} \\ \frac{\partial f}{\partial \xi_1} &\approx \frac{f^{i+1,j} - f^{i-1,j}}{2\Delta\xi_1} & \frac{\partial f}{\partial \xi_2} &\approx \frac{f^{i,j+1} - f^{i,j-1}}{2\Delta\xi_2} \end{aligned} \tag{A.7}$$

where i, j is the index of the ith vertical and jth horizontal grid line of the square mesh in the ξ_1-ξ_2 plane, $i = 1, 2, \ldots, Imax$, $j = 1, 2, \ldots, Jmax$ (the values of $Imax$ and $Jmax$ are a matter of choice) and $\Delta\xi_1 = \Delta\xi_2$ is the distance between the grid lines and it's taken to be 1 for simplifying the calculations. Then the non-linear equations that result in the coordinates of the points on the grid lines in the physical plane are given by

$$\begin{aligned} x_\alpha^{i,j} = \; & \{[(f^{i,j})^2(f^{i+1,j} - f^{i-1,j})(x_\alpha^{i+1,j} - x_\alpha^{i-1,j}) - \\ & (f^{i,j+1} - f^{i,j-1})(x_\alpha^{i,j+1} - x_\alpha^{i,j-1})]/4 + (f^{i,j})^3(x_\alpha^{i+1,j} + x_\alpha^{i-1,j}) \\ & + f^{i,j}(x_\alpha^{i,j+1} + x_\alpha^{i,j-1})\}2[(f^{i,j})^3 + f^{i,j}]. \end{aligned} \tag{A.8}$$

The form of the above non-linear equations is suitable for applying a Successive Over-Relaxation method (SOR) to solve them. The only thing remaining to be explained is the boundary conditions. We discuss two common cases. We could have a Dirichlet boundary condition where points on the boundary in the physical domain have a one to one correspondence with the points on the boundary of the uniform square grid in the fictitious plane. Thus (A.8) is solved for the points inside the domain. But we could also have the case in which points on the boundary(s) correspond to the points on two parallel sides of the square and one of the coordinate lines that is

perpendicular to the boundary(s) (and is to be found) is related to the other two sides of the square thus the points corresponding to $i = 1$ and $i = Imax$ for example, end up in the same place in the physical plane. Since the grid lines related to the other coordinate are perpendicular to this common one, the Neuman condition at these boundaries of the square can be written as

$$\frac{\partial x_\alpha}{\partial \xi_1} = 0, \quad \forall j, \quad i = 1, Imax. \tag{A.9}$$

If the sides $j = 1$ and $j = Jmax$ are mapped to the same coordinate line in the physical plane, then (A.9) changes to

$$\frac{\partial x_\alpha}{\partial \xi_2} = 0, \quad \forall i, \quad j = 1, Jmax. \tag{A.10}$$

The annulus grid used for example 6.1 is a result of such a case. For that grid, $Imax = 11$ and $Jmax = 73$. Points on the inner circle correspond to $i = 1$ and points on the outer circle correspond to $i = Imax$. Coordinate lines corresponding to $j = 1$ and $j = Jmax$ are mapped to one of the radial lines in the grid. In this case, it is obvious that hoops and radial lines are the coordinate lines. Another example that is interesting to consider is example 6.4. There, the grid for a quarter of the square is generated by this method and the rest of the grid is produced by symmetry. For example, let's consider the upper–right quarter. For that grid $Imax = 11$ and $Jmax = 20$. Points on the bottom and left sides are equally spaced and they correspond to $j = 1$. Points on the other sides are spaced in such a way that they get closer to eachother as we approach the upper–right corner of the square. The right side corresponds to $i = 1$ and the top edge corresponds to $i = Imax$. Finally, the corner node (where) singularity occurs) corresponds to all the points with $j = Jmax$. Figure (A.1) shows a few other interesting grids that are generated by this method.

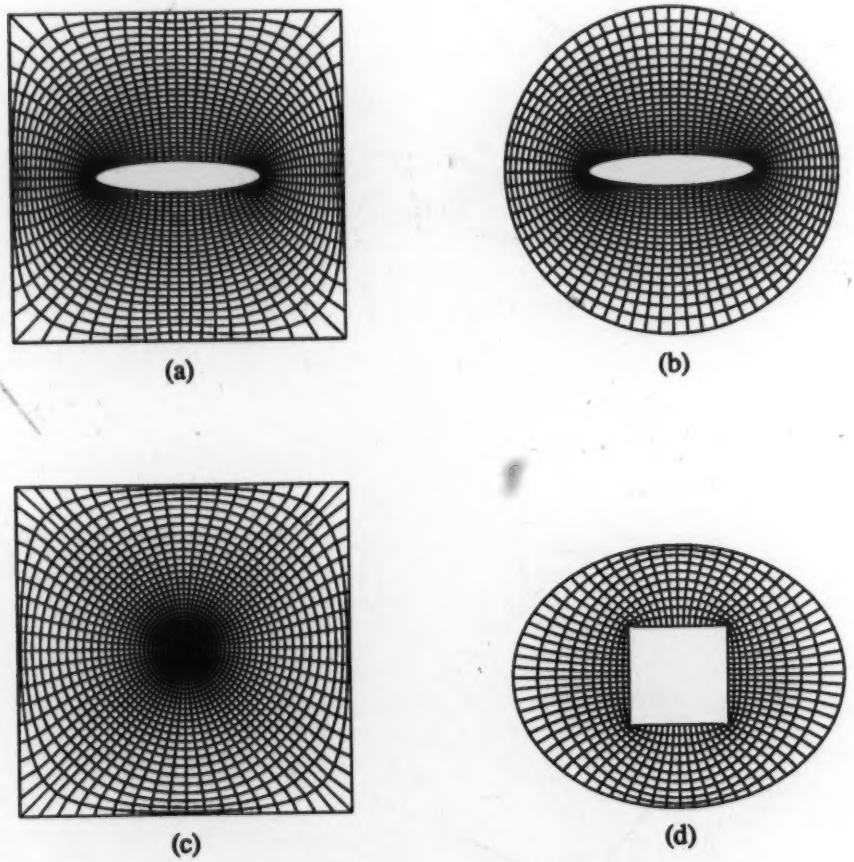

Figure A.1: A few grids generated by orthogonal mapping

Appendix B

Source Code

```
C     This program analyses a membrane (flat in unstreched config.)
C     under a variety of external loads like prescribed traction and
C     displacement, point load and pressure, attached and shearless
C     Cable reinforcement.

      Character filein*12,fileout*12,txt*80
      Double precision x(2,5605),r(3,5605),dx1(200),dx2(200),dx3(200)
      Double precision G(1),usm,usc,pp,fx(200),fy(200),fz(200),fn(18000)
      Double precision TE(3,2,5680),fp(18000),ff(18000),u(18000),A(5680)
      Double precision RR(18000),udotp(18000),udotc(18000),P(18000)
      Double precision Gcbl(10),Fcbl(18000),Lcbl(200),Ma(18000),ds
      Double precision nn(3,5680),tx(500),ty(500),tz(500),ftrac(18000)
      Double precision Lnewj2(100,200),Lcbl2(200),cstrn(200),cstrn2(200)
      Integer cblcnmt(2,200),maticbl(200),n2trc(500),ncmax(200)
      Integer conmat(4,5680),matindx(5680),nfxd(200),nprsc(200)
      Integer nfre(5605),nodcirc(2,72,5605),nodelcom(72,5605)
      Integer nndelmax(5605),nfrc(200),nsw(2,200),nltrc(500)
      Integer nfretrc1(500),nfretrc2(500),nodpc(500),ipdirid(500)
      Integer cblcnmt2(100,200),maticbl2(200),nfcbl(2,200)
      Integer nfcbl2(100,200),nfrepc(500)
      nschk=72

C     Asking for the filenames and parameters

      Write(*,*) 'Enter input file name :'
      Read (*,*)  filein
      Write(*,*) 'Enter output file name :'
      Read (*,*)  fileout
      Write(*,*) 'Enter mass matrix entry :'
      Read (*,*) usm
      Write(*,*) 'Enter damping coefficient :'
      Read (*,*) usc
```

```
C     Reading data from input datafile

      Open(1,File=filein)
      Read(1,*)txt
      Read(1,*)txt
      Read(1,*)txt
      Read(1,*)txt
      Read(1,*)nnode,nmat,nelem,nfixed,nprscrbd,nforce,nsew,ncable
     *,ncable2,nmaxcbl,nmatcbl,nprstrac,npconst
      Call Indata(nnode,x,G,nelem,conmat,matindx,nfixed,nfxd
     *,nprscrbd,nprsc,dx1,dx2,dx3,pp,nforce,nfrc
     *,fx,fy,fz,nsew,nsw,nmat,ncable,cblcnmt,nmatcbl,Gcbl,maticbl
     *,nprstrac,nltrc,n2trc,tx,ty,tz,npconst,nodpc,ipdirid,ncable2
     *,cblcnmt2,maticbl2,nmaxcbl,ncmax,cstrn,cstrn2)
      nfree=nnode-nfixed-nprscrbd

C     Indexing the free nodes

      ii=0
      Do 10 i=1 , nnode
         Do 20 j=1 , nfixed
            If (i .EQ. nfxd(j)) Go To 10
20       Continue
         Do 30 j=1 , nprscrbd
            If (i .EQ. nprsc(j)) Go To 10
30       Continue
         ii=ii+1
         nfre(ii)=i
10    Continue

C     Forming matrices nodcirc and nodelcom and array nndelmax
C     which show which free node number is surrounded by how many
C     zones and which zone numbers, This makes things a lot easier
C     when calculating the Piola stress

      nsmax=0
      Do 40 i=1 , nfree
         ii=0
         Do 50 j=1 , nelem
            If (conmat(1,j) .EQ. nfre(i)) Then
               ii=ii+1
               nodelcom(ii,i)=j
               nodcirc(1,ii,i)=conmat(2,j)
               nodcirc(2,ii,i)=conmat(4,j)
               Go To 50
            Else if (conmat(2,j) .EQ. nfre(i)) Then
               ii=ii+1
               nodelcom(ii,i)=j
               nodcirc(1,ii,i)=conmat(3,j)
               nodcirc(2,ii,i)=conmat(1,j)
               Go To 50
            Else if (conmat(3,j) .EQ. nfre(i)) Then
               ii=ii+1
               nodelcom(ii,i)=j
               nodcirc(1,ii,i)=conmat(4,j)
               nodcirc(2,ii,i)=conmat(2,j)
               Go To 50
            Else if (conmat(4,j) .EQ. nfre(i)) Then
               ii=ii+1
```

```
                nodelcom(ii,i)=j
                nodcirc(1,ii,i)=conmat(1,j)
                nodcirc(2,ii,i)=conmat(3,j)
              Endif
50          Continue
            if (nsmax .LT. ii) Then
               nsmax=ii
            Endif
          nndelmax(i)=ii
40      Continue
        Do 100 i=1 , nsew
          Do 110 j=1 , nfree
            If (nfre(j) .EQ. nsw(1,i)) Then
               j1=j
            Endif
            If (nfre(j) .EQ. nsw(2,i)) Then
               j2=j
            Endif
110       Continue
          nndj12=nndelmax(j1)+nndelmax(j2)
          if (nsmax .LT. nndj12) Then
            nsmax=nndj12
          Endif
          Do 120 j=nndelmax(j1)+1 , nndj12
            nodelcom(j,j1)=nodelcom(j-nndelmax(j1),j2)
            nodcirc(1,j,j1)=nodcirc(1,j-nndelmax(j1),j2)
            nodcirc(2,j,j1)=nodcirc(2,j-nndelmax(j1),j2)
120       Continue
          Do 130 j=nndelmax(j2)+1 , nndj12
            nodelcom(j,j2)=nodelcom(j-nndelmax(j2),j1)
            nodcirc(1,j,j2)=nodcirc(1,j-nndelmax(j2),j1)
            nodcirc(2,j,j2)=nodcirc(2,j-nndelmax(j2),j1)
130       Continue
          nndelmax(j1)=nndj12
          nndelmax(j2)=nndj12
100     Continue
        If (nsmax .NE. nschk) Then
          Write(*,*)'Maximum number of surrounding elements violated.'
          Write(*,*)'Maximum allowed :',nschk
          Write(*,*)'Maximum computed :',nsmax
          Stop
        End If

C       Calculating the force on the free nodes due to prescribed traction

        Do 140 i=1 , nprstrac
          Do 150 j=1 , nfree
            If (nfre(j).eq.n1trc(i)) Then
               nfretrc1(i)=j
            End If
            If (nfre(j).eq.n2trc(i)) Then
               nfretrc2(i)=j
            End If
150       Continue
140     Continue
        Do 160 i=1 , nprstrac
          ds=Sqrt((x(2,n1trc(i))-x(2,n2trc(i)))**2D0+(x(1,n1trc(i))-x(
     *       1,n2trc(i)))**2D0)
          i1=nfre(nfretrc1(i))
```

```
          i2=nfre(nfretrc2(i))
          ftrac((i1-1)*3+1)=ftrac((i1-1)*3+1)+tx(i)*ds/2D0
          ftrac((i1-1)*3+2)=ftrac((i1-1)*3+2)+ty(i)*ds/2D0
          ftrac((i1-1)*3+3)=ftrac((i1-1)*3+3)+tz(i)*ds/2D0
          ftrac((i2-1)*3+1)=ftrac((i2-1)*3+1)+tx(i)*ds/2D0
          ftrac((i2-1)*3+2)=ftrac((i2-1)*3+2)+ty(i)*ds/2D0
          ftrac((i2-1)*3+3)=ftrac((i2-1)*3+3)+tz(i)*ds/2D0
160     Continue

C       Calculating the free nodes index corresponding to partially
C       constrained nodes

        Do 180 i=1 , npconst
           Do 190 j=1 , nfree
              If (nfre(j) .eq. nodpc(i)) Then
                 nfrepc(i)=j
              End If
190        Continue
180     Continue


        Do 60 i=1 , nfixed
           r(1,nfxd(i))=x(1,nfxd(i))
           r(2,nfxd(i))=x(2,nfxd(i))
           r(3,nfxd(i))=0D0
60      Continue
        Do 70 i=1 , nprscrbd
           r(1,nprsc(i))=x(1,nprsc(i))+dx1(i)
           r(2,nprsc(i))=x(2,nprsc(i))+dx2(i)
           r(3,nprsc(i))=0D0+dx3(i)
70      Continue
        Do 80 j=1 , nforce
           Do 90 i=1 , nfree
              If (nfre(i) .NE. nfrc(j)) Go To 90
                 fn((i-1)*3+1)=fx(j)
                 fn((i-1)*3+2)=fy(j)
                 fn((i-1)*3+3)=fz(j)
90         Continue
80      Continue

C       Calling the Dynamic Relaxation subroutine

        Call DR(x,r,nfree,nfre,nodcirc,nodelcom,nndelmax,G,conmat,matindx
       *,usm,usc,pp,fn,nsew,nsw,nelem,nnode,nmat,nsmax,A,TE,fp,ff,u,Ma,RR,
       *udotp,udotc,P,ncable,cblcnmt,nmatcbl,Gcbl,Fcbl,Lcbl,maticbl,nfcbl,
       *nn,ftrac,npconst,nfrepc,ipdirid,ncable2,cblcnmt2,maticbl2,nmaxcbl
       *,Lcbl2,ncmax,nfcbl2,Lnewj2,cstrn,cstrn2)

C       generating the output datafile

        Call Output(nnode,x,r,G,conmat,matindx,fileout,nelem,nmat,A)
        Stop
        End
```

```
      Subroutine Fintext(x,r,nfre,nfree,nodcirc,nodelcom,nndelmax,P,co
     *nmat,G,matindx,pp,fn,ff,nelem,nnode,nmat,nsmax,A,TE,fp,ncable
     *,cblcnmt,nmatcbl,Gcbl,Fcbl,Lcbl,maticbl,nfcbl,nn,ncable2
     *,cblcnmt2,Lcbl2,maticbl2,nfcbl2,nmaxcbl,ncmax,Lnewj2)

C     This subroutine calculates the internal force vector at the nodes
C     due to the piola stress. It also calculates the external nodal force
C     vector due to pressure, point load and prescribed traction.


         Double precision x(2,nnode),r(3,nnode),T(3,2),G(nmat),sump1
         Double precision sump2,A(nelem),lambda,mu,TE(3,2,nelem)
         Double precision sump3,P(nfree*3),pp,fn(nfree*3),ff(nfree*3)
         Double precision sumf1,sumf2,sumf3,nn(3,nelem),fp(nfree*3)
         Double precision Gcbl(nmatcbl),Fcbl(nfree*3),Lcbl(ncable)
         Double precision Lcbl2(ncable2),Lnewj2(nmaxcbl,ncable2)
         Integer cblcnmt(2,ncable),maticbl(ncable),nfcbl(2,ncable)
         Integer nodcirc(2,nsmax,nfree),nodelcom(nsmax,nfree)
         Integer nndelmax(nfree),matindx(nelem),conmat(4,nelem)
         Integer nfre(nfree),cblcnmt2(nmaxcbl,ncable2)
         Integer maticbl2(ncable2),nfcbl2(nmaxcbl,ncable2)
         Integer ncmax(ncable2)

C  Calculating Piola stress for all zones

         Do 1005 i=1 , nelem
            Call Piola(x,r,i,T,conmat,G,matindx,A,lambda,mu,nn,nnode,
     *                 nelem,nmat)
            Do 1007 j=1 ,3
               Do 1009 k=1 , 2
                  TE(j,k,i)=T(j,k)
1009           Continue
1007        Continue
1005     Continue

C  Calculating internal force vector from Piola stress using
C  Green's thm.

         Do 1000 i=1 , nfree
            sump1=0D0
            sump2=0D0
            sump3=0D0
            sumf1=0D0
            sumf2=0D0
            sumf3=0D0
            Do 1010 j=1 , nndelmax(i)
               jelem=nodelcom(j,i)
               sump1=sump1+(TE(1,1,jelem)*(x(2,nodcirc(2,j,i))-x(2,nodci
     *         rc(1,j,i)))-(TE(1,2,jelem)*(x(1,nodcirc(2,j,i))-x(1,nodci
     *         rc(1,j,i)))))/2D0
               sump2=sump2+(TE(2,1,jelem)*(x(2,nodcirc(2,j,i))-x(2,nodci
     *         rc(1,j,i)))-(TE(2,2,jelem)*(x(1,nodcirc(2,j,i))-x(1,nodci
     *         rc(1,j,i)))))/2D0
               sump3=sump3+(TE(3,1,jelem)*(x(2,nodcirc(2,j,i))-x(2,nodci
     *         rc(1,j,i)))-(TE(3,2,jelem)*(x(1,nodcirc(2,j,i))-x(1,nodci
     *         rc(1,j,i)))))/2D0
               sumf1=sumf1+pp*nn(1,jelem)*lambda*mu*A(jelem)
               sumf2=sumf2+pp*nn(2,jelem)*lambda*mu*A(jelem)
               sumf3=sumf3+pp*nn(3,jelem)*lambda*mu*A(jelem)
```

```
1010        Continue

C  Forming the nodal internal force vector

            P((i-1)*3+1)=sump1
            P((i-1)*3+2)=sump2
            P((i-1)*3+3)=sump3

C  Forming the nodal force vector due to pressure

            fp((i-1)*3+1)=sumf1/(1D0*nndelmax(i))
            fp((i-1)*3+2)=sumf2/(1D0*nndelmax(i))
            fp((i-1)*3+3)=sumf3/(1D0*nndelmax(i))
1000      Continue

C  Calculating the nodal force vector due to the pressence of
C  cables (attached and shearless)

          Call Fcable(r,nfree,nfre,nnode,ncable,cblcnmt,nmatcbl,Gcbl,Fcbl
     *               ,Lcbl,maticbl,nfcbl,ncable2,cblcnmt2,Lcbl2,maticbl2
     *               ,nfcbl2,nmaxcbl,ncmax,Lnewj2)

C  Finalizing the nodal internal and external force vectors by
C  adding forces due to cable, pressure, point load and prescribed
C  traction.

          Do 1020 i=1 , nfree*3
             P(i)=P(i)+Fcbl(i)
             ff(i)=fp(i)+fn(i)
1020      Continue
       Return
       End



       Subroutine Piola(x,r,j,T,conmat,G,matindx,A,lambda,mu,nn,nnode,
      *                 nelem,nmat)

C      This subroutine calculates the piola stress for a specified
C      zone.

          Double precision F(3,2),x(2,nnode),r(3,nnode),T(3,2),C(2,2)
          Double precision lambda,mu,L(2),M(2),ll(3),mm(3),wmu,wlambda
          Double precision wphatlambda,G(nmat),A(nelem),nn(3,nelem)
          Integer conmat(4,nelem),matindx(nelem)

C  Calculating the deformation gradient F

          Call Defgrad(x,r,j,F,conmat,A,nnode,nelem)

C  Calculating the Cauchy-Green strain tensor C

          Call CGStrain(C,F)

C  Calculating the principal stretches from C
```

```
      Call Pplstrch(C,lambda,mu)

C  Calculating the ppl vectors of C ,i.e. L & M, and
C  their deformed configurations l & m

      Call Cevector(C,F,L,M,ll,mm,lambda,mu)

C  Calculating the normal to the zone n=lxm

      nn(1,j)=(ll(2)*mm(3)-ll(3)*mm(2))
      nn(2,j)=(ll(3)*mm(1)-ll(1)*mm(3))
      nn(3,j)=(ll(1)*mm(2)-ll(2)*mm(1))

C  Calculating the derivative of strain energy W with respect to the
C  ppl stretches using the Neo-Hookian strain energy

      Call Strnenrgy(wmu,wlambda,wphatlambda,lambda,mu,j,G,matindx,
     *                nelem,nmat)

C  Calculating the Piola stress

      If ((lambda .LE. 1D0) .AND. (mu. LE. 1D0)) Then
         Do 2000 i=1 , 3
            Do 2010 ia=1 , 2
               T(i,ia)=0D0
2010        Continue
2000     Continue
      Else if ((lambda .GT. 1D0) .AND. (mu .LE. 1D0/Sqrt(lambda)))
     *Then
         Do 2020 i=1 , 3
            Do 2030 ia=1 , 2
               T(i,ia)=wphatlambda*ll(i)*L(ia)
2030        Continue
2020     Continue
      Else if ((lambda .GT. 1D0/Sqrt(mu)) .AND. (mu .GT. 1D0/
     *Sqrt(lambda))) Then
         Do 2040 i=1 , 3
            Do 2050 ia=1 , 2
               T(i,ia)=wlambda*ll(i)*L(ia)+wmu*mm(i)*M(ia)
2050        Continue
2040     Continue
      Endif
    Return
    End



    Subroutine Defgrad(x,r,j,F,conmat,A,nnode,nelem)

C     This subroutine calculates the deformation gradient F
```

```
      Double precision x(2,nnode),r(3,nnode),F(3,2),A(nelem)
      Integer conmat(4,nelem)
      n1=conmat(1,j)
      n2=conmat(2,j)
      n3=conmat(3,j)
      n4=conmat(4,j)
      Do 3020 i=1 , 3
         F(i,1)=((x(2,n4)-x(2,n2))*(r(i,n3)-r(i,n1))-(x(2,n3)-x(2,n1)
     *)*(r(i,n4)-r(i,n2)))/(2D0*A(j))
         F(i,2)=-((x(1,n4)-x(1,n2))*(r(i,n3)-r(i,n1))-(x(1,n3)-x(1,n1
     *))*(r(i,n4)-r(i,n2)))/(2D0*A(j))
3020    Continue
      Return
      End



      Subroutine CGStrain(C,F)

C     This subroutine calculates the Cauchy-Green strain tensor

      Double precision C(2,2),F(3,2)
      Do 4000 ia=1 , 2
         Do 4010 ib=1 , 2
            C(ia,ib)=F(1,ia)*F(1,ib)+F(2,ia)*F(2,ib)+F(3,ia)*F(3,ib)
4010     Continue
4000    Continue
      Return
      End



      Subroutine Pplstrch(C,lambda,mu)

C     This subroutine calculates the ppl stretches from C

      Double precision C(2,2),lambda,mu,x1,x2,trc,detc
      trc=C(1,1)+C(2,2)
      detc=C(1,1)*C(2,2)-C(1,2)**2D0
      x1=Abs(trc+Sqrt(Abs(trc**2D0-4D0*detc)))/2D0
      x2=Abs(trc-Sqrt(Abs(trc**2D0-4D0*detc)))/2D0
      If (x1 .GT. x2) Then
         lambda=Sqrt(x1)
         mu=Sqrt(x2)
      Else
         lambda=Sqrt(x2)
         mu=Sqrt(x1)
      Endif
      Return
      End
```

```
      Subroutine Cevector(C,F,L,M,ll,mm,lambda,mu)

C     This subroutine calculates the ppl vectors of C and their deformed
C     configuration

         Double precision C(2,2),F(3,2),L(2),M(2),ll(3),mm(3),lambda,mu
         L(1)=Abs(C(1,2))/Sqrt((lambda**2D0-C(1,1))**2D0+C(1,2)**2D0)
         L(2)=Abs(C(1,2))/Sqrt((lambda**2D0-C(2,2))**2D0+C(1,2)**2D0)
         M(1)=Abs(C(1,2))/Sqrt((mu**2D0-C(1,1))**2D0+C(1,2)**2D0)
         M(2)=Abs(C(1,2))/Sqrt((mu**2D0-C(2,2))**2D0+C(1,2)**2D0)
         If ((C(1,1)-lambda**2D0)*C(1,2) .LT. 0D0) Then
            M(1)=-M(1)
         Else
            L(2)=-L(2)
         Endif
         If (Abs(C(1,2)) .LE. 1D-14) Then
            If (C(1,1) .GT. C(2,2)) Then
               L(1)=1D0
               L(2)=0D0
               M(1)=0D0
               M(2)=1D0
            Else
               L(1)=0D0
               L(2)=1D0
               M(1)=1D0
               M(2)=0D0
            Endif
         Endif
         Do 5000 i=1 , 3
            ll(i)=(F(i,1)*L(1)+F(i,2)*L(2))/lambda
            mm(i)=(F(i,1)*M(1)+F(i,2)*M(2))/mu
5000     Continue
      Return
      End
```

```
      Subroutine Strnenrgy(wmu,wlambda,wphatlambda,lambda,mu,j,G,matind
     *x,nelem,nmat)

C     This subroutine calculates the derivatives of the strain energy
C     w.r.t. ppl stretches using the Neo-Hookian strain energy.

         Double precision wmu,wlambda,wphatlambda,lambda,mu
         Double precision G(nmat)
         Integer matindx(nelem)
         wmu=(mu-1D0/(mu**3D0*lambda**2D0))*G(matindx(j))
```

```
        wlambda=(lambda-1D0/(mu**2D0*lambda**3D0))*G(matindx(j))
        wphatlambda=(lambda-1D0/lambda**2D0)*G(matindx(j))
      Return
      End



      Subroutine DR(x,r,nfree,nfre,nodcirc,nodelcom,nndelmax,G,conmat,ma
     *tindx,usm,usc,pp,fn,nsew,nsw,nelem,nnode,nmat,nsmax,A,TE,fp,ff,u,
     *Ma,RR,udotp,udotc,P,ncable,cblcnmt,nmatcbl,Gcbl,Fcbl,Lcbl,maticbl
     *,nfcbl,nn,ftrac,npconst,nfrepc,ipdirid,ncable2,cblcnmt2,maticbl2
     *,nmaxcbl,Lcbl2,ncmax,nfcbl2,Lnewj2,cstrn,cstrn2)

C     This subroutine solves the non-linear equations of equilibrium
C     using Dynamic Relaxation

        Double precision x(2,nnode),r(3,nnode),udotp(nfree*3),Rmax
        Double precision udotc(nfree*3),h,er,P(nfree*3),RR(nfree*3)
        Double precision cc,ff(nfree*3),A(nelem),G(nmat),u(nfree*3)
        Double precision Ma(nfree*3),usm,usc,fn(nfree*3),pp,r1,r2,r3
        Double precision TE(3,2,nelem),fp(nfree*3),nn(3,nelem)
        Double precision Gcbl(nmatcbl),Fcbl(nfree*3),Lcbl(ncable)
        Double precision ftrac(nfree*3),Lcbl2(ncable2)
        Double precision Lnewj2(nmaxcbl,ncable2),cstrn(ncable)
        Double precision cstrn2(ncable2)
        Integer cblcnmt(2,ncable),maticbl(ncable),nfcbl(2,ncable)
        Integer nodcirc(2,nsmax,nfree),nodelcom(nsmax,nfree)
        Integer nndelmax(nfree),conmat(4,nelem),nsw(2,nsew)
        Integer nfre(nfree),matindx(nelem),nfrepc(npconst)
        Integer ipdirid(npconst),cblcnmt2(nmaxcbl,ncable2)
        Integer maticbl2(ncable2),ncmax(ncable2)
        Integer nfcbl2(nmaxcbl,ncable2)
        character filetemp*12

C     Calculating the area of the zones, unstretched length of the
C     cables, and indexing free nodes lying on the cables

        Call CalcArea(x,nelem,A,conmat,nnode)
        Call Calcl(x,nnode,ncable,cblcnmt,Lcbl,ncable2,cblcnmt2,Lcbl2
     *            ,ncmax,nmaxcbl,cstrn,cstrn2)
        Call nfrecbl(nfre,nfree,cblcnmt,ncable,nfcbl,ncable2,cblcnmt2
     *            ,ncmax,nmaxcbl,nfcbl2)

C     Specifying time step and tolerance

        h=1D0
        er=1D-5
        n=0
        cc=usc

C     Initializing the displacement and mass vectors

        Do 6000 i=1 , nfree*3
           u(i)=0D0
           Ma(i)=usm
6000    Continue
```

```
C     Updating the position vectors

6010     Do 6020 i=1 , nfree
            r(1,nfre(i))=x(1,nfre(i))+u((i-1)*3+1)
            r(2,nfre(i))=x(2,nfre(i))+u((i-1)*3+2)
            r(3,nfre(i))=u((i-1)*3+3)
6020     Continue

c     Equating the nodal positions for nodes lying on the suturing seam

         Do 6170 i=1 , nsew
            r1=r(1,nsw(1,i))
            r2=r(2,nsw(1,i))
            r3=r(3,nsw(1,i))
            r(1,nsw(2,i))=r1
            r(2,nsw(2,i))=r2
            r(3,nsw(2,i))=r3
6170     Continue

C     Calculating the external and internal nodal force vectors

         Call Fintext(x,r,nfre,nfree,nodcirc,nodelcom,nndelmax,P,conma
     *t,G,matindx,pp,fn,ff,nelem,nnode,nmat,nsmax,A,TE,fp,ncable,
     *cblcnmt,nmatcbl,Gcbl,Fcbl,Lcbl,maticbl,nfcbl,nn,ncable2,cblcnmt2
     *,Lcbl2,maticbl2,nfcbl2,nmaxcbl,ncmax,Lnewj2)

C     Calculating the residual vector

         Do 6030 i=1 , nfree*3
            RR(i)=P(i)+ff(i)+ftrac(i)
6030     Continue

c     Modifying the residual vector for partially constrained nodes

         Do 6035 i=1 , npconst
            RR((nfrepc(i)-1)*3+ipdirid(i))=0d0
6035     Continue

C        Finding Maximum absolute value of residual

         Rmax=0D0
         Do 6040 i=1 , nfree*3
            If (Abs(RR(i)) .GT. Rmax) Then
               Rmax=Abs(RR(i))
            Endif
6040     Continue

C     Check for convergence

         If (Rmax .LT. er) Go To 6160

C        Calculating velocity at time step n+1/2

         If (n .EQ. 0) Then
            Do 6130 i=1 , nfree*3
               udotc(i)=h*RR(i)/(2D0*Ma(i))
6130        Continue
         Else
            Do 6140 i=1 , nfree*3
```

```
        udotc(i)=(2D0-cc*h)*udotp(i)/(2D0+cc*h)+2D0*h*RR(i)/((2D0+cc*
     *h)*Ma(i))
6140        Continue
        End if

C       Calculate displacement at time step n+1

        Do 6150 i=1 , nfree*3
           u(i)=u(i)+h*udotc(i)
           udotp(i)=udotc(i)
6150    Continue
        n=n+1
        Go To 6010
6160  Return
      End




      Subroutine  CalcArea(x,nelem,A,conmat,nnode)

C     This subroutine calculates the area of each zone to be used in
C     calculating deformation gradient F

         Double precision x(2,nnode),A(nelem)
         Integer conmat(4,nelem)
         Do 9000 i=1 , nelem
           n1=conmat(1,i)
           n2=conmat(2,i)
           n3=conmat(3,i)
           n4=conmat(4,i)
           A(i)=((x(2,n4)-x(2,n2))*(x(1,n3)-x(1,n1))-(x(1,n4)-x(1,n2))*
     *           (x(2,n3)-x(2,n1)))/2D0
           If (A(i) .LE. 0D0) Then
              Write(*,*)'n1,2,3,4=',n1,n2,n3,n4
              Write(*,*)'elem #=',i
              write(*,*)'A=',A(i)
              Stop
           Endif
9000     Continue
       Return
       End




      Subroutine nfrecbl(nfre,nfree,cblcnmt,ncable,nfcbl,ncable2,
     *                   cblcnmt2,ncmax,nmaxcbl,nfcbl2)

C     This subroutine indexes the free nodes lying on the cables

         Integer nfre(nfree),cblcnmt(2,ncable),nfcbl(2,ncable)
         Integer cblcnmt2(nmaxcbl,ncable2),ncmax(ncable2)
```

```
      Integer nfcbl2(nmaxcbl,ncable2)
      Do 13000 i=1 , nfree
         Do 13010 j=1 , ncable
            If (nfre(i) .EQ. cblcnmt(1,j)) Then
               nfcbl(1,j)=i
               Go To 13010
            End If
            If (nfre(i) .EQ. cblcnmt(2,j)) Then
               nfcbl(2,j)=i
            End If
13010    Continue
13000  Continue
       Do 13020 i=1 , nfree
          Do 13030 j=1 , ncable2
             Do 13040 k=1 , ncmax(j)
                If (nfre(i).eq.cblcnmt2(k,j)) Then
                   nfcbl2(k,j)=i
                End If
13040        Continue
13030     Continue
13020  Continue
     Return
     End
```

```
      Subroutine Fcable(r,nfree,nfre,nnode,ncable,cblcnmt,nmatcbl,Gcbl
     *,Fcbl,Lcbl,maticbl,nfcbl,ncable2,cblcnmt2,Lcbl2,maticbl2,nfcbl2
     *,nmaxcbl,ncmax,Lnewj2)

C     This subroutine calculates the nodal force vector due to the cables

         Double precision r(3,nnode),Gcbl(nmatcbl)
         Double precision Fcbl(nfree*3),FF(3),Lcbl(ncable)
         Double precision Lcbl2(ncable2),Lnewj2(nmaxcbl,ncable2)
         Integer nfre(nfree),cblcnmt(2,ncable),maticbl(ncable)
         Integer nfcbl(2,ncable),cblcnmt2(nmaxcbl,ncable2)
         Integer maticbl2(ncable2),nfcbl2(nmaxcbl,ncable2)
         Integer ncmax(ncable2)
         Do 10000 i=1 , nfree
            Fcbl((i-1)*3+1)=0D0
            Fcbl((i-1)*3+2)=0D0
            Fcbl((i-1)*3+3)=0D0
10000    Continue
         Do 10010 j=1 , ncable
            If (nfcbl(1,j) .NE. 0) Then
               Call Fcb(r,nnode,cblcnmt,j,1,Lcbl,FF,ncable,Gcbl,
     *                  maticbl,nmatcbl)
               Fcbl((nfcbl(1,j)-1)*3+1)=Fcbl((nfcbl(1,j)-1)*3+1)+FF(1)
               Fcbl((nfcbl(1,j)-1)*3+2)=Fcbl((nfcbl(1,j)-1)*3+2)+FF(2)
               Fcbl((nfcbl(1,j)-1)*3+3)=Fcbl((nfcbl(1,j)-1)*3+3)+FF(3)
            End If
            If (nfcbl(2,j) .NE. 0) Then
```

```
            Call Fcb(r,nnode,cblcnmt,j,2,Lcbl,FF,ncable,Gcbl,
     *                  maticbl,nmatcbl)
            Fcbl((nfcbl(2,j)-1)*3+1)=Fcbl((nfcbl(2,j)-1)*3+1)+FF(1)
            Fcbl((nfcbl(2,j)-1)*3+2)=Fcbl((nfcbl(2,j)-1)*3+2)+FF(2)
            Fcbl((nfcbl(2,j)-1)*3+3)=Fcbl((nfcbl(2,j)-1)*3+3)+FF(3)
         End If
10010    Continue
         Do 10020 i=1 , ncable2
            Call Calclnewj(r,nnode,i,cblcnmt2,nmaxcbl,ncmax,Lnewj2,
     *                     ncable2)
            Do 10030 j=1 , ncmax(i)
               If (nfcbl2(j,i).NE.0) Then
                  Call Fcb2(r,nnode,cblcnmt2,i,j,Lcbl2,FF,ncable2,Gcbl,
     *                 maticbl2,nmatcbl,nmaxcbl,ncmax,Lnewj2)
                  Fcbl((nfcbl2(j,i)-1)*3+1)=Fcbl((nfcbl2(j,i)-1)*3+1)
     *            +FF(1)
                  Fcbl((nfcbl2(j,i)-1)*3+2)=Fcbl((nfcbl2(j,i)-1)*3+2)
     *            +FF(2)
                  Fcbl((nfcbl2(j,i)-1)*3+3)=Fcbl((nfcbl2(j,i)-1)*3+3)
     *            +FF(3)
               End If
10030       Continue
10020    Continue
      Return
      End




      Subroutine Fcb(r,nnode,cblcnmt,j,k,Lcbl,FF,ncable,Gcbl,maticbl
     *            ,nmatcbl)

C     This subroutine calculates the force vector at each free node on  the
C     attached cable.

         Double precision r(3,nnode),Lcbl(ncable),FF(3),Lnewj,lam,eps
         Double precision Gcbl(nmatcbl),Fj
         Integer cblcnmt(2,ncable),maticbl(ncable)
         FF(1)=0D0
         FF(2)=0D0
         FF(3)=0D0
         Lnewj=((r(1,cblcnmt(2,j))-r(1,cblcnmt(1,j)))**2D0+
     *          (r(2,cblcnmt(2,j))-r(2,cblcnmt(1,j)))**2D0+
     *          (r(3,cblcnmt(2,j))-r(3,cblcnmt(1,j)))**2D0)**5D-1
         lam=Lnewj/Lcbl(j)
         If (lam .GT. 1D0) Then
            eps=lam-1D0
            Fj=Gcbl(maticbl(j))*eps
            If (k .EQ. 1) Then
               FF(1)=(r(1,cblcnmt(2,j))-r(1,cblcnmt(1,j)))*Fj/Lnewj
               FF(2)=(r(2,cblcnmt(2,j))-r(2,cblcnmt(1,j)))*Fj/Lnewj
               FF(3)=(r(3,cblcnmt(2,j))-r(3,cblcnmt(1,j)))*Fj/Lnewj
            Else
               FF(1)=(r(1,cblcnmt(1,j))-r(1,cblcnmt(2,j)))*Fj/Lnewj
               FF(2)=(r(2,cblcnmt(1,j))-r(2,cblcnmt(2,j)))*Fj/Lnewj
```

```
            FF(3)=(r(3,cblcnmt(1,j))-r(3,cblcnmt(2,j)))*Fj/Lnewj
         End If
      End If
   Return
   End



   Subroutine Fcb2(r,nnode,cblcnmt2,j,k,Lcbl2,FF,ncable2,Gcbl,
  *          maticbl2,nmatcbl,nmaxcbl,ncmax,Lnewj2)

C     This subroutine calculates the force vector at each free node on
C     the shearless cable.

      Double precision r(3,nnode),Lcbl2(ncable2),FF(3),Lnewj,lam,eps
      Double precision Gcbl(nmatcbl),Fj,Lnewj2(nmaxcbl,ncable2),sum
      Integer ncmax(ncable2)
      Integer cblcnmt2(nmaxcbl,ncable2),maticbl2(ncable2)
      FF(1)=0D0
      FF(2)=0D0
      FF(3)=0D0
      sum=0D0
      Do 15000 i=1 , ncmax(j)-1
         sum=sum+Lnewj2(i,j)
15000 Continue
      Lnewj=sum
      lam=Lnewj/Lcbl2(j)
      If (lam .GT. 1D0) Then
         eps=lam-1D0
         Fj=Gcbl(maticbl2(j))*eps
         If (k .EQ. 1) Then
            FF(1)=(r(1,cblcnmt2(2,j))-r(1,cblcnmt2(1,j)))*Fj/
     *           Lnewj2(1,j)
            FF(2)=(r(2,cblcnmt2(2,j))-r(2,cblcnmt2(1,j)))*Fj/
     *           Lnewj2(1,j)
            FF(3)=(r(3,cblcnmt2(2,j))-r(3,cblcnmt2(1,j)))*Fj/
     *           Lnewj2(1,j)
         Else If (k.eq.ncmax(j)) Then
            FF(1)=(r(1,cblcnmt2(k-1,j))-r(1,cblcnmt2(k,j)))*Fj
     *           /Lnewj2(k-1,j)
            FF(2)=(r(2,cblcnmt2(k-1,j))-r(2,cblcnmt2(k,j)))*Fj
     *           /Lnewj2(k-1,j)
            FF(3)=(r(3,cblcnmt2(k-1,j))-r(3,cblcnmt2(k,j)))*Fj
     *           /Lnewj2(k-1,j)
         Else
            FF(1)=(r(1,cblcnmt2(k-1,j))-r(1,cblcnmt2(k,j)))*Fj
     *           /Lnewj2(k-1,j)+(r(1,cblcnmt2(k+1,j))-r(1,
     *           cblcnmt2(k,j)))*Fj/Lnewj2(k,j)
            FF(2)=(r(2,cblcnmt2(k-1,j))-r(2,cblcnmt2(k,j)))*Fj
     *           /Lnewj2(k-1,j)+(r(2,cblcnmt2(k+1,j))-r(2,
```

```
     *              cblcnmt2(k,j)))*Fj/Lnewj2(k,j)
                 FF(3)=(r(3,cblcnmt2(k-1,j))-r(3,cblcnmt2(k,j)))*Fj
     *              /Lnewj2(k-1,j)+(r(3,cblcnmt2(k+1,j))-r(3,
     *              cblcnmt2(k,j)))*Fj/Lnewj2(k,j)
           End If
        End If
      Return
      End




      Subroutine Calclnewj(r,nnode,i,cblcnmt2,nmaxcbl,ncmax,Lnewj2
     *                     ,ncable2)

C     This subroutine calculates the deformed length of each piece of
C     shearless cable

         Double precision r(3,nnode),Lnewj2(nmaxcbl,ncable2)
         Integer cblcnmt2(nmaxcbl,ncable2),ncmax(ncable2)
         Do 16000 j=1 , ncmax(i)-1
            Lnewj2(j,i)=((r(1,cblcnmt2(j,i))-r(1,cblcnmt2(j+1,i)))**2D0+
     *       (r(2,cblcnmt2(j,i))-r(2,cblcnmt2(j+1,i)))**2D0+
     *       (r(3,cblcnmt2(j,i))-r(3,cblcnmt2(j+1,i)))**2D0)**5D-1
16000    Continue
      Return
      End



      Subroutine Calcl(x,nnode,ncable,cblcnmt,Lcbl,ncable2,cblcnmt2,
     *                 Lcbl2,ncmax,nmaxcbl,cstrn,cstrn2)

C     This subroutine calculates the unstretched length of each piece of
C     shearless and attached cables.

         Double precision x(2,nnode),Lcbl(ncable),Lcbl2(ncable2)
         Double precision cstrn(ncable),cstrn2(ncable2)
         Integer cblcnmt(2,ncable),cblcnmt2(nmaxcbl,ncable2)
         Integer ncmax(ncable2)
         Do 12000 i=1 , ncable
            Lcbl(i)=(((x(1,cblcnmt(1,i))-x(1,cblcnmt(2,i)))**2D0+
     *(x(2,cblcnmt(1,i))-x(2,cblcnmt(2,i)))**2D0)**5D-1)/(1D0+cstrn(i))
12000    Continue
         Do 12010 i=1 , ncable2
            sum=0D0
            Do 12020 j=1 , ncmax(i)-1
               sum=sum+((x(1,cblcnmt2(j,i))-x(1,cblcnmt2(j+1,i)))**2D0
     *          +(x(2,cblcnmt2(j,i))-x(2,cblcnmt2(j+1,i)))**2D0)**5D-1
12020       Continue
            Lcbl2(i)=sum/(1D0+cstrn2(i))
12010    Continue
      Return
      End
```

```
      Subroutine Indata(nnode,x,G,nelem,conmat,matindx,nfixed,nfxd
     *,nprscrbd,nprsc,dx1,dx2,dx3,pp,nforce,nfrc,fx,fy,fz,nsew,nsw
     *,nmat,ncable,cblcnmt,nmatcbl,Gcbl,maticbl,nprstrac,n1trc,
     *n2trc,tx,ty,tz,npconst,nodpc,ipdirid,ncable2,cblcnmt2
     *,maticbl2,nmaxcbl,ncmax,cstrn,cstrn2)

C     This subroutine reads the data from input datafile

         Double precision x(2,nnode),dx1(nprscrbd),dx2(nprscrbd)
         Double precision dx3(nprscrbd),fx(nforce),fy(nforce)
         Double precision G(nmat),fz(nforce),pp,Gcbl(nmatcbl)
         Double precision tx(nprstrac),ty(nprstrac),tz(nprstrac)
         Double precision cstrn(ncable),cstrn2(ncable2)
         Integer cblcnmt(2,ncable),maticbl(ncable),ipdirid(npconst)
         Integer conmat(4,nelem),matindx(nelem),nfxd(nfixed)
         Integer nprsc(nprscrbd),nfrc(nforce),nsw(2,nsew)
         Integer n1trc(nprstrac),n2trc(nprstrac),nodpc(npconst)
         Integer cblcnmt2(nmaxcbl,ncable2),maticbl2(ncable2)
         Integer ncmax(ncable2)
         Read (1,*) nnnode
         Do 7000 i=1 , nnode
            Read (1,*) ii,x(1,i),x(2,i)
7000     Continue
         Read (1,*) nnmat
         Do 7010 i=1 , nmat
            Read (1,*) ii,G(i)
7010     Continue
         Read (1,*) nnelem
         Do 7020 i=1 , nelem
          Read (1,*) ii,conmat(1,i),conmat(2,i),conmat(3,i),conmat(4,i),
     *matindx(i)
7020     Continue
         Read (1,*) nnfixed
         Do 7030 i=1 , nfixed
            Read (1,*) nfxd(i)
7030     Continue
         Read (1,*) nnprscrbd
         Do 7040 i=1 , nprscrbd
            Read (1,*) ii,nprsc(i),dx1(i),dx2(i),dx3(i)
7040     Continue
         Read (1,*) nnforce
         Do 7050 i=1 , nforce
            Read (1,*) ii,nfrc(i),fx(i),fy(i),fz(i)
7050     Continue
         Read (1,*) pp
         Read (1,*) nnsew
         Do 7060 i=1 , nsew
            Read (1,*) ii,nsw(1,i),nsw(2,i)
7060     Continue
         Read (1,*) ncable
         Do 7070 i=1 , ncable
            Read(1,*) ii,cblcnmt(1,i),cblcnmt(2,i),maticbl(i),cstrn(i)
```

```
7070     Continue
         Read (1,*) ncable2
         Do 7110 i=1 ,ncable2
            Read(1,*)ii,ncmax(i),(cblcnmt2(j,i),j=1,ncmax(i)),
     *      maticbl2(i),cstrn2(i)
            If (ncmax(i).gt.nmaxcbl) Then
               write(*,*)'Maximum # of cables in the string is violated'
               Stop
            End If
7110     Continue
         Read (1,*) nmatcbl
         Do 7080 i=1 , nmatcbl
            Read(1,*) ii,Gcbl(i)
7080     Continue
         Read(1,*)nprstrac
         Do 7090 i=1 , nprstrac
            Read(1,*)ii,n1trc(i),n2trc(i),tx(i),ty(i),tz(i)
7090     Continue
         Read(1,*)npconst
         Do 7100 i=1 , npconst
            Read(1,*)nodpc(i),ipdirid(i)
7100     Continue
         Close (1)
      Return
      End
```

```
      Subroutine Output(nnode,x,r,G,conmat,matindx,fileout,nelem,nmat,A)

C     This subroutine generates the output datafile

         Character fileout*12,date*30
         Double precision x(2,nnode),r(3,nnode),G(nmat),F(3,2),C(2,2)
         Double precision lambda,mu,L(2),M(2),ll(3),mm(3),wmu
         Double precision wlambda,wphatlambda,A(nelem),T(3,2)
         Integer conmat(4,nelem),matindx(nelem),es
         Open(1,File=fileout)
         Do 8000 i=1 , nnode
            Write(1,*)i,r(1,i),r(2,i),r(3,i)
8000     Continue
         Do 8010 i=1 , nelem
            Call Defgrad(x,r,i,F,conmat,A,nnode,nelem)
            Call CGStrain(C,F)
            Call Pplstrch(C,lambda,mu,F)
            Call Cevector(C,F,L,M,ll,mm,lambda,mu)
            Call Strnenrgy(wmu,wlambda,wphatlambda,lambda,mu,i,G,matind
     *      x,nelem,nmat)
            If ((lambda .LE. 1D0) .AND. (mu. LE. 1D0)) Then
            Do 8020 ji=1 , 3
```

```
               Do 8030 ia=1 , 2
                  T(ji,ia)=0D0
8030           Continue
8020        Continue
               es=0
            Else if ((lambda .GT. 1D0) .AND. (mu .LE. 1D0/Sqrt(lambda)))
     *Then
            Do 8040 ji=1 , 3
               Do 8050 ia=1 , 2
                  T(ji,ia)=wphatlambda*ll(ji)*L(ia)
8050           Continue
8040        Continue
               es=1
            Else if ((lambda .GT. 1D0/Sqrt(mu)) .AND. (mu .GT. 1D0/
     *Sqrt(lambda))) Then

            Do 8060 ji=1 , 3
               Do 8070 ia=1 , 2
                  T(ji,ia)=wlambda*ll(ji)*L(ia)+wmu*mm(ji)*M(ia)
8070           Continue
8060        Continue
               es=2
            Endif
            Write(1,*)i,lambda,mu,es,ll(1),ll(2),ll(3),mm(1),mm(2),mm(3)
            Write(1,*)T(1,1),T(1,2),T(2,1),T(2,2),T(3,1),T(3,2)
8010     Continue
      Return
      End
```